

2010

ANALYZING EFFICIENCY OF SWITCH-MODE WELDING POWER SUPPLY

Muhammad Imtiaz

Follow this and additional works at: <https://ir.lib.uwo.ca/digitizedtheses>

Recommended Citation

Imtiaz, Muhammad, "ANALYZING EFFICIENCY OF SWITCH-MODE WELDING POWER SUPPLY" (2010).
Digitized Theses. 3719.
<https://ir.lib.uwo.ca/digitizedtheses/3719>

This Thesis is brought to you for free and open access by the Digitized Special Collections at Scholarship@Western. It has been accepted for inclusion in Digitized Theses by an authorized administrator of Scholarship@Western. For more information, please contact wlsadmin@uwo.ca.

ANALYZING EFFICIENCY OF SWITCH-MODE WELDING POWER SUPPLY

(Spine title: Analyzing efficiency of switch-mode welding power supply)
(Thesis Format: Monograph)

By

Muhammad Imtiaz

Graduate program
in
Engineering Sciences
Electrical and Computer Engineering

A thesis submitted in partial fulfillment
Of the requirements for the degree of
Master of Engineering Science

School of Graduate and Postdoctoral Studies
The University of Western Ontario
London, Ontario, Canada

© Muhammad Imtiaz 2010

Certificate of Examination

The UNIVERSITY OF WESTERN ONTARIO
SCHOOL OF GRADUATE AND POSTDOCTORAL STUDIES
CERTIFICATE OF EXAMINATION

Chief Advisor:

Examining Board:

Dr. Lyndon Brown

Dr. Gerry Moschopoulos

Advisory Committee:

Dr. Ilia Polushin

Dr. Samuel F. Asokanthan

The thesis by
Muhammad Imtiaz

entitled:

Analyzing Efficiency of Switch-Mode Welding Power Supply

is accepted in partial fulfillment of the
requirements for the degree of

Master of Engineering Science

Date: _____

Chair of Examining Board
Dr. R. Eagleson

ABSTRACT

Researches and studies have indicated that many of the welding quality issues are related to the weld schedule or power supply. During a weld, a certain amount of energy is lost which can be reduced to improve the efficiency of the power supply. This thesis presents a DC/DC buck converter power supply for small scale resistance spot welding (SSRSW), which can provide a testing platform for studies of different control modes, and at the end implement the results of the experiments and research done with this power supply.

In this thesis, a model of the small scale resistance spot welding power supply has been implemented. The power supply uses pulse width modulation technique with MOSFETs to convert the power of a 12V battery to the weld current up to 1000A. Various measurements of voltage and current were taken at the respective terminals to calculate the energy losses. Capacitances were added with gradually increased values and again measurements were taken to calculate and analyze the energy losses in presence of the capacitances based on their numerical values. It was noted that the energy losses were reduced appreciably by this technique. So, the efficiency of the converters can be improved.

ACKNOWLEDGEMENTS

I wish to express my most sincere gratitude to my supervisor Dr. Lyndon Brown under whose supervision this Masters thesis was conducted throughout all stages of the thesis. I really admire his extraordinary support throughout my studies as a MESC student.

Sincere thanks are also given to the technicians in the Engineering Electronics Workshop, my colleagues in our research group for the discussion at the University of Western Ontario for their great help during the experimental work.

Finally, I would like to thank my family for their moral support and encouragement and all my friends for their great assistance.

London, Ontario, 2010

Muhammad Imtiaz

TABLE OF CONTENTS

CERTIFICATE OF EXAMINATION	I
ABSTRACT	II
ACKNOWLEDGEMENTS	III
TABLE OF CONTENTS	IV
LIST OF FIGURES	VIII
LIST OF TABLES	XII
NOMENCLATURE	XIII
1. Introduction	1
1.1 Resistance Spot Welding	1
1.2 Contribution of this thesis work	5
1.3 Switching power supplies	6
1.4 Non-isolated switched-mode DC-DC converters	7
1.5 Single switch converters	7
1.5.1 Hard switching converters	10
1.5.2 Soft switching converters	12
1.6 Isolated switched-mode DC-DC converters	15
1.7 Outline of thesis	16
2. Analysis of a Buck Converter in SSRSW	18
2.1 System Description	18
2.1.1 Power section	19
2.1.2 Control Electronics	19
2.2 Buck Converter	19

2.2.1	Modes of operations of the Buck DC-DC Converter -----	20
2.2.2	Steady State Analysis -----	22
2.2.2.1	Analysis of the powering state, Q_1 OFF, Q_2 ON --	23
2.2.2.2	Analysis of freewheeling state Q_1 ON, Q_2 OFF --	25
2.3	Conclusion -----	26
3	Background Knowledge in minimizing switching losses -----	27
3.1	Introduction -----	27
3.2	Research Motivation and objective -----	28
3.2.1	Problems and proposed solution -----	28
3.3	Snubbers -----	30
3.5.1	Dissipative Snubber Circuit -----	31
3.5.2	Active-Clamp Snubber Circuit -----	32
3.5.3	Reactor Snubber Circuit -----	33
3.4	Snubbers for Power MOSFETs -----	33
3.4.1	Energy Recovery from Snubbers -----	34
3.5	Literature Review -----	34
4	Simulations, Experimental setup and results of model power supply -----	44
4.1	Analysis of model SSRSW with and without capacitors -----	44
4.1.1	Inductance & Resistances of wires of the model power supply --	47
4.1.2	Inductance and resistance of the capacitor C3 -----	47
4.2	Experimental setup -----	48
4.3	Operation and Analysis -----	48

4.4	Experiments without capacitors -----	49
4.5	Experiments with capacitors -----	54
4.6	Comparison of Energy -----	59
4.7	Comparison of Simulations with Experiments for model power supply -	67
4.8	Conclusion -----	69
5	Measuring Losses in Small Scale Resistance Spot Welding -----	70
5.1	Experimental setup -----	70
5.2	Experimental Procedure -----	71
5.3	Application of K.V.L. to find the voltage drops -----	73
5.4	Inductor current -----	75
	5.4.1 Inductor current correction -----	75
5.5	Calculation of power losses -----	77
	5.5.1 Current through capacitor -----	77
	5.5.2 Current in the MOSFETs -----	80
5.6	Comparison of the energy losses -----	81
5.7	Conclusion -----	87
6	Simulation analysis of SSRSW -----	88
6.1	Power MOSFET characteristics -----	88
	6.1.1 Output characteristics -----	88
	6.1.2 On-Resistance $R_{DS(on)}$ -----	89
	6.1.3 Transconductance g_{fs} -----	89
	6.1.4 Intrinsic Capacitances -----	90
	6.1.5 Intrinsic resistance -----	91

6.1.6	Gate charge -----	91
6.2	Analysis with the actual small scale resistance spot welding -----	91
6.2.1	Internal inductance and resistance of battery -----	94
6.2.2	Calculation of inductance and resistance of capacitor C3 -----	95
6.2.3	Calculation of inductance and resistance of long wires -----	95
6.3	Comparison of the simulations with the experiments -----	97
6.4	Conclusion -----	103
7	Conclusion and future work -----	104
7.1	Summary -----	104
7.2	Conclusions -----	105
7.3	Contributions -----	105
7.4	Future work -----	106
	Bibliography -----	108
	Curriculum Vitae -----	115

LIST OF FIGURES

1.1	DC-DC boost converter -----	8
1.2	Switch voltage and inductor current waveforms for the boost converter -----	9
1.3	Switching of power switches -----	11
1.4	Reverse recovery characteristics of a regular and fast recover diode -----	12
2.1	Resistance Spot welding system -----	18
2.2	Power Section -----	21
2.3	Steady State Equivalent Circuit -----	
	2.3 (a) Powering Q_1 OFF, Q_2 ON -----	22
	2.3 (b) Freewheeling Q_1 ON, Q_2 OFF -----	23
2.4	Steady State Waveforms -----	24
2.5	Waveforms from the experimental data -----	25
3.1	RC and RCD Snubber circuits -----	31
3.2	Active-clamp lossless snubber -----	32
3.3	Reactor snubber circuit -----	33
3.4	Buck and boost converters employing snubbers -----	39
3.5	Conventional and proposed soft switching buck-boost converter -----	41
4.1	Model power supply for simulation without capacitors -----	44
4.2	Model power supply for simulation with capacitors -----	45
4.3	Actual Experimental setup in lab -----	49
4.4	Schematic of the model SSRSW without capacitors -----	50
4.5	High-side switching from OFF to ON without Capacitor -----	51
4.6	High-side switching from ON to OFF without Capacitor -----	52

4.7	Low-side switching from OFF to ON without Capacitor -----	53
4.8	Low-side switching from ON to OFF without Capacitor -----	53
4.9	Schematic of the prototype SSRSW with capacitors -----	54
4.10	Waveforms of the rise time with and without capacitors -----	55
4.11	High-side switching from OFF to ON with 0.01 uf capacitor -----	56
4.12	High-side switching from ON to OFF with 0.01 uf capacitor -----	56
4.13	Low-side switching from OFF to ON with 0.01 uf capacitor -----	57
4.14	Low-side switching from ON to OFF with 0.01 uf capacitor -----	57
4.15	High-side switching from OFF to ON with 0.1 uf capacitor -----	58
4.16	High-side switching from ON to OFF with 0.1 uf capacitor -----	58
4.17	Low-side switching from OFF to ON with 0.1 uf capacitor -----	58
4.18	Low-side switching from ON to OFF with 0.1 uf capacitor -----	59
4.19	High-side MOSFET switching from OFF to ON without capacitors-----	59
4.20	High-side MOSFET switching from OFF to ON with 0.01 uf capacitors -----	60
4.21	High-side MOSFET switching from OFF to ON with 0.1 uf capacitors-----	60
4.22	High-side MOSFET switching from ON to OFF without capacitors -----	60
4.23	High-side MOSFET switching from ON to OFF with 0.01 uf capacitors -----	61
4.24	High-side MOSFET switching from ON to OFF with 0.1 uf capacitors -----	61
4.25	Low-side MOSFET switching from OFF to ON without capacitors -----	63
4.26	Low-side MOSFET switching from OFF to ON with 0.01 uf capacitors -----	63
4.27	Low-side MOSFET switching from OFF to ON with 0.1 uf capacitors -----	64
4.28	Low-side MOSFET switching from ON to OFF without capacitors -----	64
4.29	Low-side MOSFET switching from ON to OFF with 0.01 uf capacitors -----	64

4.30	Low-side MOSFET switching from ON to OFF with 0.1 uf capacitors -----	65
4.31	Comparison of high-side MOSFET OFF and ON without capacitors -----	67
4.32	Comparison of low-side MOSFET OFF and ON without capacitors -----	68
5.1	Block diagram of experimental setup to measure energy losses -----	70
5.2	Actual small scale resistance spot welding used for experiments -----	71
5.3	Schematic of the SSRSW power supply -----	72
5.4	Block diagram to measure voltage drop across components of the welder -----	72
5.5	Voltage drops across various components of the power supply -----	74
5.6	Inductor voltage and voltage across shunt-2 -----	75
5.7	Inductor voltage and corrected inductor current -----	76
5.8	Block diagram to calculate current in the capacitor -----	78
5.9	Capacitor current -----	79
5.10	Measured and simulink capacitor voltage -----	79
5.11	Simulink model to measure the current through the capacitor -----	80
5.12	Voltages and currents across high-side and lowside MOSFETs -----	81
5.13	I_b , I_{ind} , I_c , I_{hs} and I_{ls} -----	82
5.14	Powers of Z_1 , Z_2 , Z_3 , Z_{11} , Z_{12} and Z_{13} -----	83
5.15	Powers of Z_{4a} , Z_5 , Z_6 , Z_7 , Z_8 and Z_9 -----	83
5.16	P_b , P_{hs} and P_{ls} -----	84
6.1	Characteristics of a N-channel power MOSFET -----	89
6.2	Power MOSFET parasitic components -----	90
6.3	Small scale resistance spot welding used for simulation -----	92
6.4	Experimental and simulated currents across Inductor, battery and capacitor -----	97

6.5	Experimental and simulated voltages of Z1+Z2+Z3 -----	98
6.6	Experimental and simulated voltages across load resistor -----	98
6.7	Experimental and simulated inductor voltage -----	99
6.8	Experimental and simulated voltages of Z4a+Z6+Z7+Z8 -----	99
6.9	Experimental and simulated voltages of Z11+Z12+Z13 -----	100
6.10	Experimental and simulated capacitor voltage -----	100
6.11	Experimental and simulated voltage of high-side MOSFET -----	101
6.12	Experimental and simulated voltage of low-side MOSFET -----	101
6.13	Experimental and simulated current of high-side MOSFET -----	102
6.14	Experimental and simulated current of low-side MOSFET -----	102

LIST OF TABLES

1.1	Comparison of the current typical power supplies for SSRSW systems -----	2
1.2	Comparison of a linear power supply & a switched-mode power supply -----	14
1.3	Summary of various non-isolated converter topologies -----	15
1.4	Summary of various isolated converter topologies -----	16
4.1	The components and their numerical values used in power supply circuit -----	47
4.2	Inductance and resistance of the wires of the prototype power supply -----	48
4.3	Energy comparison of the high-side MOSFETs -----	63
4.4	Energy comparison of the low-side MOSFETs -----	67
4.5	Comparison of energies between experimental and simulated results of the model power supply -----	69
5.1	Description about the voltage drops measured across various junctions -----	74
5.2	Energy losses measured across the power supply -----	86
6.1	Parameter values of the MOSFET -----	93
6.2	Inductances and resistances of the long wires in the power supply -----	96

NOMENCLATURE

PWM	Pulse width modulation
MOSFET	Metal oxide semiconductors field effect transistors
EMI	Electromagnetic interference
DC	Direct current
AC	Alternating current
ZVS	Zero voltage switching
ZCS	Zero current switching
QRC	Quasi resonant circuits
SSRSW	Small scale resistance spot welding
SR	Synchronous rectification
DCM	Discontinuous conduction mode
CCM	Continuous conduction mode
SOA	Safe Operating Area
K.V.L.	Kirchoff's Voltage Law
V_{DS}	Drain-to-source voltage
V_{GS}	Gate-to-source voltage
V_{TO}	Gate threshold voltage
$R_{DS(ON)}$	On-resistance of MOSFET
I_{DS}	Drain-to-source current
G_{fs}	Trans-conductance
C_{GS}	Gate-to-source capacitance
C_{GD}	Gate-to-drain capacitance
C_{DS}	Drain-to-source capacitance
t_{rr}	Reverse recovery time
Q_{rr}	Excess charge

Chapter 1

Introduction

1.1 Resistance spot welding:

Welding is an industrial process of joining materials like metals and thermoplastics. Welding process is widely used in many different industries, such as automobile, aerospace, appliance and metal processing, etc. When the joint materials are metals, the welding process is called metal welding. In a metal welding process two pieces of metal are melted, and inter-atomic penetration takes place at the boundary surfaces of the work pieces. The boundary surfaces will more or less disappear during the process, and integrating crystals will develop across the joining pieces. Welding is conducted by using heat or pressure or both and with or without added metal. The major solid state welding processes include friction welding, ultrasonic welding, and resistance welding. The common resistance welding processes are:

1. Resistance Flush Butt Welding
2. Resistance Upset Butt Welding
3. Resistance Projection Welding
4. Resistance Seam Welding
5. Resistance Spot Welding

The selection of a specific welding process depends upon many factors, such as the geometric shape, material, size, thickness, costs, portability, and skills needed, etc. The geometric shape of the weldment itself is the result of joint design, which, in several forms, is central to the issue of process applicability. Among those common welding processes the resistance spot welding is widely and commercially used. In this thesis, the

RSW is studied. In particular, the case where the energy during the process is produced by the resistance of the work pieces to the passage of electric current is considered.

The large-scale resistance spot welding (LSRSW) systems often use direct energy (AC) power supplies [42]. Downsized welder power supplies are used for small-scale RSW systems (SSRSW). Most SSRSW applications use “closed loop” controlled power supplies including constant current, voltage and power control modes and providing faster speed and smaller time intervals (1 millisecond), such as downsized HFDC power supplies and Linear DC power supplies. Nevertheless, some of the SSRSW applications also use CD power supplies, which use “open loop” control scheme. The main features of these power supplies are described in table 1.1, [42] [43] [44].


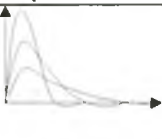
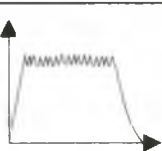

Comparison of the current typical power supplies for SSRSW systems					
Power supply type	Main components	Weld time resolution	Advantages	Limitations	Waveforms
AC	<ul style="list-style-type: none"> - Transformer - Control circuit 	> 8 msec or 16.6 msec	<ul style="list-style-type: none"> - Rugged - Inexpensive 	- Poor control	
CD	<ul style="list-style-type: none"> - Transformer - Capacitor bank - Pulse generator 	1-5 msec	<ul style="list-style-type: none"> - simple - Inexpensive - Rugged 	<ul style="list-style-type: none"> - Open loop - Fixed weld time 	
HFDC	<ul style="list-style-type: none"> - Small-size Transformer - Full-bridge converter - Pulse-width modulation 	0.1 – 1 msec	<ul style="list-style-type: none"> - excellent control - small transformer - extensive programmability 	- Higher cost	
Linear DC	<ul style="list-style-type: none"> - Transformer - Power transistors - AC/DC converter - Capacitor bank 	0.01 msec	<ul style="list-style-type: none"> - excellent control - repeatability - good for thin foils and fine wires 	<ul style="list-style-type: none"> - Highest cost - Larger - Heavier - Limited duty cycle - Heat dissipation limitation 	

Table 1.1 Comparison of the current typical power supplies for SSRSW systems

Since the power resources for the existing power supplies are the AC power from the power line, large size welding transformers and welding capacitors are used to avoid the line voltage fluctuation and power factor affection. That is why the existing power supplies are large, heavy, complex and expensive. The power required for a typical large scale weld is 60 KVA. The cost involved to bring this power to a site for establishing a large scale power welding power supply can be on the order of 10,000 dollars. The power supply approach presented here has the ability to provide output bursts of power necessary for RSW while drawing power continuously from the 110V, 20A household outlet. While the welder presented here has a goal of providing a maximum of 12 KVA power, it can be easily implemented as parallel modules when in the current control mode to provide power for a traditional large scale RSW machine. This work explores the possibility that today's low cost power MOSFETS will allow solid state DC-DC converters to be economically viable competitors with traditional AC transformers. This leads directly to the improvement in the size, weight and cost of the system.

Resistance spot welding is a process of joining sheet metal of thickness up to 0.125 inches by resistance to the flow of electric current through work pieces that are held together under force by electrodes. The contacting surfaces in the region of current concentration are heated by a short-time pulse of low-voltage, high-amperage current to form a fused nugget of weld metal. When the flow of current ceases, the electrode force is maintained while the weld metal rapidly cools and solidifies and the electrodes are retracted after each weld.

The operation of spot welding involves a coordinated application of current of the proper magnitude for the correct length of time. Its continuity is assured by forces applied

to the electrodes, which are shaped to provide the necessary density of current and pressure. The entire sequence of operations is required to develop sufficient heat to raise a confined volume of metal, under pressure, to temperature must be such that fusion is obtained, but not so high that molten metal will be forced from the weld zone. The rates of the rise and fall of temperature must be sufficiently rapid to obtain commercial welding speeds, but neither rate may be permitted to be so rapid that either inconsistent or brittle welds will be produced. The heat required for any resistance welding process is produced by the resistance offered to the passage of an electric current through the work pieces typically in the range from 10^{-3} to 10^{-5} ohms. Since the electrical resistance of metals is low, high welding currents are required to develop the necessary welding heat. Typically the currents are in the range of 1000's of Amps, while the voltage is at the level of a few volts only.

The rate of heat generation depends upon the flow of current in amperes or voltage across the weld interface and the resistance offered by the materials. Any of the formulas, $P = V*I = V^2/R = I^2*R$ are equally valid means of describing the rate of heat input into weld. A satisfactory weld depends on optimum setting of variables such as time, current or voltage and electrode force.

Containers such as receptacles are spot welded. The attachment of braces, brackets, pads or clips to formed sheet-metal parts such as cases, covers, bases or trays is another common application of spot welding. One of the most important applications of resistance spot welding is in automotive industry in which, the car frame body is constructed by spot welding of individual stamping parts, with manual portable welding guns, semi-automatic machines or fully automatic robots.

Major advantages of resistance spot welding are high speed and suitability for automation and inclusion in high-production assembly lines with other fabricating operations. With computer PLC control of current, timing and electrode forces; sound spot welds can be produced consistently at high production rates. Because of these advantages, much effort has been put into the research of welding processes and the development of new methods to improve the welding quality and productivity in the previous few decades. Due to the increasing need for RSW of very thin metal sheets in manufacturing electronic components and devices in recent time, small-scale resistance spot welding (SSRSW) has attracted the attention of many researchers.

According to a study, almost 20% of the welding quality issues are related to the weld schedule or power supply. Therefore, the development of highly flexible power supplies is of great value. This allows exploration of weld schedules and control modes that will contribute to welding quality improvement.

1.2 Contribution of This Thesis Work:

In this thesis, the analysis of a small scale resistance spot welding used for RSW is studied. It is the one type of resistance welding processes that involves the joining of two or more metal parts together in a localized area by the application of heat and pressure. The heat is generated within the material being joined by the resistance to the passage of a high current through the metal parts, which are held under a pre-set pressure.

The aim for this thesis is to present a SSRSW power supply containing a DC-DC buck converter with a passive technique to improve the efficiency of the converter at a frequency of 20-KHz. Resistance spot welding (RSW) is widely used in industries such

as automotive, aerospace, appliance, medical devices and electronic equipment etc.

Focusing on the SSRSW, this thesis has the following main objectives:

- To present a SSRSW power supply, this uses 20-KHz switching frequency and pulse width modulation (PWM) techniques to convert the power from a 12V battery to weld current up to 1000A to power the SSRSW system.
- To analyze and determine the steady state operating characteristics.
- To develop spice models of power supply. These can be used to discover primary mechanisms that limit the power supply and design strategies to optimize the power supply.

1.3 Switching Power supplies:

SMPS (switching mode power supply) is a device that transforms the input voltage level to the required value. The SMPS ensures that the right amount of power is delivered to end appliances and also ensures that there is no 'meltdown' with unregulated power supply. SMPS is basically a circuit that operates in a closed loop system to regulate the power supply output.

Increase in personal computers, telecommunication equipment and automotive electronics has prompted intensive research and development activity in the areas of switching power supplies. The reduction in size of the electronic equipment requires ever-increasing power densities of the supply systems. Power density is defined, as the ratio of available power to volume of the power supply, can only be high in highly efficient systems.

The input voltage for switching power supplies is obtained from batteries, photovoltaic cells or from utility lines. The current drawn by the load can vary, affecting

the output voltage. In certain applications, such as laboratory power supplies, wide range adjustability of the output voltage or current is required. There are two types of switching power supplies namely Non-isolated switched-mode DC-DC converters and isolated switched-mode DC-DC converters.

1.4 Non-isolated switched-mode DC-DC converters:

Basic non-isolated switched-mode dc-to-dc converters are single-switch networks that, besides the switch, contain a diode, one or two inductors, and one or two capacitors, one of them connected across the output terminals (which is not the case in our SSRSW because it would not work at the very high current level that we are operating at). Switched-mode dc-to-dc converters operate in the steady state with constant duty ratios of their switches. The capacitors smooth the output voltage. Increasing the switching frequency allows reduction in size of the capacitor, inductors and, transformers etc. In case of PWM power converters, the switching frequency involved represents a trade off between the quality and the efficiency of the converter performance. Ultrasonic (above 20 KHz) frequencies are used to eliminate acoustic noise emitted by the electromagnetic components.

A quality converter should be simple, reliable, efficient, compact and characterized by low ripple of the output voltage and possibly of the input current. The most common topologies of non-isolated switched-mode dc-to-dc converters are described below.

1.5 Single switch converters:

There are several types of single-switch power converters. The most fundamental single-switch converters are the buck converter, which can step down voltage, the boost converter, which can step up voltage, and the buck-boost converter, which can do both.

The buck, boost, buck-boost and the cuk converters can be used as DC/DC converters. Most DC-DC converters are switch-mode converters that operate with active semiconductor devices (i.e. MOSFETs, IGBTs, etc) acting as on-off switches. These switches are repeatedly and periodically turned on and off with high switching frequencies ($f_{sw} = 20 \text{ KHz}-1\text{MHz}$). The output DC voltage is dependent on the duty cycle D , which is defined as the length of time that a switch is on (t_{on}) over the duration of a switching cycle ($T_{sw} = 1/f_{sw}$).

$$D = t_{on} / T_{sw} \quad (1.1)$$

Figure 1.1 shows a DC/DC boost converter consisting of inductor L_{in} , a switch, main diode D_1 and output capacitor C_o . The converter works as follows.

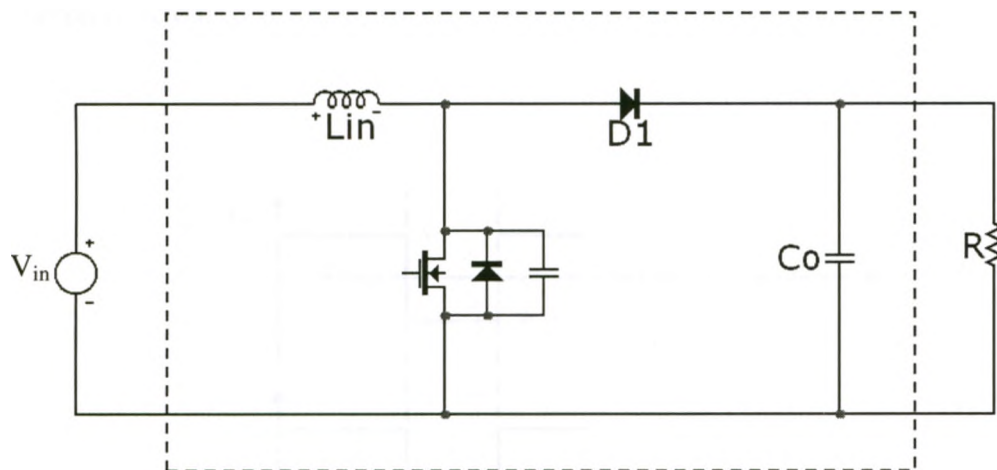


Figure 1.1 DC/DC boost converter

When the switch is turned on, input voltage V_{in} is applied across L_{in} to store energy in the inductor. When the switch is turned off, a negative voltage, $V_{in}-V_o$, is applied across the L_{in} and energy is transferred into the output capacitors. The output

voltage of a boost converter will always be greater than input voltage as the ratio of output to input voltage is

$$\frac{V_o}{V_{in}} = \frac{1}{1-D} \quad (1.2)$$

in order to operate the MOSFET switch in the converter in Fig. 1.1, a periodic pulse such as the one shown as V_{gs} in Fig. 1.2 must be applied between the gate and source of the device through a drive circuit. The MOSFET is on when the V_{gs} pulse is high and off when it is low. Since $T_{on} = DT_{sw}$, the duty cycle of the converter and therefore the ratio of output to input voltage is determined by the width of the V_{gs} pulse so, it is this pulse width that is ultimately used to control and regulate the output voltage. This method of converter, which is common to most power electronics converters, is called pulse width modulation (PWM).

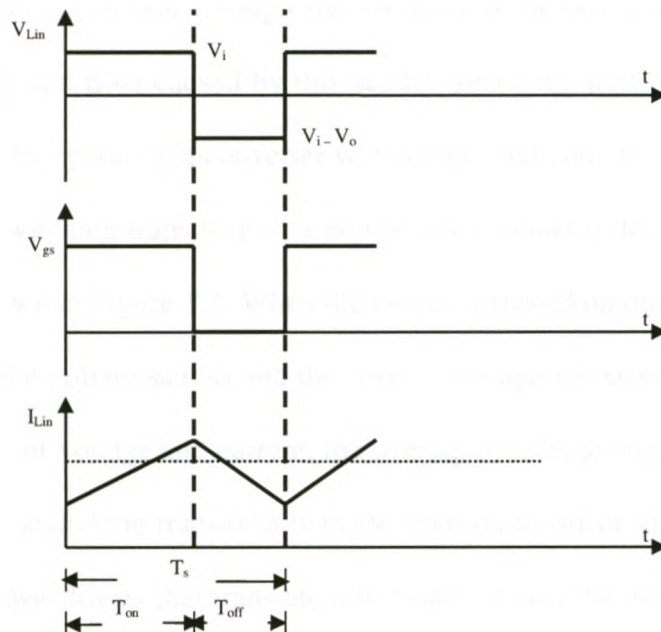


Figure 1.2 Switch voltage and inductor current waveforms for the boost converter

1.5.1 Hard-Switching Converters:

DC-DC PWM power converters are widely used in power supplies for computers, telecom, medical, aerospace and other industrial applications. The size of the converters manufactured now a day is decreasing to increase the power density (W/cm^3). The size of the energy storage components, such as inductors and capacitors, accounts for most of the overall size of the converter. These components, such as the inductor and capacitor in the boost converter shown in Figure 1.1, are needed to store and transfer energy in the converter. Their values depend on the frequency that the converter switch is turned on and off. As the switching frequency is increased, the values of L and C decrease and so do the size of L and C; therefore the higher converter switching frequency means smaller converter size. Higher switching frequency operation, however, results in increased switching losses and EMI noise emission. This is especially true if the converter switches are operated with hard switching when they are operated so that the transition in the state of voltage across and the current through the switches is sudden. Problems associated with switching losses and EMI caused by this sudden switching transition can offset the advantages achieved by operating a converter with a high switching frequency.

The typical switching trajectory of a power semiconductor device operating with hard switching is shown in Figure 1.3. When the switch is turned on or turned off, there is an overlap between the voltage across and the current through the switch. Since power is related to the product of voltage and current, the overlap in voltage and current that exists in the switch when a switching transition is made from on to off or vice versa results in the switch having power losses that translate into heat that must be dissipated. It is these losses that are referred to as switching losses in the power electronics literature.

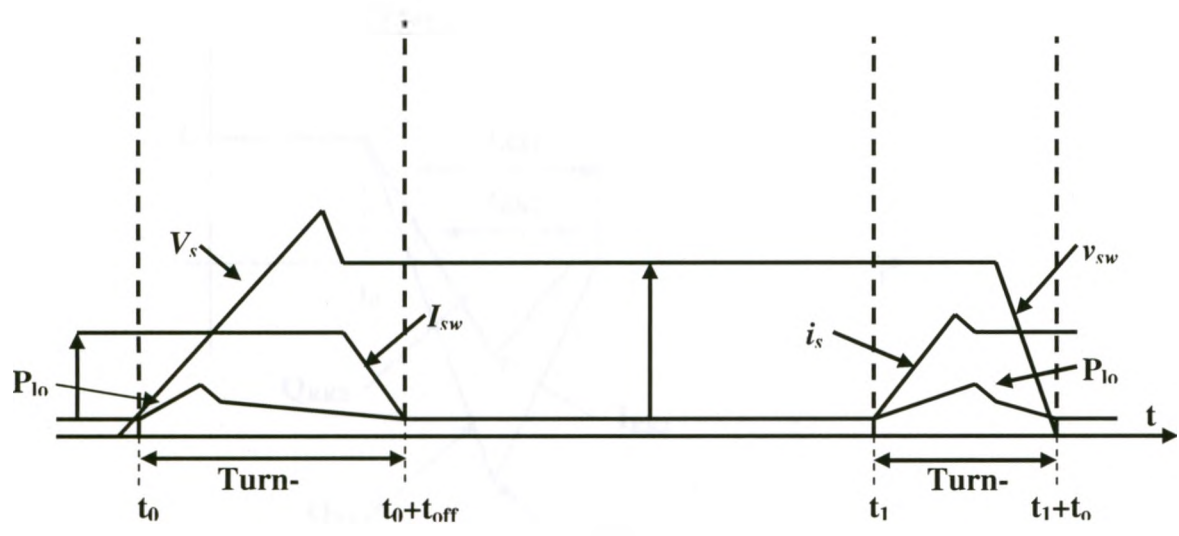
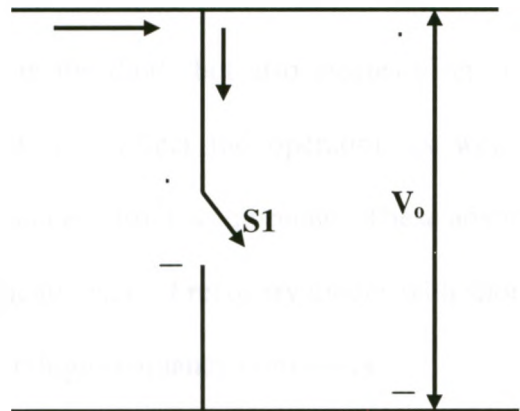


Figure 1.3 Switching of power switches

Single-switch converters typically have a power diode that can conduct current when the main power switch is off. The current is transferred from the diode to the switch and the diode stops conducting current when the switch is turned on. While the diode stops conducting, there is a duration of time commonly referred to as reverse recovery time t_{rr} , (as shown in figure 1.4 for a regular diode t_{RR1} and a fast recovery diode t_{RR2}) during which there is reverse current flowing through it and reverse voltage across it.

Therefore, the conduction losses are generated. The reverse recovery current not only leads to power losses in the diode but also creates electromagnetic interference in the converter systems that may affect the operation as well performance of the other surrounding electrical and electronics equipment. These adverse effects can be significant in high frequency applications. Fast recovery diodes with short reverse recovery times are therefore widely used in high frequency converters.

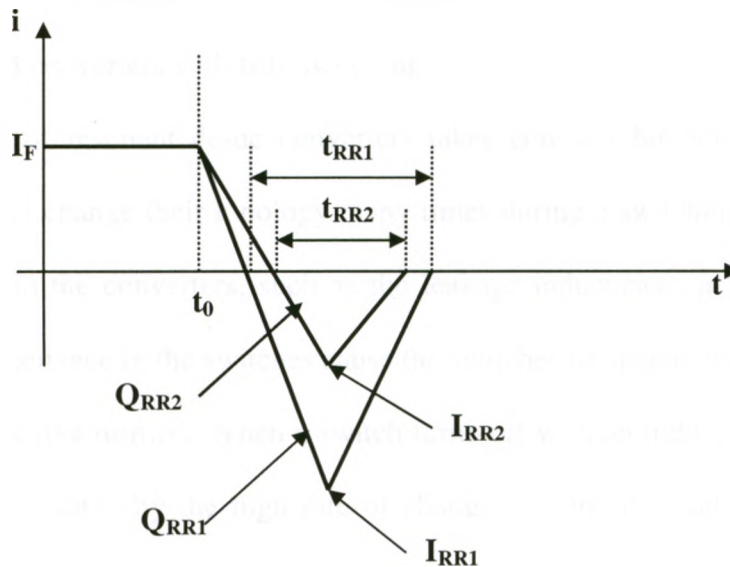


Figure 1.4 Reverse recovery characteristics of a regular and fast recover diode.

1.5.2 Soft-Switching Converters:

The term “soft-switching” refers to any method of switching where the main power switch in a single-switch converter turns on and/or turns off with a gradual rise or fall of voltage and/or current. The gradual rise and fall of voltage and current can reduce EMI noise and it can also reduce switching losses due to a reduction in the overlap between switch voltage and current during a transition. A device operating with soft

switching can be made to operate with zero voltage across it or with zero current flowing through it when the device is turned on or off. There are therefore two general types of soft switching: zero-voltage switching (ZVS) and zero-current switching (ZCS). Of the two types, ZVS operation is preferred when using MOSFETs in high switching frequency single-switch converters because it minimizes the power loss due to the discharging of the MOSFETs drain-source capacitance when the device is turned on. Various methods by which ZVS in a single-switch converter can be implemented are as follows.

- Resonant Converters with soft-switching
- PWM converters with soft-switching

Analysis of resonant dc-dc converters takes considerable time and effort as their power circuits change their topology many times during a switching cycle. The parasitic inductances in the converters, such as the leakage inductances in transformers and the junction capacitance in the switches cause the switches to operate with the inductive turn-off and capacitive turn-on. When a switch turns-off with an inductive load, high voltage spikes are generated by the high rate of change of current values. On the other hand, when turning on, the energy stored in the junction capacitance is trapped and dissipated in the device. Also a switching noise is induced that may interfere with proper operation of the converter itself or neighbouring sensitive systems. At high switching frequency levels, the resonant Soft switching converters offer an attractive alternative to the hard-switching, switched mode converters. Table 1.2 shows a Comparison of a linear power supply and a switched-mode power supply. To reduce the cost of the power supply, transformer is prohibitive in our application of SSRSW.

Comparison of a linear power supply and a switched-mode power supply			
	Linear power supply	Switching power supply	Notes
Size and weight	1) If a transformer is used, large due to low operating frequency (mains power frequency is at 50 or 60 Hz). 2) Small if there is no transformer.	Smaller due to higher operating frequency (typically 50 kHz–1 MHz)	A transformer's power handling capacity increases with frequency if hysteresis losses are kept down. Therefore, higher frequency means either higher capacity or smaller transformer.
Output voltage	1) If regulated, output voltage is regulated by dissipating excess power as heat 2) If unregulated, transformer's iron and copper losses are significant.	Output is regulated using duty cycle, which draws only the power required by the load. In all SMPS topologies, the transistors are always switched fully on or off.	Switching losses in the transistors, on-resistance of transistors, ESR of inductor and capacitors, core losses in the inductor, and rectifier voltage drop contribute to the efficiency. A proper SMPS design can minimize the amount of power losses.
Complexity	1) Unregulated can have diode and capacitor. 2) Regulated has a voltage regulating IC or discrete circuit and a noise filtering capacitor.	Consists of a controller IC, power transistors and diodes as well as inductors and filter capacitors.	Multiple voltages can be generated by one transformer core. For this, SMPSs have to use duty cycle control.
RFI	High-frequency interference may be generated by AC rectifier diodes under heavy current loading.	EMI/RFI produced due to the current being switched on and off sharply.	Long wires between the components may reduce the high frequency filter efficiency provided by the capacitors at the inlet and outlet.
Electric noise at the output terminals	Unregulated PSU may have a little AC ripple superimposed upon the DC component..	Noisier due to the switching frequency of the SMPS.	This can be suppressed with capacitors and other filtering circuitry in the output stage. With a switched mode PSU the switching frequency can be chosen to keep the noise out of the circuits
Electric noise at the input terminals	Causes harmonic distortion to the input AC, but relatively little or no high frequency noise.	SMPS may couple electrical switching noise back onto the mains power line, causing interference.	This can be prevented if an EMI/RFI filter is connected between the input terminals and the bridge rectifier.
Acoustic noise	Faint, usually due to vibration of windings in the transformer.	Inaudible to humans.	The frequency of an unloaded SMPS is sometimes in the audible range.
Power factor	Low for a regulated supply because current is drawn from the mains at peaks of the voltage sinusoid.	Ranging from low to medium since a simple SMPS without PFC draws current spikes at peaks of the AC sinusoid.	Active/passive power factor correction in the SMPS can offset this problem.
Risk of equipment damage	Very low, unless shorted between the primary and secondary windings.	Can fail to make output voltage very high.	

Table 1.2 Comparison of a linear power supply and a switched-mode power supply

Table 1.3 gives a brief summary of various non-isolated converter topologies. SEPIC and Zeta converters are both minor rearrangements of the Cuk converter. Switches become less efficient as duty cycle becomes extremely short.

Type	Power	Typical efficiency	Energy storage	Voltage relation	Features
Buck	0–1000	80–90%	Single inductor	$0 \leq \text{Out} \leq \text{In}$, $\text{Out} = \text{In} \times D$	Continuous output
Boost	0–150	70%	Single inductor	$\text{Out} \geq \text{In}$, $\text{Out} = \text{In}/(1-D)$	Continuous input
Buck-Boost	0–150	78%	Single inductor	$\text{Out} \leq 0$, $\text{Out} = -\text{In} \times D/(1-D)$	Inverted output voltage.
Split Pi (or, boost-buck)	0–2000	78%	Two inductors + three capacitors	Up or down	Bidirectional power control; in or out
Cuk			Capacitor and two inductors	Any inverted, $\text{Out} = -\text{In} \times D/(1-D)$	Continuous input and output
SEPIC			Capacitor + two inductors	Any, $\text{Out} = \text{In} \times D/(1-D)$	Continuous input
Zeta			Capacitor + two inductors	Any, $\text{Out} = \text{In} \times D/(1-D)$	Continuous output

Table 1.3 Summary of various non-isolated converter topologies.

1.6 Isolated switched-mode DC-DC converters:

All isolated switched-mode dc-dc converters include a transformer, and thus can produce an output of higher or lower voltage than input by adjusting the turns ratio. For some topologies, multiple windings can be placed on the transformer to produce multiple output voltages. Some converters use transformer for energy storage, while other use a separate inductor. The isolated dc-dc converters can be classified as either single switch or multiple switch converters. Table 1.4 shows the summary of various features of the isolated converters.

Type	Power	Typical efficiency	Input range	Energy storage	Features
Fly-back	0–250	78%	5–600	Transformer	Isolated form of the buck-boost converter.
Ringing choke converter	0–150	78%	5–600	Transformer	Low-cost self-oscillating fly-back variant
Half-forward	0–250	75%	5–500	Inductor	
Forward	100-200	78%	60–200	Inductor	Isolated form of buck converter
Resonant forward	0–60	87%	60–400	Inductor + capacitor	Single rail input, unregulated output, high efficiency, low EMI
Push-Pull	100–1000	72%	50–1000	Inductor	
Half-bridge	0–2,000	72%	50–1000	Inductor	
Full-bridge	400–5,000	69%	50–1000	Inductor	Very efficient use of transformer, used for highest powers.
Resonant, zero voltage switched	>1000				
Isolated Cuk				Two capacitors + two inductors	

Table 1.4 Summary of various isolated converter topologies.

1.7 Outline of This Thesis:

This thesis is organised as follows:

Chapter 1 provides a brief introduction about resistance spot welding (RSW) and small scale resistance spot welding (SSRSW) power supply. It also provides an introduction about the switch mode power supplies, their types and utilization based on the requirement. Chapter 2 presents the operation of a DC-DC buck converter used in small scale resistance spot welding power supply. In Chapter 3, objectives, structure of this thesis and a literature review of minimizing power losses in dc-dc converters are presented. Chapter 4 provides the simulation analysis for the model small scale resistance spot welding power supply. It also presents the application of a passive technique on the same model power supply to analyse energy losses in MOSFETs and provides a

comparison of the energy losses with and without capacitors. Chapter 5 describes the procedure and experimental data to measure power losses across different components in an existing small scale resistance spot welding (SSRSW) in lab. Chapter 6 gives the simulation procedure and analysis. A comparison of the switching losses under different measurements has been analyzed based on the experimental results as well as the simulation data. The test results demonstrate feasibility of the proposed converter. Chapter 7 provides the summary of the contributions and concludes the achievements of this thesis and provides suggestions for future work.

Chapter 2

Analysis of a Buck Converter in SSRSW

In this chapter, the operation of a Buck converter that will be used in the small scale resistance spot welding power supply is discussed. The stages of operation that the converter goes through during a switching cycle along with the system description, and the control electronics are explained, and a mathematical analysis for each stage is performed. The results of the analysis will be used to examine the steady state characteristics of the converter later.

2.1 System Description:

The small scale resistance spot welding system consists of three major sections: the power section, the control electronics and Function Generator (for the model power supply) and dspace software (for the existing power supply), which will be used as a source for PWM signal. The welding power supply has been designed by the University of Western Ontario, and described in [27] with major modifications. Figure 2.1 gives the system block diagram.

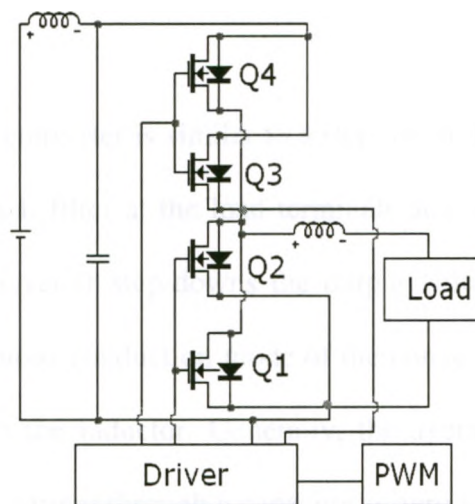


Figure 2.1 Resistance spot welding system

In the power section, the MOSFETs are used as the switching components to regulate the output and the control electronics section includes the driver circuit for the MOSFETs. The control scheme is implemented to provide the PWM signal to drive the MOSFETs in the power section.

2.1.1 Power Section:

The power supply is a pulse width modulated DC-DC converter. Thus its nominal output is given by the duty cycle times the maximum voltage of the input voltage, i.e. 13.5 volts. Power capacitor is used to compensate for the induction of the battery cables. An output inductor is used to filter the output current.

2.1.2 Control Electronics:

The control electronics section is used to drive the MOSFETs according to the PWM signals, and measure the load current. The driver circuit takes the logic level PWM signal, outputs gate signals to drive the high-side and the low-side MOSFETs Q_1 , Q_2 . The function generator implements the control scheme in case of model while dspace software in case of the actual power supplies, and provides the PWM signal to drive the MOSFETs in the power section.

2.2 Buck Converter:

The circuit of the buck converter is similar to a step-down, first quadrant chopper with an addition of a low pass L filter at the load terminals and without the traditional output capacitor. The buck converter step-downs the output voltage and increases the current at the output. A continuous conduction mode of the converter is considered, that means a continuous current in the inductor. Generally, the average voltage across an inductor as well as the average current through a capacitor is zero when averaged over an

integer number of cycles. Therefore, the average inductor current in the buck converter equals the output current, which can easily be determined if the load is known.

The duty ratio D is defined as the ratio of the on-time (t_{on}) divided by the switching period (T):

$$D = t_{on}/(t_{on} + t_{off}) = t_{on} / T = t_{on} f \quad (2.1)$$

where, f is the switching frequency in hertz and 20 KHz is used in our converter.

The average (dc) component of the output voltage is:

$$V_o = \frac{1}{T} \int v_o(t) dt = \frac{1}{T} \int v_s dt = V_s D \quad (2.2)$$

The duty cycle 'D' is a fraction from 0 to 1 but there is limit of duty cycle, e.g. if we want to step down 100 V to 10 V, that means "0.1 duty cycle" and we are trying to transfer power in a very short period of time and that will put stress on the switches, therefore the output voltage V_o (load voltage) is less than or equal to the input voltage V_s .

2.2.1 Modes of operations of the Buck DC-DC Converter:

Figure 2.2 explains the configuration of the power section, which contains the following four components:

A half bridge of power MOSFETs, Q_1 & Q_2

An inductor, L

Capacitor, C

Battery, V_s

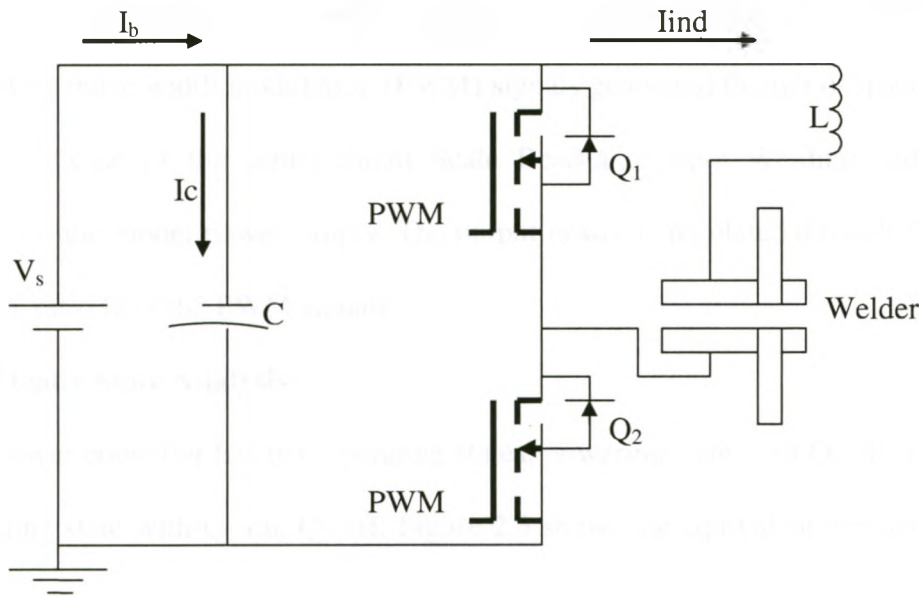


Figure 2.2 Power Section

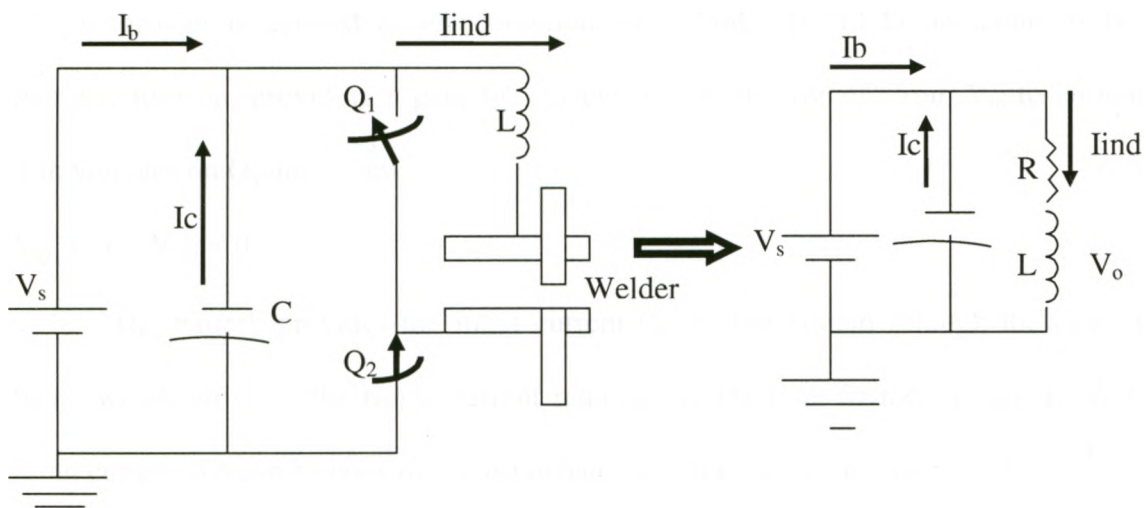
The half bridge (Q_1 and Q_2) works as a buck converter with the capability of free wheeling the load current through MOSFET Q_1 . For high current rating design, switching components MOSFETs are put in parallel. The low-side MOSFET Q_2 is the main power switch, which regulates the output power. The high-side MOSFET Q_1 works as a freewheeling switch that gives a current path for the load current when Q_2 is off. The capacitor C helps in providing the ripple current required by the high frequency switching. The inductor L filters the ripple on the load current caused by the high frequency switching. The battery V_s is the energy source of the power supply.

The selection of the switching frequency is usually a trade-off of the switching loss, the component sizes and the acoustic noise. Since the switching loss is proportional to the switching frequency, a lower frequency is required for lower switching loss. On the other hand, the higher value of inductor will be needed in the circuit, if the switching frequency is on the lower end; therefore the response of the circuit is also slower. Hence, a higher switching frequency must be selected to reduce the sizes of the capacitor C and

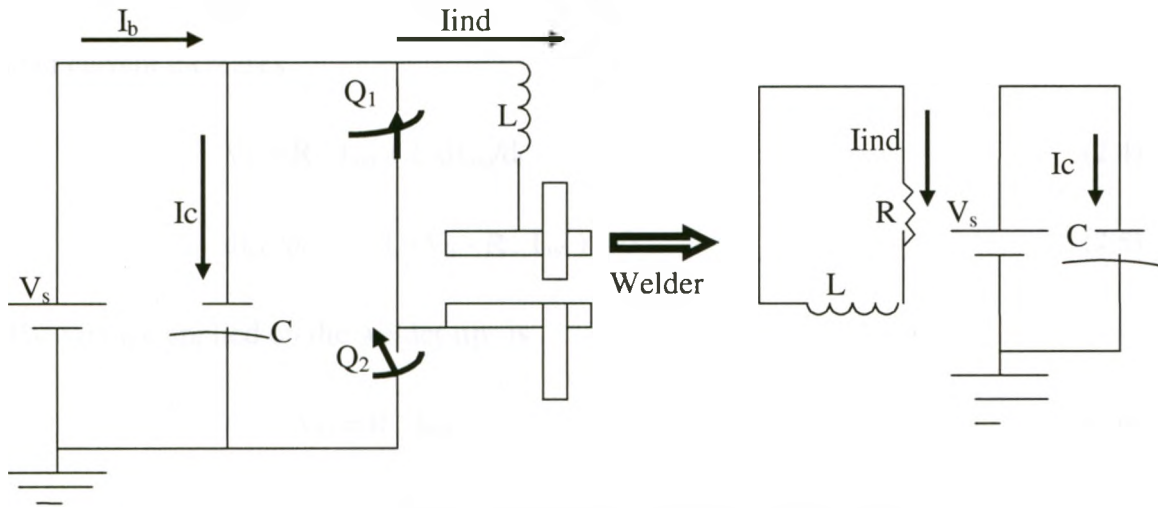
the inductor L . In this thesis, a switching frequency of 20 kHz is used. The MOSFETs are controlled by pulse width modulation (PWM) signals generated through d-Space software controller in case of the actual Small Scale Resistance Spot Welding and function generator for the model power supply. The output power is regulated through the control of the duty ratio D of the PWM signals.

2.2.2 Steady State Analysis:

The power converter has two operating states: powering state with Q_1 off, Q_2 on, and freewheeling state with Q_1 on, Q_2 off. Figure 2.3 shows the equivalent circuits for these two states.



(a) Powering, Q_1 off, Q_2 on



(b) Freewheeling, Q_1 on, Q_2 off

Figure 2.3 Steady state equivalent circuits

2.2.2.1 Analysis of powering state, Q_1 off, Q_2 on:

When Q_2 is turned on, Q_1 will be turned off to avoid the failure of shoot through (shoot through is defined as the condition when both MOSFETs are either fully or partially turn on, providing a path for current to “shoot through” from V_{in} to Ground).

The voltages on Q_1 and Q_2 are:

$$V_{Q1} = V_s; V_{Q2} = 0.$$

The battery provides the input current (I_b) to the system through the capacitor bank, which provides the ripple current required by the high frequency switching. The input current (I_b) can be considered as unchanged within the switching period.

The relationship between the input current (I_b), capacitor current (I_c) and inductor current is:

$$I_b = I_{ind} + I_c. \quad (2.3)$$

The source voltage (V_s) is applied to the load (welder) and the inductor. Therefore the load current increases.

$$V_s = R \cdot I_{ind} + L \frac{dI_{ind}}{dt} \quad (2.4)$$

$$\frac{dI_{ind}}{dt} = 1/L (V_s - R \cdot I_{ind}) > 0 \quad (2.5)$$

The voltage applied on the welder tips is

$$V_o = R \cdot I_{ind} \quad (2.6)$$

Figure 2.4 illustrates the waveforms of these variables during the switching.

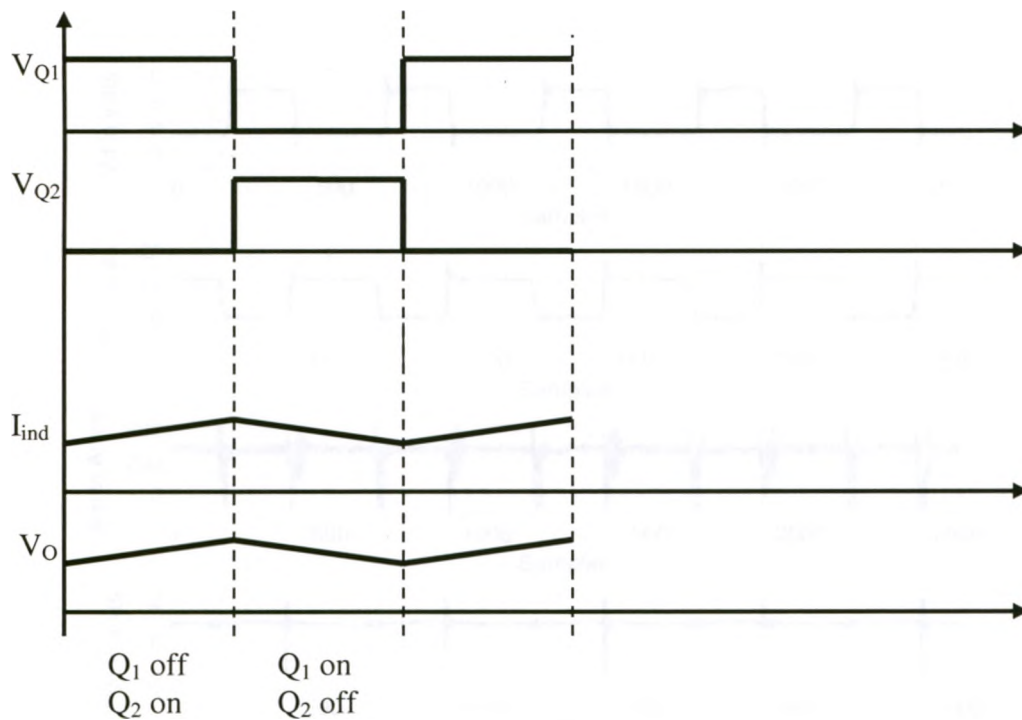


Figure 2.4 Steady state waveforms

2.2.2.2 Analysis of freewheeling, Q₁ on, Q₂ off:

When Q₂ is turned-off, Q₁ will be turned-on to provide a freewheeling path for the inductive load current (I_{ind}). The voltages on Q₁ and Q₂ are:

$$V_{Q1} = 0 ; V_{Q2} = V_s .$$

The load current (I_{ind}) loops back through Q₁, and no energy is drawn from the power source. The capacitor takes all the input current (I_b) to charge up, since

$$I_c = I_b. \tag{2.7}$$

The inductor discharges the stored energy to keep the current flowing, and the load current (I_{ind}) decreases, so that

$$0 = R \cdot I_{ind} + L \frac{dI_{ind}}{dt} , \quad L \frac{dI_{ind}}{dt} = - R/L \cdot I_{ind} < 0 \tag{2.8}$$

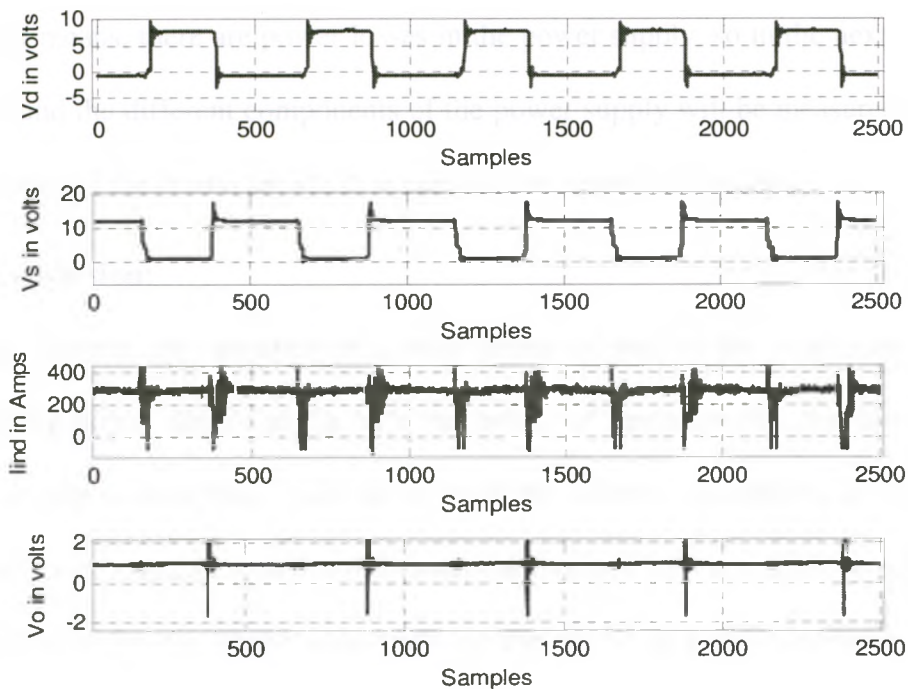


Figure 2.5 Waveforms from the Experimental data

Figure 2.5 shows the actual voltage and current obtained from the experimental data. V_d represents the voltage across the high-side MOSFET Q_1 which is at 12 volts in the first mode of the operating cycle while V_s is the voltage across low-side MOSFET Q_2 which must be at zero volt because it is on in the first mode. In the freewheeling mode, voltage at the high-side MOSFET Q_1 switches to zero while 12 volts on the low-side MOSFET Q_2 . I_m is the middle stage current which increases in the first mode as we are drawing power from both the battery and the capacitor. I_{ind} represents the actual measured inductor current which also is in accordance with the operation of the converter. V_o is the voltage across the welder which must be increasing in the power cycle and should decrease in the freewheeling mode to cool down the welder. As in this thesis a duty cycle of 0.45 has been used for experiments, so based on this duty cycle, V_o must be around 5.5 volts but actually, the output voltage is found to be between 0.9 to 1.0 volts. That means, there are power losses in the power supply, so in the next chapter, the losses around the different components of the power supply will be measured to improve the efficiency of the converter which is currently at around 15 percent.

2.3 Conclusion:

In this chapter, the operation of a Buck converter used in the small scale resistance spot welding power supply along with the modes of operation that the converter goes through during a switching cycle along with the system description, and the control electronics were explained, and a mathematical analysis for each mode was performed. The waveforms for the steady state both for theoretical and experimental results were also presented to show the behaviour of the buck converter.

Chapter 3

Background Knowledge on Minimizing Switching Losses

In order to provide detailed picture on minimizing switching losses in power converters (buck converters), some background knowledge is presented in this chapter. The first section describes the general information. Next, the existing techniques of reducing switching losses in DC-DC buck converters are reviewed.

3.1 Introduction:

With the rapid development of digital devices and semiconductor technology, switching power supplies are used in almost all applications such as wireless base station, computers, cell phones and various types of battery chargers. Two types of commonly used switching power supplies are AC-DC and DC-DC. With AC-DC power supplies, the input voltage is from the AC utility and the output is DC voltage, for loads such as a computer power supply, or battery charges. With DC-DC power supplies, the input voltage is DC and the output voltage is another DC level for loads such as a USB charger, or Voltage Regulator in a computer motherboard.

Power conversion efficiency and small size are very important performance features for a switching power supply. High efficiency not only means less energy loss, but also means lower temperature rise and therefore, more compact mechanical design. Closed loop operation is used to ensure stable operation of the switching power supply. In the present times, digital control has begun to find its way into switching power supplies due to reduced silicon costs and technology development.

Switching losses occurs due to simultaneous overlap of voltage and current in power switches during switching transitions. Zero voltage switching (ZVS) is a technique

that nearly eliminates turn on switching loss in power transistors by allowing the voltage across the switch (Voltage from Drain to Source) to go to zero before the switch turns on. This technique requires a negative current (Current from Drain to Source) at turn on. The negative current is used to discharge a capacitor across drain to source to zero before the MOSFET is turned on. Adding a small snubber capacitor across drain and source terminals can significantly reduce the turn off losses.

3.2 Research Motivation and Objective:

3.2.1 Problems and proposed solution:

In previous research, different people have tried to reduce the switching losses by different techniques. Here is the summary of the similar work done in the recent past. The snubber circuit in [7] explains a way without increasing circuit complexity and cost to overcome the issue of the snubber circuit (A snubber consists of a small resistor 'R' in series with a small capacitor 'C'. This combination can be used to suppress the rapid rise in voltage across a switch. Snubbers are often used to prevent spikes and electrical interference), which performs well when an off-line power supply is operated in constant output voltage mode. An off-line power supply is one, in which the ac line voltage is rectified and filtered without using a line frequency isolation transformer or a power supply, switched into service upon line loss to provide power to the load without significant interruption. However, when an off-line power supply is operated in constant power or current limit mode, resistor-capacitor-diode (RCD) and lossless snubber circuits lose their effectiveness. In [4], the converter consists of a partial resonant circuit using a step-up inductor and lossless snubber capacitor. In this scheme, the accumulated energy in the loss-less snubber capacitor is regenerated into the input power source by the partial

resonant operation. This technique helps in reducing the switching losses and stresses of the resonant devices which ultimately improves the efficiency of the converter. A soft switching “two switches forward converter” (TSFW) converter with active energy recovery snubber is described in [8], using an auxiliary switch to enable energy circulating and soft switching of the main switches, so the switching losses are reduced appreciably. The proposed current snubber converter in [3] is a compromise solution, which permits to significantly reduce the switching losses in a switch and in a diode during switch turn ON transition. Power dissipated, core size and core cost in the snubber are reduced as compared to a simple resistor-inductor-diode (RLD) snubber. A soft-switching buck boost converter using the pulse current regenerative snubber circuit has been proposed in [6]. It is observed that the efficiency of the proposed new soft-switching converter increases when the passive snubber circuit is implemented compared to the hard-switching operation. Energy recovery snubber circuits can be used advantageously in gate turn-off (GTO) chopper converters [1]. Each energy recovery circuit presented in [5], employing a step-up transformer to transfer the snubber energy to the load, is an evolution and refinement of the previous ones, starting from the conventional snubber circuits. A complete analysis of a buck converter using the proposed commutation cell is presented in [9]. This cell allows obtaining better operating performances than those known for the hard-switching PWM converters. Besides, it permits to operate for a wide range of power and high switching frequencies. The presented cell is therefore an alternative to overcome quasi-resonant-circuits (QRCs) and PWM-QRCs limitations. Two passive lossless snubber circuits for current doubler rectification are proposed in [2]. It was observed that both proposed snubber circuits attenuate the ringing and clamp

voltage spikes of the rectifier diodes because of their “unidirectional” architecture. Higher efficiencies are achieved compared to the conventional resistor-capacitor (RC) or RCD snubber because the proposed snubber has limited losses.

Based on the above discussion, the objective of this thesis is to find the best passive technique to reduce the power losses during high frequencies switching in DC-DC buck converter and to improve the efficiency of the converter. We are not planning on developing new circuit topologies but want to research others topologies and find the best one for our circumstances

3.3 Snubbers:

Switches in Power electronics converters have various kinds of stresses. For example, a sudden change of the switched current at turn-off would produce very damaging voltage spikes in stray inductances of the power circuit. At turn-on, a simultaneous occurrence of the high voltage and current could take the operating point of a switch well beyond the safe operating area (SOA). Therefore, switching aid circuits called snubbers, often accompany semiconductor power switches. Their purpose is to prevent transient over-voltages and over-currents, reduce switching losses and ensure that the switch does not operate outside its SOA. Snubbers also help to maintain uniform distribution of voltages across switches that are connected in series to increase the effective voltage rating, or currents in switches that are connected in parallel to increase the effective current rating. Following sub-sections describe the various types of snubbers for current doubler rectification.

3.3.1 Dissipative Snubber Circuit:

Due to reverse-recovery effect of rectifier diodes or synchronous rectification (SR) body diodes, voltage ringing is generated across these diodes. Resistive snubber circuits are commonly used to absorb the extra energy resulted from the reverse recovery. RC and RCD snubber circuits are the simplest dissipative snubbers, which are usually connected in parallel with SR switches or diodes as shown in figure 3.1.

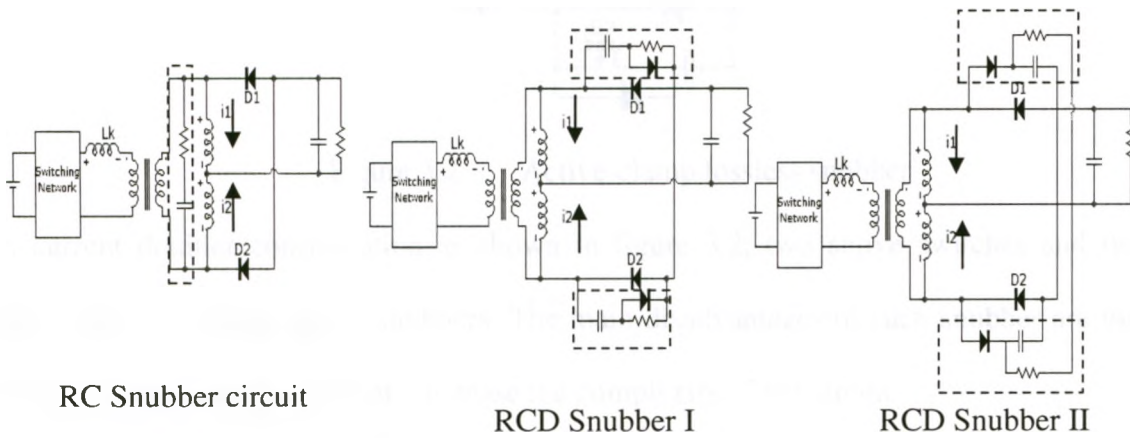


Figure 3.1 RC and RCD Snubber circuits

For the current doubler Rectifiers configuration, two RC snubbers may be combined into one. In such RC and RCD snubbers, the reverse recovery related energy is transferred to snubber capacitor and partly recycled. Therefore, they are considered to be dissipative snubbers.

3.3.2 Active-Clamp Snubber Circuit:

Resistive snubber circuits damp the ringing by dissipating the redundant energy. By resonant manner, the reverse recovery related energy is recycled instead of dissipated in resistive snubber.

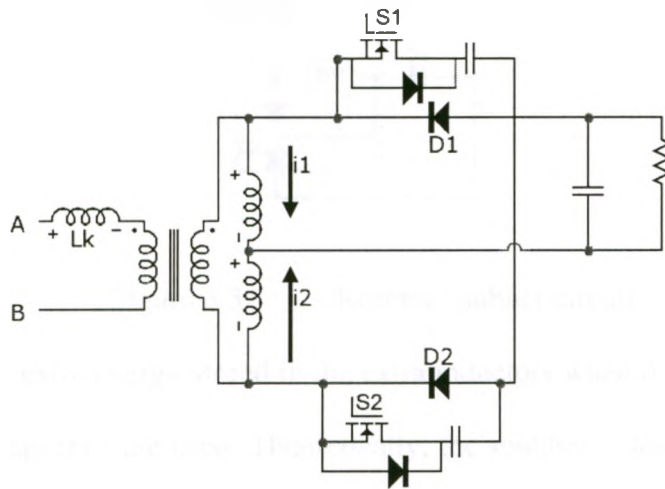


Figure 3.2 Active-clamp lossless snubber

In current doubler configuration as shown in figure 3.2, two active switches and two capacitors are used as active snubbers. The main disadvantages of such snubber are that active switches and their drivers increase the complexity of the circuit.

3.3.3 Reactor Snubber Circuits:

The reverse d_i/d_t through the diodes is critical factor to affect the reverse peak current. The larger reverse d_i/d_t , higher the reverse recovery peak current. Considering d_i/d_t is inversely proportional to the inductance, connecting inductor in series with diodes may decrease the reverse d_i/d_t . Figure 3.3 shows the circuit diagram of the reactor snubber circuit.

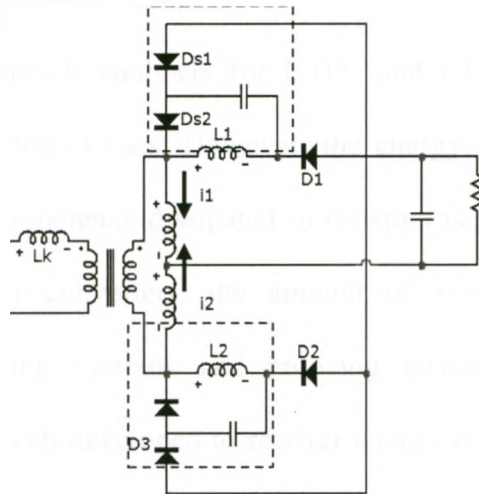


Figure 3.3 Reactor snubber circuit

To recycle the extra energy stored in the extra inductors when diodes are turned off, two diodes and a capacitor are used. Theoretically, the snubber is lossless if the reactors are regarded as lossless components and the snubber diodes have zero forward voltage drops. Unfortunately, the current flowing through snubber diodes is shifted to main diode, which causes undesirable conduction losses especially for high output current converters.

3.4 Snubbers for Power MOSFETs:

Since hybrid semiconductor power switches operate in a manner similar to BJTs, the same snubber configurations are applicable to converters based on power MOSFETs. To protect the internal freewheeling diodes and reduce the EMI, simple RC snubbers in parallel with the switches are recommended. In bridge converters, a single inductor can be placed in series with the input terminals of the bridge.

3.4.1 Energy recovery from snubbers:

The turn-on and turn-off snubbers for GTOs and BJTs modify the switching trajectory and reduce switching losses. However, the energy temporarily stored in the inductive and capacitive components dissipated in resistors is permanently lost. In high frequency and high power converters, the amount of energy lost in snubbers is substantial, stressing cooling systems and reducing efficiency of the converters. Therefore, measures have been developed to recover energy from snubbers and direct it to the load or return it to the supply source. The energy recovery system can be active or passive, the latter involving an auxiliary power converter.

3.5 Literature Review:

There are two types of switching techniques used in power converters namely active technique and passive technique to reduce switching losses. For PWM converters passive soft switching technique reduce switching losses by lowering the main switch's d_i/d_t and d_v/d_t to achieve nearly zero current turn-on and zero voltage turn-off. By controlling the d_i/d_t on the rectifier, the reverse recovery current of diode can also be controlled. Switching losses can be equal to zero in the optimum active soft switching technique. This is also known that the switching losses include the following losses

- Current and voltage overlap losses during the switching intervals.
- Capacitor discharging loss during turning-on.
- Additional conduction losses because of the diode reverse recovery.

It is been observed that in some cases the passive soft switching techniques are much better than active soft switching methods because they do not require an extra switch or additional resonant network. They are less expensive, more reliable and the performance-

cost ratio is higher than active methods. The passive soft switching method utilizes a loss-less snubber circuit with a small inductor and a small capacitor to reduce ZC turning-on and turning-off losses. The inductor also limits the recovery current of the diode. Additional circuitry carrying the inductor and capacitor is used to recover their energy to either the load or the input.

The snubbers help the commutations (The commutation cell is used to chop DC power into square wave alternating current. This is done so that an inductor and a capacitor can be used in an LC circuit to change the voltage. The output is then run through a filter to produce clean DC power. By controlling the duty cycle of the switch in the commutation cell, the output voltage can be regulated) of the device by reducing the dissipated energy in the GTO or dc-dc converters (choppers) used in electrical railways [5], by keeping the derivative of the current at turn-on under a certain limit, by dumping the applied voltage spikes and by making a path for the current which flows in an array of devices during turn-off. The snubber circuits can be grouped, by their function, into the series or L-snubbers (on-snubber) and the parallel or C-snubber (off-snubber). The values of their components devices makes the snubbers good choice and are chosen according to their applications and on the basis of the semiconductor they are connected to.

The series inductor limits the d_i/d_t value at turn-on or limits the instantaneous variation of the current that is flowing through it. That's why it takes its name as it is connected in series with the switching device. The parallel snubber is connected in parallel to the switching device. The C-snubber limits d_v/d_t at turn-off. It provides a path to the current, flowing through the storing elements (design inductances and stray inductances of the circuit).

The L and the C-snubbers are coupled networks. They form an R-L-C filter that gets rid of the applied voltage spike. The filter parameters have to be approximately chosen to avoid oscillations that could damage the switching device. During operation the snubbers trap some energy which is dissipated by the resistances. The dissipated energy can be reduced by means of the optimization of the snubber components devices. The energy recovery method normally makes use of a transformer that transfers the energy trapped in the L and C-snubbers to the load. The main problem with circuit is the saturation of the transformer core. The winding of the transformer carry a current which always has the same direction and to which an offset flux is added at each commutation cycle of the converter. The transformer must discharge the snubber before a new commutation and its core must be reset between two subsequent commutations of the converter.

With the increased demands for PWM converters with high frequency and high power density, switching techniques have attracted great attention. These techniques enable the power semiconductor devices to operate under zero-voltage switching (ZVS) and zero-current switching (ZCS). The ZVS is more attractive for devices such as power MOSFETS [9]. Using MOSFETs has two advantages: less losses due to the less voltage drop across MOSFET and the good load current sharing feature of MOSFETs. The MOSFET has a positive thermal feature, i.e. the higher the junction temperature, the higher the on-state resistor. On the other hand, ZCS is more appropriate for insulated gate bipolar transistors-IGBTs. Due to the intrinsic characteristics of the IGBTs, they are more suitable for high-voltage applications than MOSFETs. Generally IGBT's are more useful

when voltages can exceed 200V. Since our nominal voltages are 12V and peak voltages are less than 30V, MOSFETs are the most appropriate choice.

Another method to reduce switching losses is named as “two switches forward PWM (TSFW) converter” with active snubber [8]. The experimental and simulation analysis of this converter gives the following advantages.

1. When the main switches are turning-on, their current rising rates are limited by the resonant inductance. Hence the losses during the turn-on transition of IGBTs are decreased. Similarly, the voltage rising rates of switches when they turn-off are limited by snubber capacitors. The main switches turning-off losses are also decreased.
2. The snubber inductor and capacitor energy circulations are realized by changing the turning off time sequence of the switches.
3. The auxiliary switch can be turned-on and turned-off without losses. The current rating of this auxiliary switch is much lower than that of the main switches.
4. When load current is decreased, the snubber capacitor energy may not be fully released. It also will not be released through main switches. Hence the main switches will be hard switching at light load, and does not carry additional capacitance discharging loss.

This converter also has some draw backs. The secondary side switching frequency and the duty cycle ratio are lower compared with the full bridge pulse width modulated converter with same operation frequency of main switches. Hence a larger filter inductance is needed given the high currents in our application; increasing inductor size

is highly undesirable. An additional auxiliary switch is needed in the active snubber. The control complexity is thus also larger.

There is also interest in high power, high switching frequency and high efficient operation for dc-dc power converters. It is also known that these three desired characteristics can not be achieved by using either hard PWM or Quasi-Resonant techniques. In the recent past, the LC-PWM-SF-RDC cells [9] with and without resonant cycle interruption have been used. Soft switching of these converters is achieved by using an auxiliary Quasi-Resonant circuit associated with a main PWM converter. This method provides the advantages of PWM as well as the Quasi-Resonant converters, which are constant frequency, high switching frequency without commutation losses. These converters also have other advantages like soft switching for full load range, the highest voltage on the switches is limited by the main and the auxiliary sources and conduction losses are nearly the same as those seen in the hard PWM converters.

Therefore, the LC-PWM-SF-RDC (lossless commutation pulse width modulation (PWM) source feeding resonant disconnecting circuit) converters can operate at high switching frequency, high power conversion and high efficiency. These properties can provide the required small size and weight converters. Although these cells are excellent alternative to overcome the many disadvantages of the dc-dc converters, they still need an auxiliary source to feed the resonant circuit. To avoid the use of such auxiliary source, a novel ZCS-ZVS-PWM commutation cell is implemented that also provides non dissipative switching, high switching frequency and high power operation, without the power limitation of the conventional Quasi Resonant converters. These cell, are called ZCS-ZVS-PWM-FRC, consist of an auxiliary feedback resonant circuit. The simulation

and experimental results support the effectiveness of the methods used in the cell being discussed. These converters do not have the same limitations as those found in the QRCs and the PWM-QRCs in order to keep the switching without losses.

One common problem for power suppliers especially for buck and boost converters, is the reverse recovery when we apply reverse voltage to the conducting diode. The efficiency and reliability of a power supply is very much dependent on the solution of this problem. Another technique [3] describes snubber with a constant reverse recovery current for the diode. The objective of this invention is to find an effective and low cost solution to reduce the switching losses during diode recovery with very little limitation to a PWM duty factor. The simplest solution creates power stress to the switch and diode, a high level of electromagnetic interference, when a diode is recovered without any snubber circuit that results to low efficiency of the power supply. Figure 3.4 shows the circuit diagrams of the proposed converters.

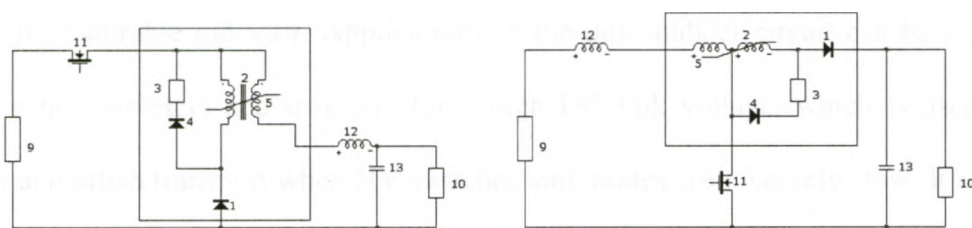


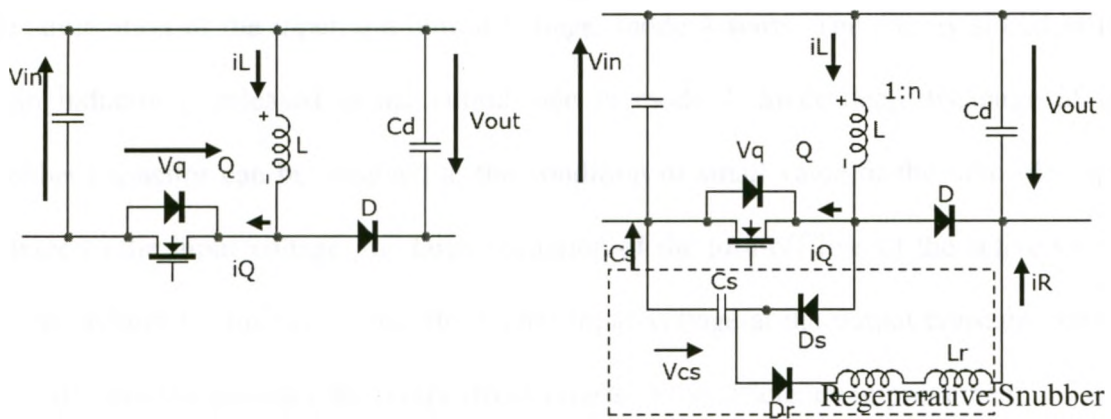
Figure 3.4 Buck and boost converters employing snubbers

LRD snubber circuit used in practice limits the derivative d_i/d_t , hence the reverse current takes the triangular waveform and a voltage across the diode starts to grow up at

the maximum reversal current. This current snubber has a low efficiency and becomes a source of electromagnetic pollution when the diode has snappy recovery behaviour. Current snubber with saturated inductor does not generate electromagnetic pollution due to small reverse current, but has low efficiency, large dimensions and cost limits duty factor for a power switch. The proposed snubber in this technique is free of the mentioned problems. During power switch-on transition, the diode current is quickly changed from forward to nearly constant value, according to current value I and the ratio of turns of windings 2 & 5. When diode 1 is recovered, current equal to IN_2/N_5 (where N_2 and N_5 are the numbers of the turns of windings 2 and 5 respectively) flows through resistor 3 and diode 4. So the core of saturated inductor starts to demagnetize. Energy stored in the core and then dissipated in resistor 3 and diode 4 is negligible. Before power switch turns-OFF, the core is still in saturation, so the forward current is produced rapidly and a part of energy, dissipated in resistor 3 and diode 4, is insignificant, so the maximum achievable duty factor is up to 100 percent. The advantages of this specific technique are recovery process is ideal, energy losses in resistor 3 are 10-50 times lesser, size and cost of the core of saturable inductor 2 can be taken several times less than size and cost of the core of the saturable inductor. Applications of the this snubber circuit can be especially effective in converters and inverters for a high DC link voltage, which is used in the railway and urban transport when HV switches and diodes are relatively slow. It may also be used in application in different types of rectifiers, especially in 3-phase thyristor rectifiers where short circuit interphases cross talk during thyristor recovery may be eliminated. Snubbers especially with active auxiliary switches, provide close to soft switching are used very rarely because of their complexity. So there is always a

compromise for simplest snubber circuit with ideal diode recovery process under constant adjustable reverse current.

DC-DC converters circuits are also commonly used for the DC power generation stage of renewable energy system like fuel cell system and a photovoltaic system. In such applications, the power conversion efficiency improvement is one of the most important issues necessary to gain the high efficiency performance of the whole generation system. To realize high conversion efficiency, a soft switching circuit is an effective technology. The soft switching topologies using auxiliary active switches have disadvantages, such as low reliability and complexity of both the power circuit and control circuit compared to the passive soft-switching. The passive regenerative snubber [6] as shown in figure 3.5 has the simple circuit configuration and wide operation region of the soft switching action, consists of the passive components applied to the buck-boost converter.



Conventional buck-boost converter

Proposed soft-switching buck-boost converter

Figure 3.5 Conventional and proposed soft switching buck-boost converter

Due to simple configuration, the converter used in this technique, can be controlled by a single PWM signal. The main power converter circuit in the proposed

converter consists of one active switch and the auxiliary passive snubber circuit. The passive snubber circuit with current regeneration for energy recovery is composed of a snubber diode, a snubber capacitor, an auxiliary diode, a secondary winding of a main inductor which has the winding turn ratio and a resonant inductor. Here is some brief description of the operation of the circuit. At mode 1, the active switch is turned on and a voltage (turns times the input voltage) appears across the secondary winding of the main inductor. As a result, resonance based on resonant inductor and snubber capacitor starts partially. The snubber capacitor is discharged towards the low level. When the regeneration current becomes zero, the second mode starts. In this mode, the main inductor energy is stored from the input side. When the active switch is turned off by the controller gate off signal of the desired duty ratio, next mode starts. In mode 3, the turn-off voltage applied to the active switch is suppressed by the snubber capacitor, and then the turn-off loss of the active switch becomes small. As the capacitor voltage reaches to the summation of the input and output voltage, mode 4 starts. The energy stored in the main inductor is released to the output side in mode 4. Since deep discharge of the snubber capacitor can be obtained at the condition of small value of the ratio of output voltage to the input voltage, the large reduction of the turn-off loss of the active switch can be achieved. This means that the higher input voltage at the output constant voltage control condition provides the larger effectiveness of the efficiency improvement.

It can be concluded that these two are the most appropriate approaches for reducing switching losses for the welder. LC-PWM-SF-RDC (lossless commutation pulse width modulation (PWM) cells as it source feeding resonant disconnecting circuit) converters can operate at high switching frequency, high power conversion and high

efficiency. These properties can provide the required small size and weight converters. Another method that seems very suitable is described in [5], It keeps the derivative of the current at turn-on under a certain limit, by dumping the applied voltage spikes and by making a path for the current which flows in an array of devices during turn-off.

There is also lots of literature available related to reduce the switching losses in DC-DC buck converters, which was reviewed but have not included in this thesis. A little description of some of the material that is not included with the reason is given below.

- A new Buck-Boost DC-DC converter of high efficiency by soft switching techniques [4]. The reason not to add this paper in thesis is that it has continuous and discontinuous conduction modes, which do not fulfil the purpose because our case requires a circuit with continuous conduction mode.
- A passive lossless snubber cell with minimum stress and wide soft-switching range [10]. Left it because it had a boost converter but we need a buck converter.
- Comparative study of snubber circuits for DC-DC converters utilized in high power off-line power supply applications [7]. As it was related to the AC (power factor correction), but we need a converter with DC.

The simplest possible passive technique, placing capacitors between the drain and the source of the high-side and the low-side MOSFETs in the small scale resistance spot welding, will be implemented to verify its effect on the switching losses of this power supply. If it is found suitable to reduce the switching losses, then it will be implemented on the existing SSRSW power supply.

Chapter 4

Simulations, Experimental setup and results of model power supply

In this chapter, simulation results using Micro-cap software obtained from a model SSRSW power supply, the procedure and the data analysis to reduce the energy losses by using a passive technique are presented. This model power supply was implemented with Buck DC-DC converter as discussed in chapter 2. Experimental results obtained from the model SSRSW are presented. Experimental and simulation waveforms obtained with the model welding power supply and conclusions about the results achieved during this process are also provided.

4.1 Analysis of model power supply with and without capacitors:

Figure 4.1 and 4.2 show the micro-cap models of a model power supply with and without capacitors to do the simulation analysis of this circuit.

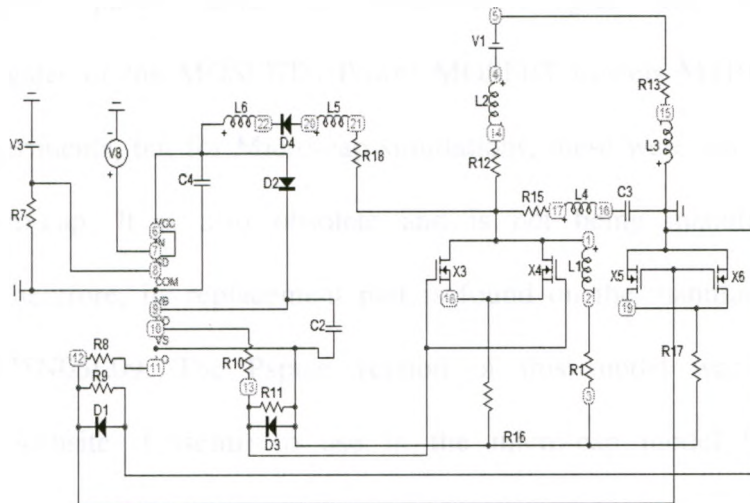


Figure 4.1 Model power supply for simulations without capacitors

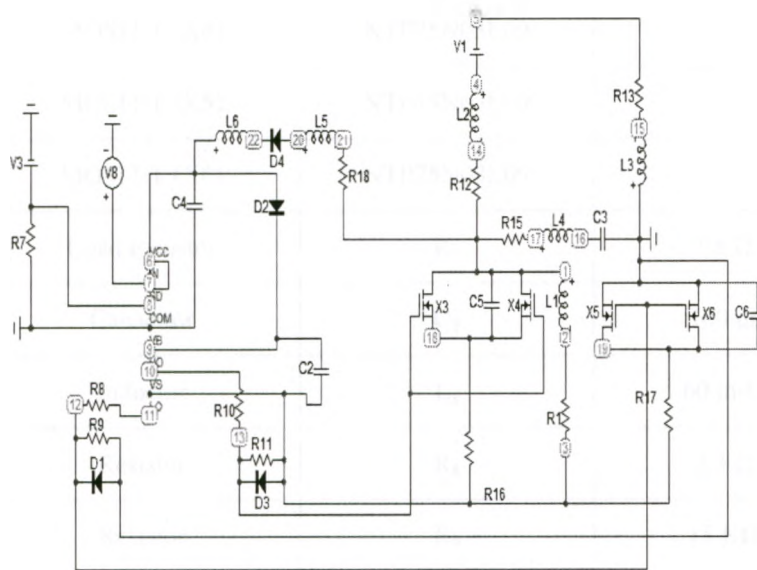


Figure 4.2 Model power supply for simulations with capacitors

X3 & X4 are two power MOSFETs in parallel as high-side MOSFETs, while X5 & X6 are two MOSFETs in parallel as low-side MOSFETs. Integrated chip (IR-2184) is used for driving the gates of the MOSFETs. Power MOSFET models MTP1306 have been used in the experiments, but for Micro-cap simulations, these were not available in the library of Micro-cap. It is also obsolete and is not being manufactured by the manufacturer. Therefore, its replacement part is found on the manufacturer's website which is NTP75N03L09. The Pspice version of this model was found on the manufacturer's website (Onsemi) to use in the micro-cap model for simulations. Similarly the driver chip's Pspice was also found on the manufacturer's website (International Rectifier) to use in the same micro-cap model. Table 4.1 details the components and their values used in the model power supply and driver's circuits.

Component Name	Description	Numerical value
MOSFET (X3)	NTP75N03L09	
MOSFET (X4)	NTP75N03L09	
MOSFET (X5)	NTP75N03L09	
MOSFET (X6)	NTP75N03L09	
Load Resistor	R_1	1.8 Ω
Capacitor	C_2	100 uf
Inductor	L_1	60 m-H
Resistor	R_8	3.3 Ω
Resistor	R_9	15 K Ω
Resistor	R_{10}	3.3 Ω
Resistor	R_{11}	15 K Ω
Diode	D_1	246b
Diode	D_3	246b
Diode	D_2	IN4007
Driver's IC	IR-2184	
Resistor	R_7	50 K Ω
Resistor	R_{16}	0.1 Ω
Resistor	R_{17}	0.1 Ω
Capacitor	C_3	1800 uf
Capacitor	C_4	10 uf
Capacitor	C_5	0.01 uf
Capacitor	C_6	0.01 uf

Table 4.1 The components and their numerical values used in Micro-cap Circuit

4.1.1 Inductance and resistances of wires of the model power supply:

Inductances of the wires are measured directly by the inductance meter LC-102 manufactured by SENCORE, while for resistance measurement; one ampere current is applied across the piece of the wire and the potential difference is noted. Once we know the current and voltage, we can calculate the resistances of the wires using ohm's law, which are listed in table 4.2.

4.1.2 Inductance and resistance of the capacitor C3:

Capacitor C3 is an 1800 uf capacitor with rated voltage of 16 volts. So, based on these parameters, its effective series resistance is looked up in the data sheet [41] and found to be 10 m-Ω at a frequency of 10-MHz.

It is known that the effective series resistance = $R + jX_L$, where R and X_L are the resistive and inductive reactance respectively. It is also known that at very high frequencies, resistive reactance becomes dominant, so the effective resistive part can be ignored and we are left with jX_L . Now in theory $X_L = 2\pi fL$ and f is 10-MHz in the data sheet at which the described value of the impedance is calculated. Hence, in this way, the effective series inductance of the capacitor can be calculated and is listed in table 4.2.

Inductance and resistance of the wires of model power supply		
Description	Inductance	Resistance
Cable from battery 12 V terminal to Drain of high-side MOSFET	$L_2 = 2.50E-07$	$R_{12} = 2.81E-02$
Across Inductor	$L_1 = 6.00E-02$	
Cable between ground and source of low-side MOSFET	$L_3 = 2.10E-07$	$R_{13} = 1.98E-02$
Cable between 12 V and VCC pin of the driver's chip	$L_5 = 0.12E-07$	$R_{18} = 2.0E-02$
Capacitor (C ₃)	$L_4 = 1.60E-09$	$R_{15} = 1.00E-02$

Table 4.2 Inductance and resistance of the wires of the model power supply

4.2 Experimental Setup:

The model power supply's experimental setup consists of the following equipment and components.

1. Bread board
2. 4-MOSFETs (MTP-1306), two for high-side and two for low-side in parallel combination.
3. Inductor
4. Load Resistor ($R_L = 1.8 \Omega$)
5. A driving chip of International Rectifier (IR-2184)
6. Function Generator **BK Precision** Model 4010A
7. **Good Will** laboratory DC power supply Model GPC-1850D
8. Tektronix TDS-2014 Oscilloscope
9. PC computer
10. Omron depress switch
11. Two 0.1Ω resistors to measure the voltage drop across the Drain of high-side and Source of Low-side MOSFETs.

Figure 4.3 shows the actual experimental setup for experiments to reduce the energy losses in the MOSFETs.



Figure 4.3 Actual Experimental setup in lab

4.3 Operation and Analysis:

Figure 4.4 shows the schematic of the model power supply circuit used for the experimental set up. Operating modes of the power supply are same as already described in chapter 2. The 0.1 ohms resistors have been connected between the source and drain used to measure the voltage drop across the MOSFETs, so that we may be able to measure the current flowing through them during both operating modes to get power to measure the switching losses in MOSFETS.

4.4 Experiments without capacitors:

Figure 4.4 shows the schematic of the model power supply to measure the voltage and current across the high and low-side MOSFETs.

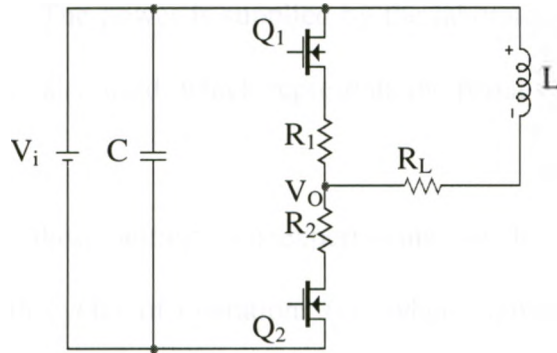


Figure 4.4 Schematic of the model SSRSW without capacitors

A floating oscilloscope is used for measuring the voltages and its reference, or the common point, is connected to the point marked V_O . Then one 0.1Ω resistor is connected between the source of high-side MOSFET and the common point while the other 0.1Ω resistor is connected between the drain of the low-side MOSFET and the common point. Then the one end of the load resistor R_L is also connected at the common point. The other end of the load resistor is connected to the Inductor which is connected to drain of the high-side (i.e. 12 V) power supply.

Following Oscilloscope settings are selected to measure the voltage drops and the currents across the MOSFETs of high-side. Probes of ch1 and ch2 are connected on the 0.1Ω resistor, which is connected between the source of the high-side MOSFET and the common point with vertical scales of 1-V and 20-mv per division respectively. Probes of ch3 and ch4 with vertical scale of 500-mv and 5-V per division respectively are connected on the inductor i.e., the drain of the high-side MOSFET. The reference of the oscilloscope is connected at the common point. The horizontal (time) scale is selected at 5 micro-seconds per division. Ch3 has been used for trigger, while the function generator

is supplying the pulse width modulation signal through the driving circuit (IR-2184 chip) to power supply. The power is supplied by the laboratory DC power supply. An Omron depress switch is also used, which represents the pedal in the actual power supply in the laboratory.

With all these settings ten experiments are done to measure the voltages and currents for both cycles of operations (i.e. when high-side MOSFET is switched from OFF to ON and ON to OFF). That data is then transferred to a personal computer to do analysis and calculation in matlab. The two signals that are measured across the source of the high-side (i.e. ch1 and ch2) at different resolution settings of the oscilloscope were then merged to get one signal that represents the current in the high-side MOSFETs. Same method is applied to the other two signals that represent the voltage across the high-side MOSFET. Based on these calculations, power and energy loss is calculated for high-side MOSFET when it is switched from OFF to ON and ON to OFF. Figure 4.5 and 4.6 shows the signals of voltage and current got on the oscilloscope when the high-side MOSFET is switching from OFF to ON and ON to OFF.

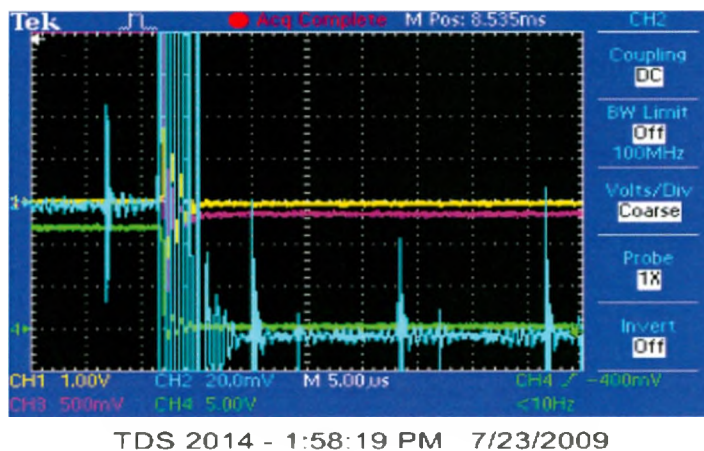
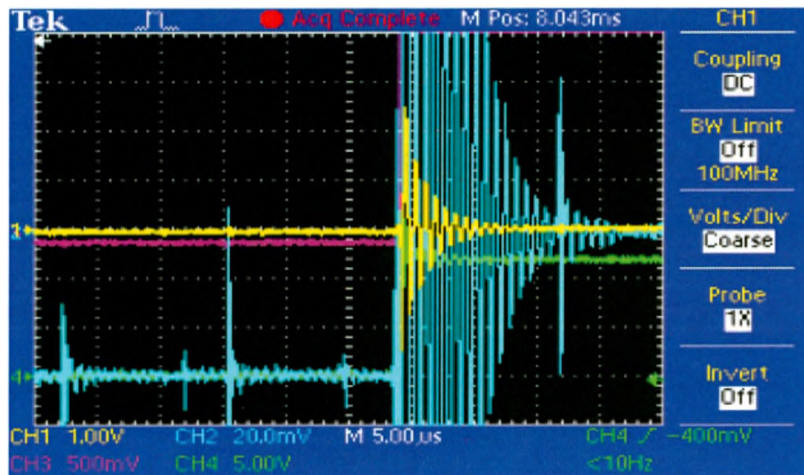


Figure 4.5 High-side switching from OFF to ON without Capacitor



TDS 2014 - 1:27:03 PM 7/22/2009

Figure 4.6 High-side switching from ON to OFF without Capacitor

The same procedure was repeated for the low-side MOSFET. Following Oscilloscope settings are selected to measure the voltage drops and the currents across the MOSFETs of low-side. Probes of ch1 and ch2 were connected on the 0.1Ω resistor, which is connected between the drain of the low-side MOSFET and the common point with vertical scales of 1-V and 20-mv per division respectively. Probes of ch3 and ch4 with vertical scale of 500-mv and 5-V per division respectively are connected on the common point i.e., the Source of the low-side MOSFET. The horizontal (time) scale is selected at 5 micro-seconds per division. The trigger is used by ch3 while the function generator is supplying the pulse width modulation signal through the driving circuit (IR-2184 chip) to the gates of the MOSFETs of the power supply. The power is supplied by the laboratory DC power supply.

With all these settings, ten experiments have been done to measure the voltage and currents for both cycles of operations (i.e. when low-side MOSFET is switched from OFF to ON and ON to OFF). That data is then transferred to a personal computer to do analysis and calculation in matlab. The two signals that are measured across the drain of

the low-side (i.e. ch1 and ch2) at different resolution settings of the oscilloscope were also merged to get one signal that represents the current in the low-side MOSFETs. Same method is applied to the other two signals that represent the voltage across the low-side MOSFET. Based on these calculations, power and energy loss is calculated for low-side MOSFET when it is switched from OFF to ON and ON to OFF. Figure 4.7 and 4.8 shows the voltages and currents signals got from the oscilloscope when the low-side MOSFET is switching from OFF to ON and ON to OFF.

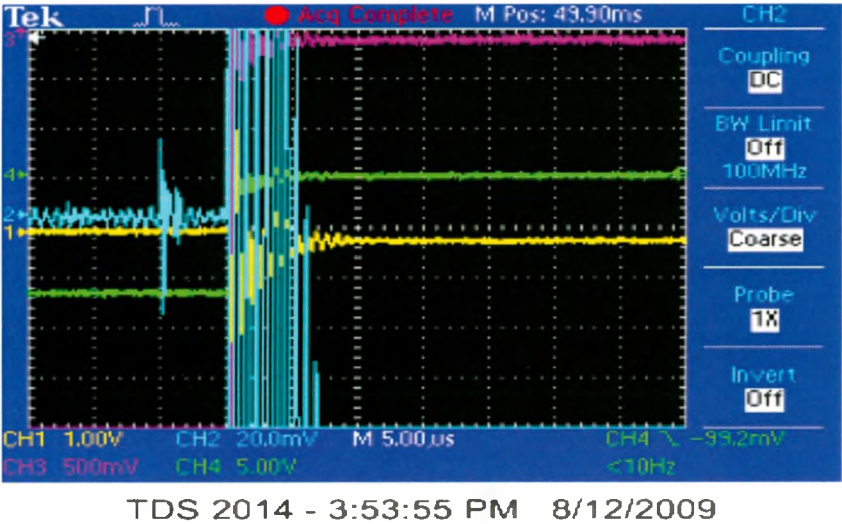


Figure 4.7 Low-side switching from OFF to ON without Capacitor

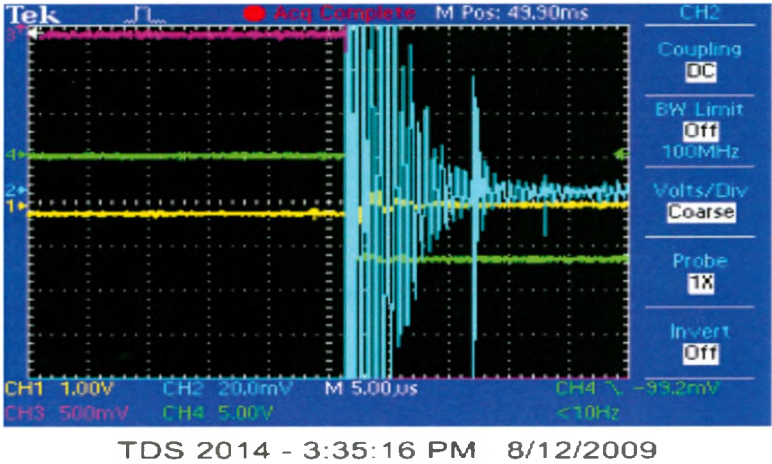


Figure 4.8 Low-side switching from ON to OFF without Capacitor

4.5 Experiments with capacitors:

Figure 4.9 shows the schematic of the same model power supply with capacitors connected between source and drain of both high and low-side MOSFETs.

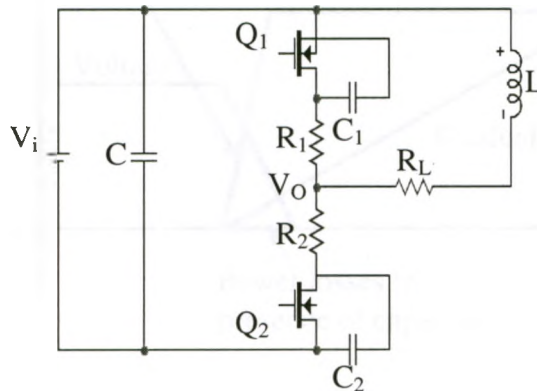


Figure 4.9 Schematic of the model SSRSW with capacitors

The rate of voltage rise is limited by the output capacitance of the MOSFET. The purpose of the capacitors C_1 and C_2 in figure 4.9 is to decrease rate of voltage increase during turn-on transition of MOSFET. By putting capacitors across power switches, there are advantages and disadvantages. The main trade-off to consider is that turn off losses will go down, but turn on losses will increase. Voltage spikes that can appear across a MOSFET when it is turned off will be reduced decreasing electromagnetic noise and improving switching stability which should also reduce power losses. If a lot of current have to be interrupted and the switch capacitance is small, then a voltage spike that may exceed the ratings of the device may appear, which can destroy the switch.

Figure 4.10 shows the waveforms of the voltage and current with and without the capacitors.

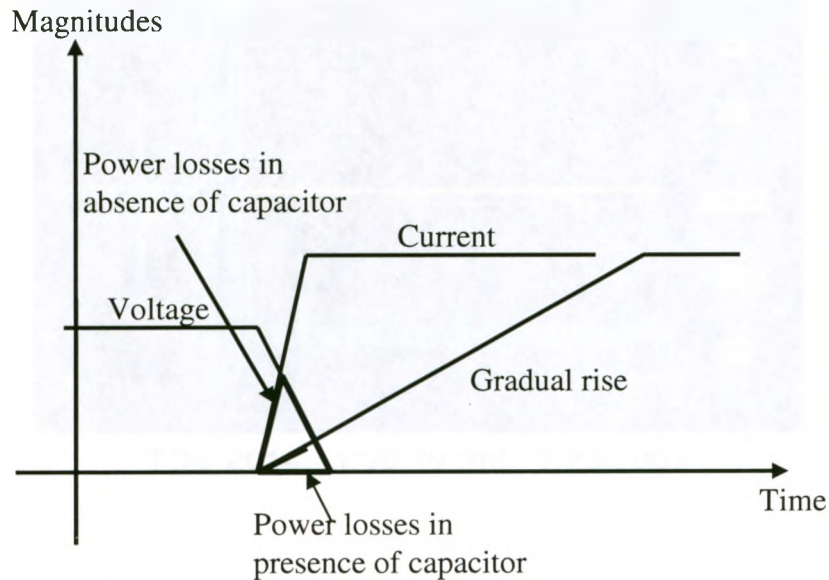
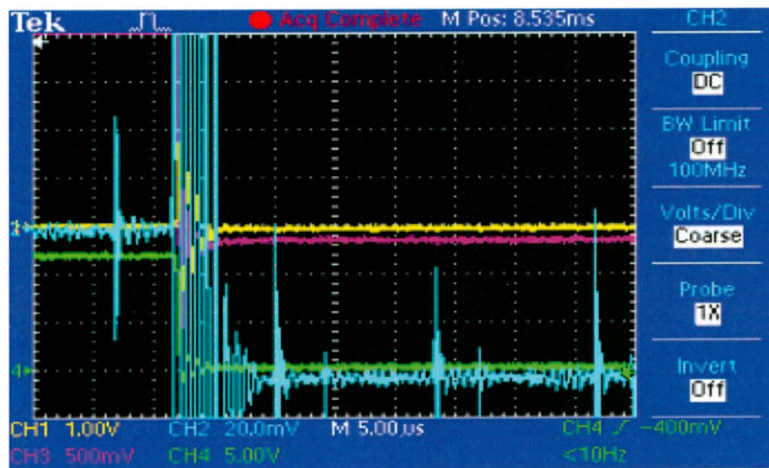


Figure 4.10 Waveforms of the rise time with and without capacitors

As, it is obvious in figure 4.10 that in absence of capacitor, the rise time of the output capacitor of the switch is short and the area under the curve of the voltage and current is larger, which means larger switching losses. By adding capacitor, the rise time of the output capacitor of the switch has increased and the area under the curve has become small, therefore less switching losses.

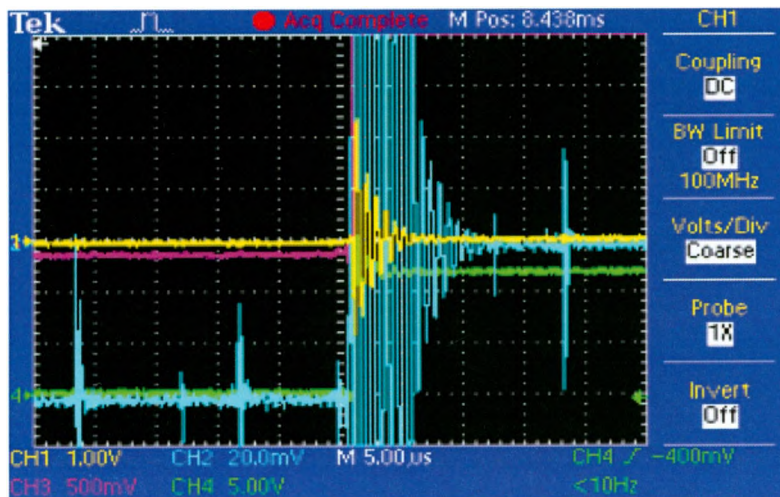
When we add an extra capacitor that means, we are storing more charge on the capacitor and we need to make an extra effort to get rid off this charge but there is always a trade off. This capacitor can also reduce the spiking and ringing. Otherwise, the switch can get damaged.

The rest of the experimental procedure is same as described in the previous section. Ten experiments are first done with 0.01 uf capacitors for both high-side and low-side MOSFETs. Figure 4.11 to 4.14 shows the signals of voltages and currents got from the Oscilloscope for both high and low-side MOSFETs.



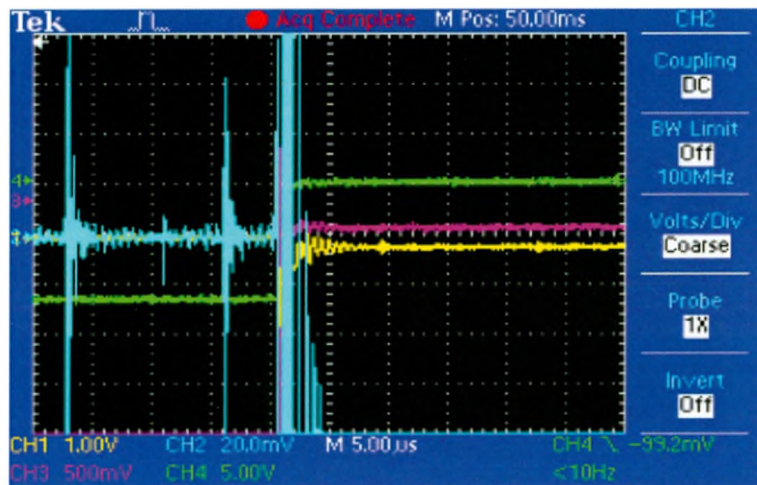
TDS 2014 - 1:58:19 PM 7/23/2009

Figure 4.11 High-side switching from OFF to ON with 0.01 uf capacitor



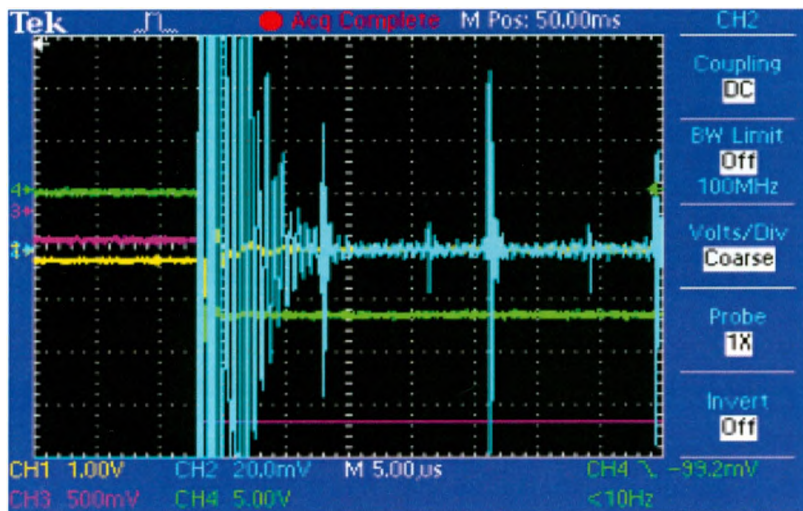
TDS 2014 - 11:32:05 AM 7/23/2009

Figure 4.12 High-side switching from ON to OFF with 0.01 uf capacitor



TDS 2014 - 2:18:16 PM 8/11/2009

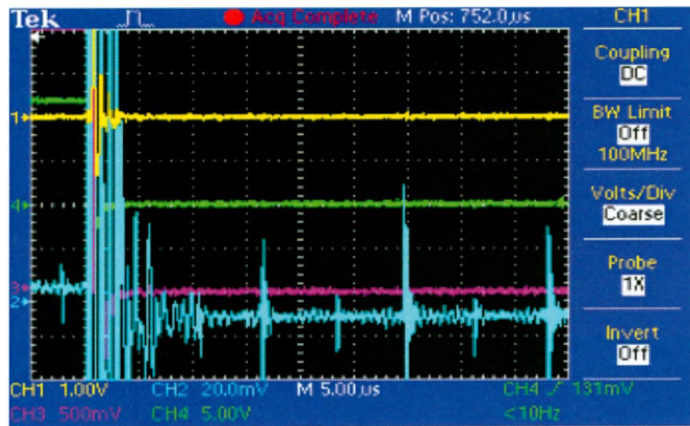
Figure 4.13 Low-side switching from OFF to ON with 0.01 uF capacitor



TDS 2014 - 2:13:05 PM 8/11/2009

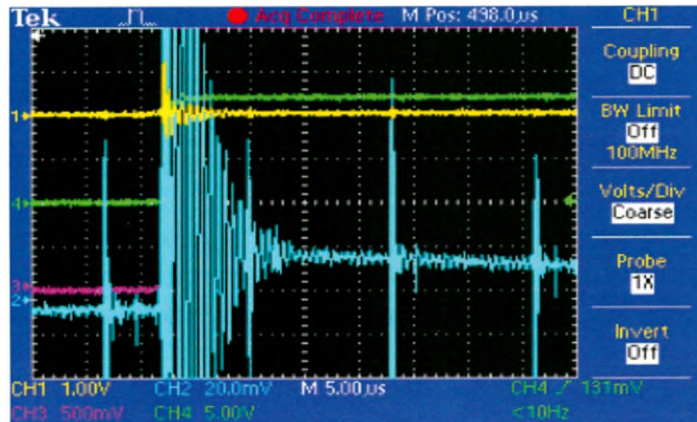
Figure 4.14 Low-side switching from ON to OFF with 0.01 uF capacitor

Again ten experiments are done with 0.1 uF capacitors for both high-side and low-side MOSFETs 'OFF' and 'ON'. Figure 4.15 to 4.18 shows the signals of voltages and currents got from the Oscilloscope for both high-side and low-side MOSFETs.



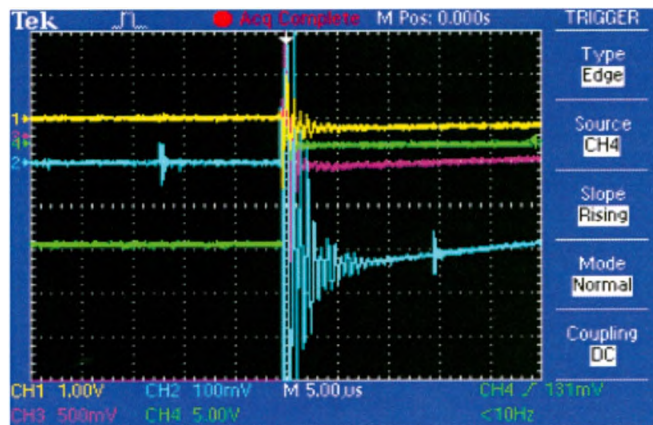
TDS 2014 - 12:40:47 PM 8/27/2009

Figure 4.15 High-side switching from OFF to ON with 0.1 uf capacitor



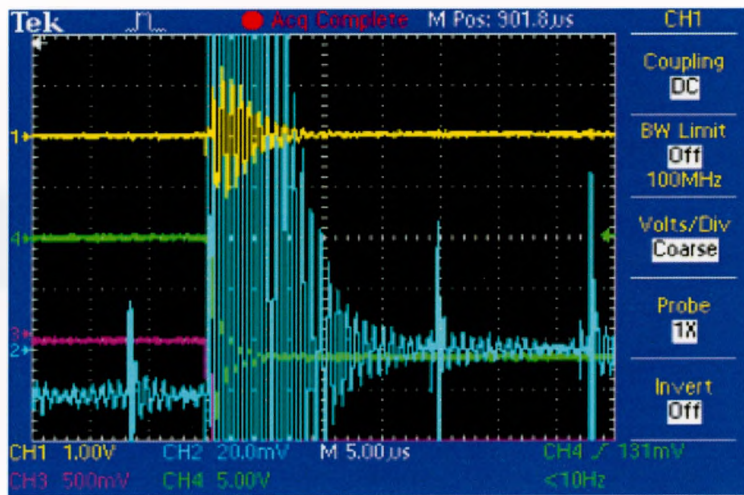
TDS 2014 - 11:22:06 AM 8/27/2009

Figure 4.16 High-side switching from ON to OFF with 0.1 uf capacitor



TDS 2014 - 3:20:41 PM 8/24/2009

Figure 4.17 Low-side switching from OFF to ON with 0.1 uf capacitor



TDS 2014 - 12:01:22 PM 9/3/2009

Figure 4.18 Low-side switching from ON to OFF with 0.1 uF capacitor

4.6 Comparison of the energy losses:

Figure 4.19 to 4.24 shows the plots of the voltage, current, power and the energy of the high-side MOSFET without capacitor, with 0.01uF and 0.1 uF capacitor. The legends of the plots represent the respective signals of current, voltage, power and energy in the MOSFETs.

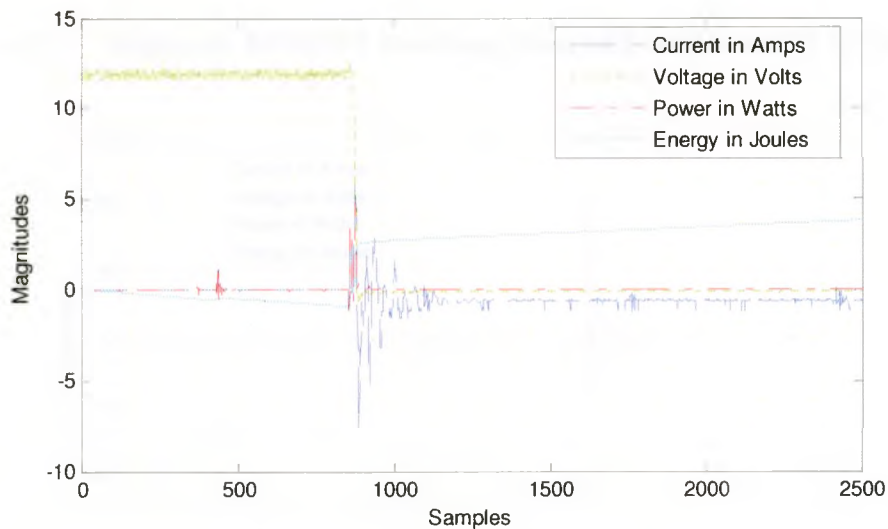


Figure 4.19 High-side MOSFET switching from OFF to ON without capacitor

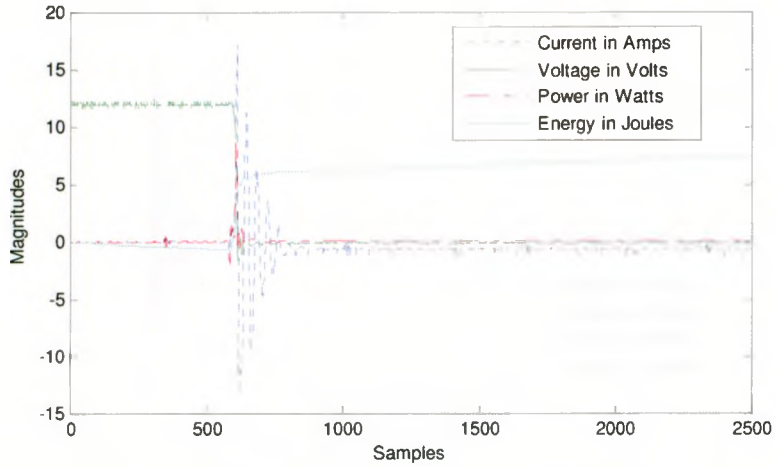


Figure 4.20 High-side MOSFET switching from OFF to ON with 0.01µf capacitor

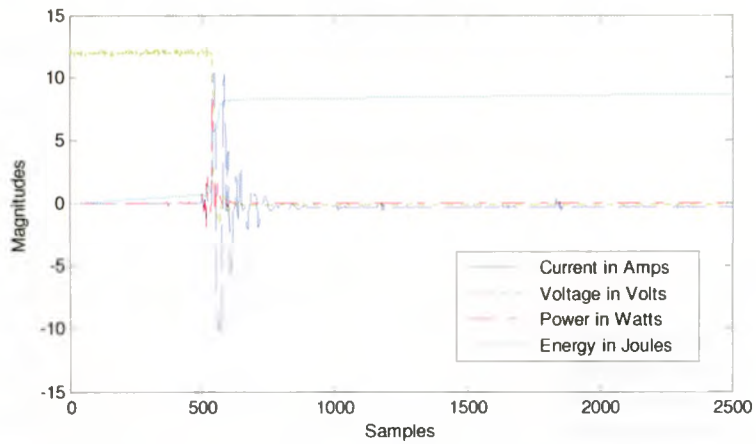


Figure 4.21 High-side MOSFET switching from OFF to ON with 0.1µf capacitor

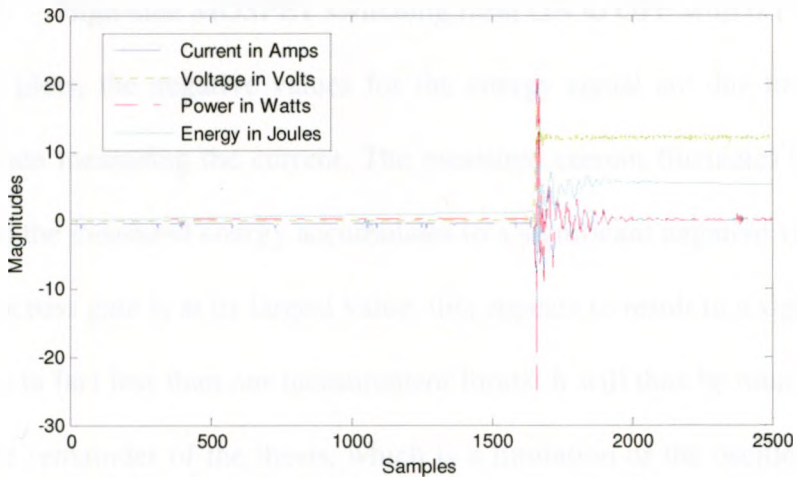


Figure 4.22 High-side MOSFET switching from ON to OFF without capacitor

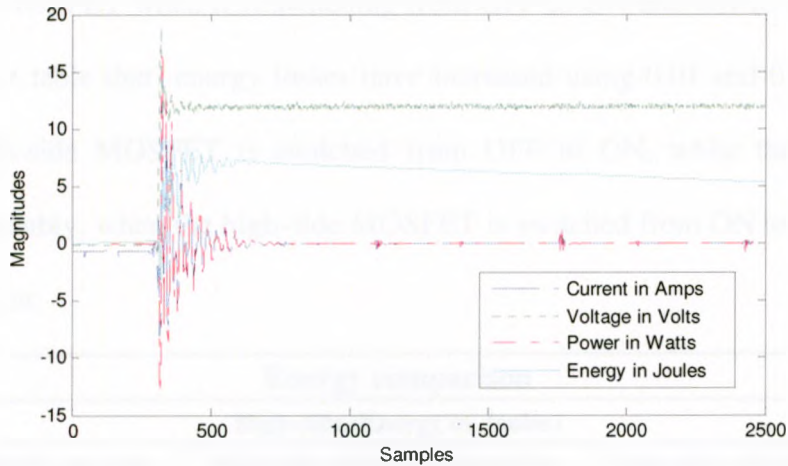


Figure 4.23 High-side MOSFET switching from ON to OFF with 0.01 uf capacitor

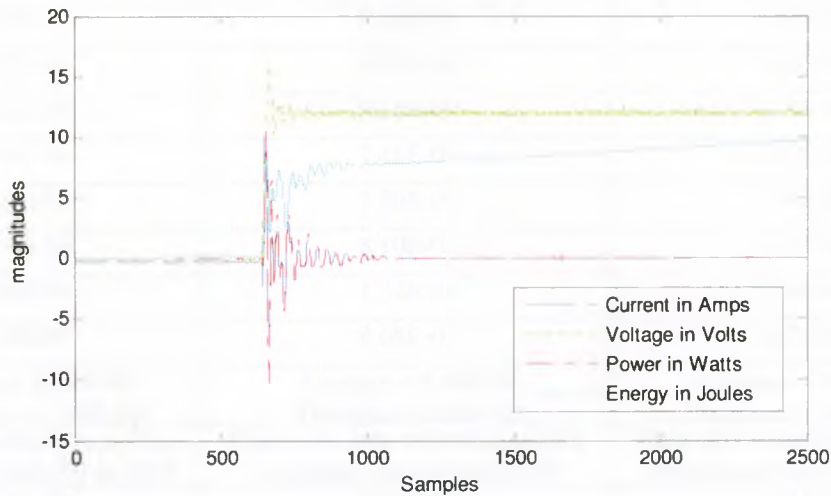


Figure 4.24 High-side MOSFET switching from ON to OFF with 0.1 uf capacitor

In the plots, the negative values for the energy signal are due to the resolution limitations when measuring the current. The measured current fluctuates between 0 and -1 bit and thus the measured energy accumulates to a significant negative value. Since the voltage drop across gate is at its largest value, this appears to result in a significant power loss when it is in fact less than our measurement limits. It will thus be rounded off to zero throughout the remainder of the thesis, which is a limitation of the oscilloscope that has been used for measurements. Table 4.3 shows comparison of the energy losses between

the high-side MOSFET when it is switching from OFF to ON and ON to OFF. It can be observed in the table that energy losses have increased using 0.01 and 0.1 uf capacitor when the high-side MOSFET is switched from OFF to ON, while these have been reduced appreciably, when the high-side MOSFET is switched from ON to OFF by using 0.01 uf capacitor.

Energy comparison		
High-side (Energy in joules)		
High-side without capacitor switching from OFF to ON	High-side with 0.01uf capacitor switching from OFF to ON	High-side with 0.1uf capacitor switching from OFF to ON
7.40E-09	1.17E-08	1.88E-08
6.66E-09	1.16E-08	1.47E-08
1.05E-08	7.88E-09	1.64E-08
7.58E-09	8.96E-09	1.50E-08
1.27E-08	9.16E-09	1.53E-08
1.22E-08	7.10E-09	1.27E-08
6.92E-09	7.80E-09	1.74E-08
7.04E-09	8.10E-09	1.27E-08
6.86E-09	1.32E-08	1.34E-08
7.20E-09	8.68E-09	1.67E-08
Average = 8.50E-09 Variance = -1.26E-18	Average = 9.40E-09 Variance = 8.82E-19	Average = 1.53E-08 Variance = -4.71E-19
High-side without capacitor switching from ON to OFF	High-side with 0.01uf capacitor switching from ON to OFF	High-side with 0.1uf capacitor switching from ON to OFF
1.76E-08	1.40E-08	1.61E-08
1.66E-08	1.27E-08	2.22E-08
1.70E-08	1.34E-08	1.47E-08
1.26E-08	1.42E-08	1.82E-08
1.08E-08	1.34E-08	2.10E-08
1.37E-08	1.26E-08	1.52E-08
1.43E-08	1.27E-08	1.34E-08
1.82E-08	1.20E-08	1.52E-08
1.35E-08	1.46E-08	1.40E-08
1.96E-08	1.26E-08	1.40E-08
Average = 1.54E-08 Variance = -1.65E-18	Average = 1.32E-08 Variance = -2.83E-19	Average = 1.64E-08 Variance = 2.58E-18

Table 4.3 Energy Comparison of the High-side MOSFETs

Figure 4.26 Low-side MOSFET switching from OFF to ON with 0.01 uf capacitor

Figure 4.25 to 4.30 shows the plots of the voltage, current, power and the energy of the low-side without capacitor, with 0.01 uf and 0.1 uf capacitor. The legends of the plots represent the respective signals of current, voltage, power and energy in the MOSFETs.

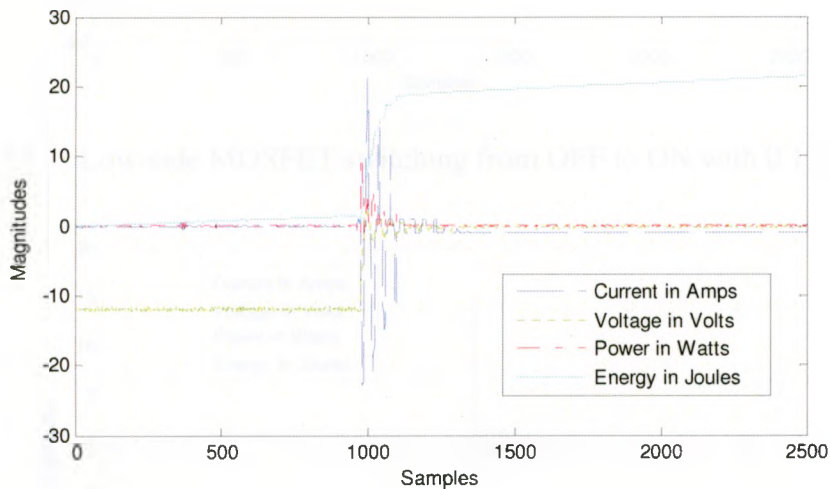


Figure 4.25 Low-side MOSFET switching from OFF to ON without capacitor

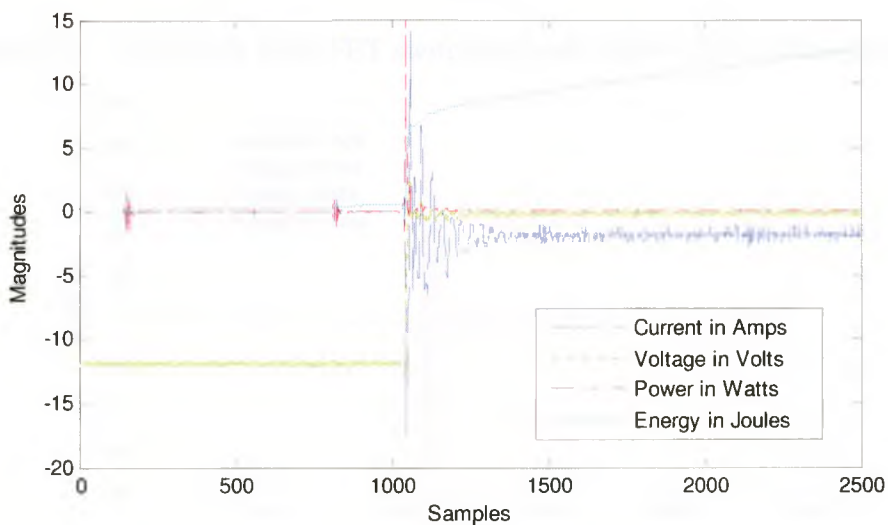


Figure 4.26 Low-side MOSFET switching from OFF to ON with 0.01 uf capacitor

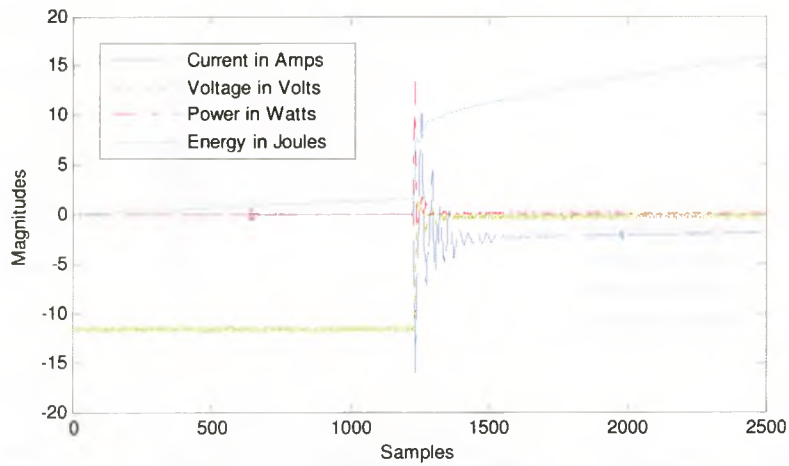


Figure 4.27 Low-side MOSFET switching from OFF to ON with 0.1 uf capacitor

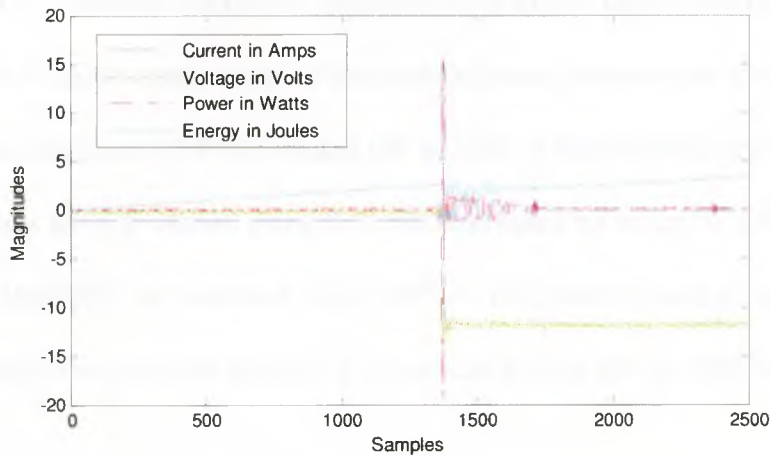


Figure 4.28 Low-side MOSFET switching from ON to OFF without capacitor

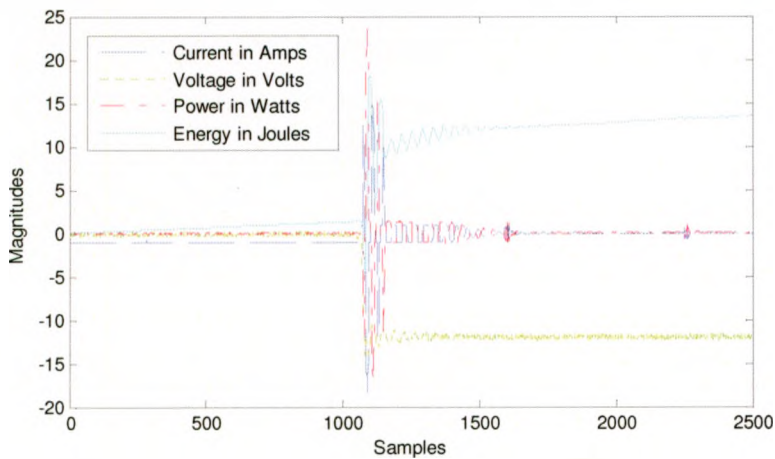


Figure 4.29 Low-side MOSFET switching from ON to OFF with 0.01 uf capacitor

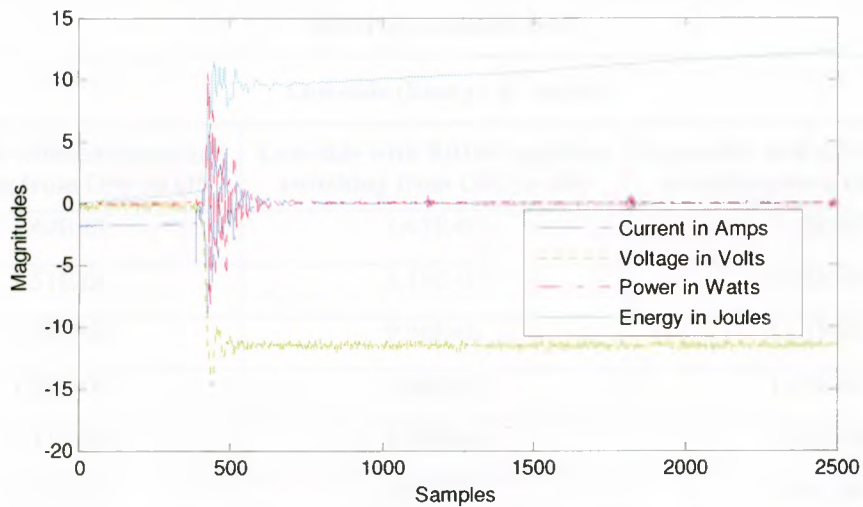


Figure 4.30 Low-side MOSFET switching from ON to OFF with 0.1 uf capacitor

Table 4.4 shows comparison of the energy losses between the low-side MOSFET when it is switching from OFF to ON and ON to OFF. It can be observed in the table that the energy losses have increased using 0.01 but decreased by using 0.1 uf capacitor when the low-side MOSFET is switched from OFF to ON, while these have been reduced appreciably when the low-side MOSFET is switched from ON to OFF by using 0.01 uf capacitor.

Energy comparison		
Low-side (Energy in joules)		
Low-side without capacitor switching from OFF to ON	Low-side with 0.01uf capacitor switching from OFF to ON	Low-side with 0.1uf capacitor switching from OFF to ON
1.49E-08	1.47E-08	1.02E-08
1.51E-08	1.17E-08	1.03E-08
1.16E-08	9.76E-09	1.01E-08
1.05E-08	1.06E-08	1.06E-08
1.11E-08	3.76E-09	1.04E-08
9.72E-09	6.86E-09	1.09E-08
1.11E-08	1.07E-08	1.06E-08
1.50E-08	1.41E-08	1.01E-08
2.02E-08	8.72E-09	9.48E-09
9.82E-09	1.32E-08	6.64E-09
Average = 1.29E-08 Variance = 2.1E-18	Average = 1.04E-08 Variance = -3.51E-18	Average = 9.92E-09 Variance = -2.41E-19
Low-side without capacitor switching from ON to OFF	Low-side with 0.01uf capacitor switching from ON to OFF	Low-side with 0.1uf capacitor switching from ON to OFF
5.70E-09	2.08E-09	1.33E-08
7.60E-09	7.04E-09	1.75E-08
1.05E-08	5.06E-09	1.28E-08
3.00E-09	5.80E-09	1.79E-08
3.06E-09	7.96E-09	1.52E-08
7.26E-09	2.70E-09	1.75E-08
1.47E-08	7.32E-09	1.68E-08
4.86E-09	3.88E-09	1.70E-08
5.74E-09	1.26E-09	1.48E-08
6.38E-09	2.06E-09	1.40E-08
Average = 6.88E-09 Variance = -7.48E-19	Average = 4.52E-09 Variance = 7.07E-19	Average = 1.57E-08 Variance = -2.30E-20

Table 4.4 Energy comparison of low-side MOSFETs

4.7 Comparison of Simulations with Experiments for model power supply:

The simulation results are compared with the experiments performed with the model power supply. PWM signals with constant frequency (20 kHz) and constant duty ratio (50%) are applied to the high-side and low-side MOSFETs. The simulation results are presented from figure 4.31 through figure 4.32.

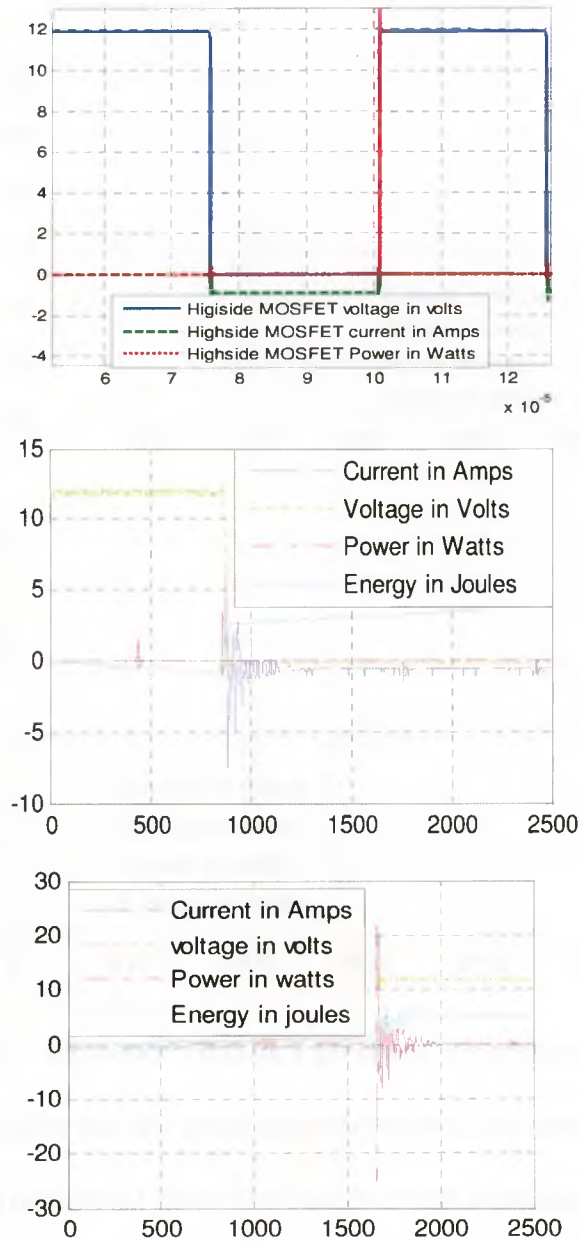


Figure 4.31 High-side MOSFET OFF and ON without capacitors

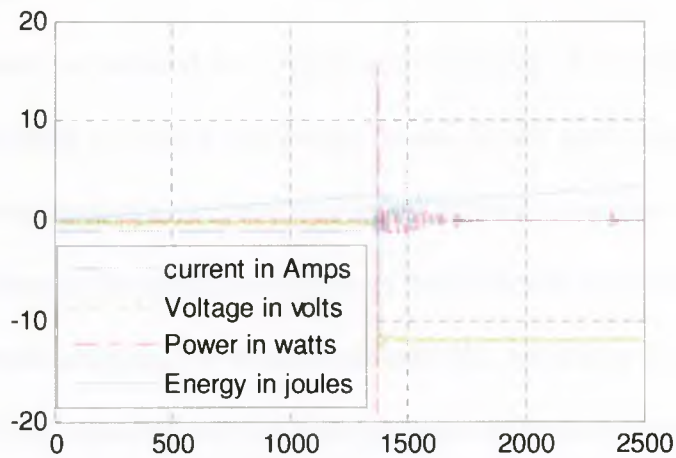
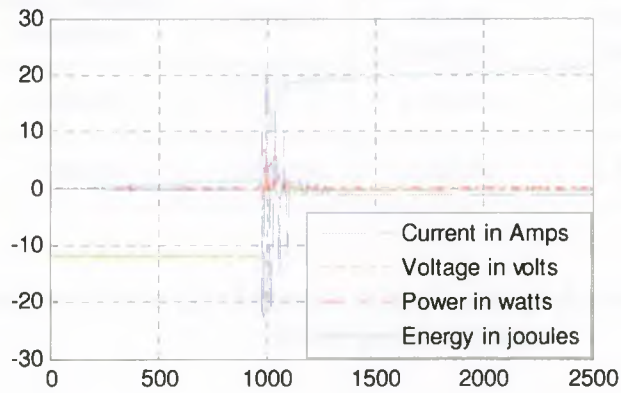
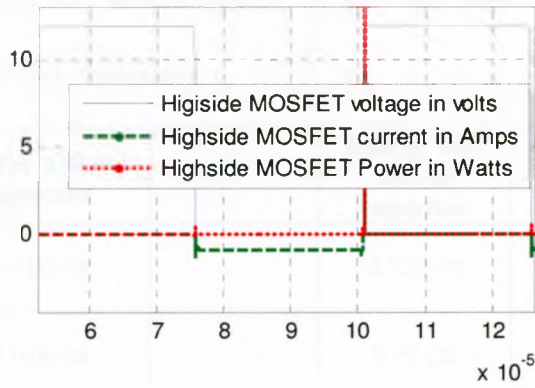


Figure 4.32 Low-side MOSFET OFF and ON without capacitors

The figures indicate that the simulation waveforms can represent the real trends of the variables in the experimental data. The ranges of the simulated variables agree with the experiments very well. Table 4.5 shows a comparison of the energies of the model

power supply as well as the actual power supply for both high-side and low-side MOSFETS with and without capacitors.

Simulated results with model power supply	Energy without capacitor		Energy with 0.01 uf capacitor	Energy with 0.01 uf capacitor	
High-side MOSFET	2.31E-08		2.32E-08	2.32E-08	
Low-side MOSFET	2.04E-08		3.1E-08	3.1E-08	
Experimental results with model power supply	Energy without capacitor	Variance	Energy with 0.01 uf capacitor	Energy with 0.01 uf capacitor	Variance
High-side MOSFET	2.39E-08	-2.91E-18	2.26E-08	2.26E-08	5.99E-19
Low-side MOSFET	1.98E-08	1.35E-18	1.49E-08	1.49E-08	-2.80E-18

Table 4.5 Comparison of energies between experimental and simulated results of the model power supply

4.8 Conclusion:

In this chapter, we studied the experimental analysis of the model power supply with a passive technique to reduce the energy losses in the small scale resistance spot welding. Experimental analysis has been performed without capacitors, with 0.01 uf, and 0.1 uf capacitors between the drain and source of the high-side and low-side MOSFETS. From the experimental analysis, we would conclude that variability of result was greater than mean, so adding a capacitor was not a useful means of reducing switching loss.

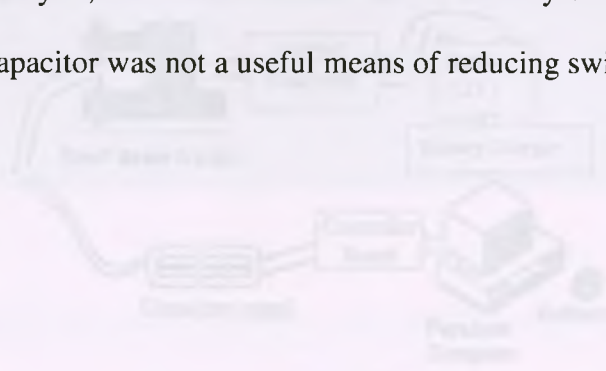


Figure 3.1 Block diagram of Experimental setup to measure energy losses

Chapter 5

Measuring Losses in Small Scale Resistance Spot Welding

The experimental procedure to measure the energy losses in the small scale resistance spot welding (SSRSW) will be discussed in detail in this chapter. Voltages across various components have been measured and Kirchoff's voltage law is applied to add all the measured voltages.

5.1 Experimental Setup:

The experimental set up consists of a small scale resistance spot welding (SSRSW) power supply head from Unitek Peco Model 80, already developed power supply, d-space software for data acquisition and a personal computer. Steel coupons are also used as welding material to measure losses. A Model CP cable foot pedal is used to apply electrode force after two over lapped coupons are manually placed between the electrodes of the welder. The Model CP cable pedal is equipped with an adjustable down-stop which enables it to apply the required force to do weld. The welding current is generated through the electrodes and coupons by the DC power supply, when the force applied by the pedal reaches the preset value. Figure 5.1 demonstrates the block diagram of the experimental setup.

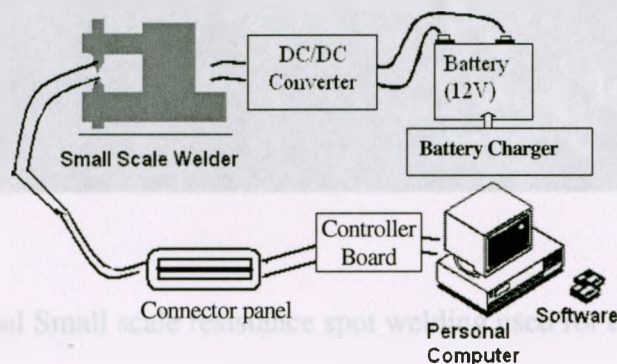


Figure 5.1 Block diagram of Experimental setup to measure energy losses

An oscilloscope was also used to measure the voltages and currents across the different components of the power supply.

5.2 Experimental procedure:

Figure 5.2 is the actual SSRSW power supply, while figure 5.3 is the schematic of the power supply and figure 5.4 shows the block diagram, according to which, the measurements of voltage and currents across different junctions of the power supply and welder are measured.



Figure 5.2 Actual Small scale resistance spot welding used for experiments

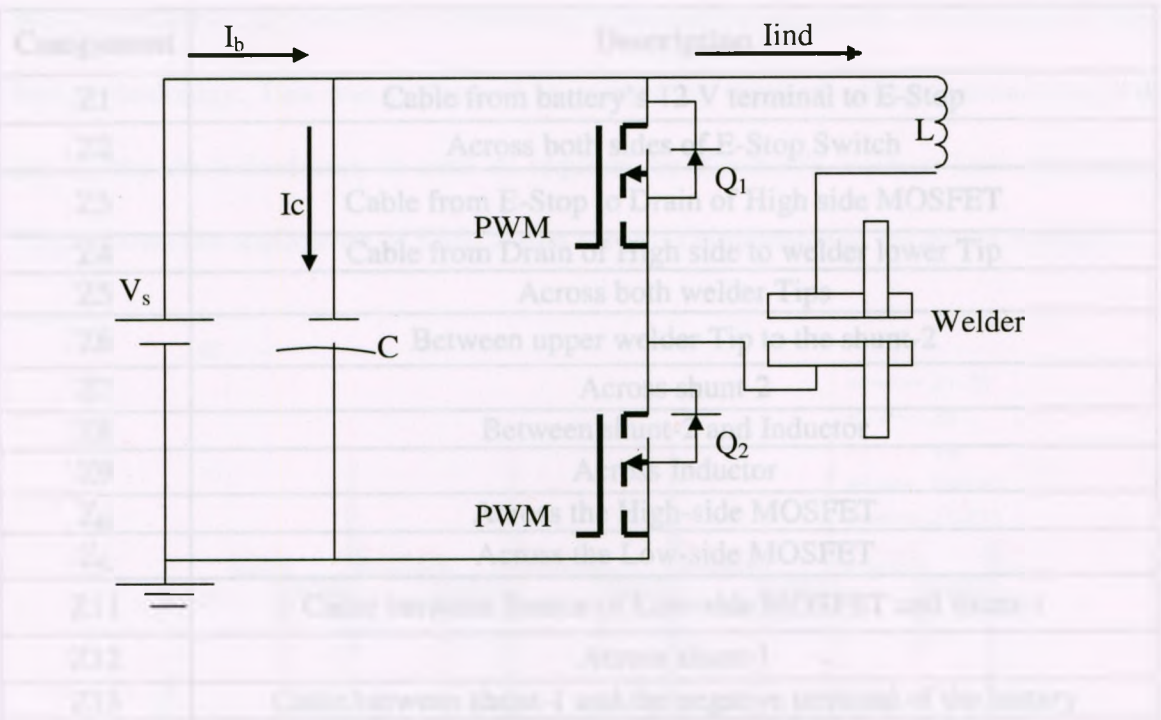


Fig. 5.3 Schematic of the SSRSW power supply

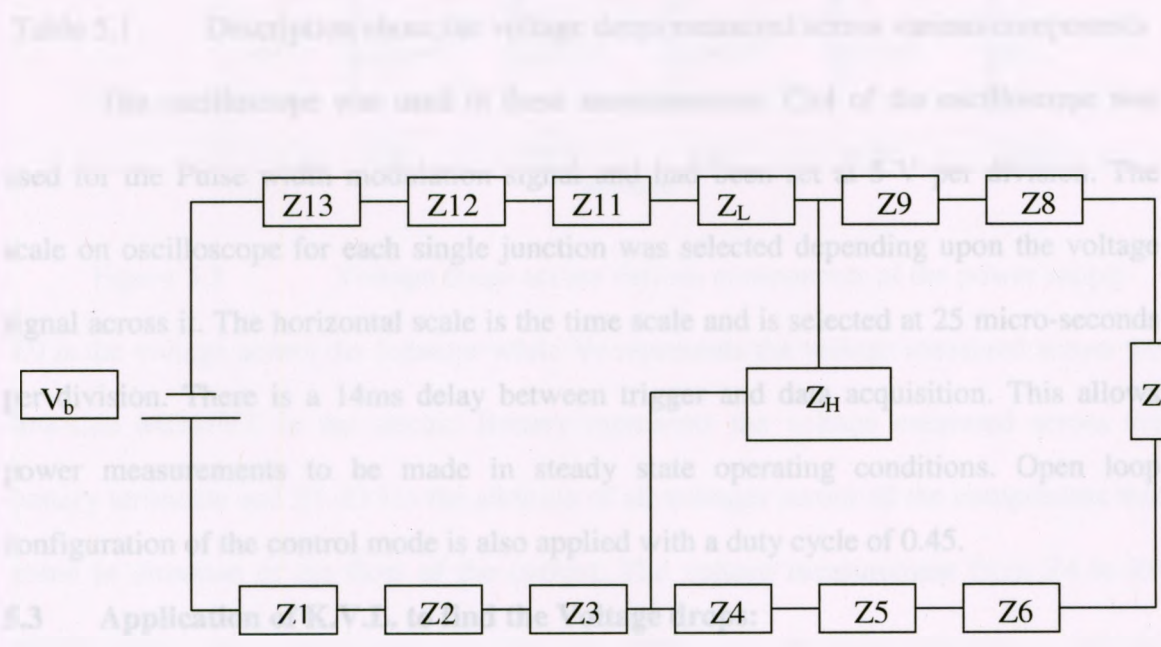


Figure 5.4 Block diagram to measure voltage drops across various components of welder

Component	Description
Z1	Cable from battery's 12 V terminal to E-Stop
Z2	Across both sides of E-Stop Switch
Z3	Cable from E-Stop to Drain of High side MOSFET
Z4	Cable from Drain of High side to welder lower Tip
Z5	Across both welder Tips
Z6	Between upper welder Tip to the shunt-2
Z7	Across shunt-2
Z8	Between shunt-2 and Inductor
Z9	Across Inductor
Z _H	Across the High-side MOSFET
Z _L	Across the Low-side MOSFET
Z11	Cable between Source of Low-side MOSFET and shunt-1
Z12	Across shunt-1
Z13	Cable between shunt-1 and the negative terminal of the battery
V _b	Across the battery terminal

Table 5.1 Description about the voltage drops measured across various components

The oscilloscope was used in these measurements. Ch4 of the oscilloscope was used for the Pulse width modulation signal and had been set at 5-V per division. The scale on oscilloscope for each single junction was selected depending upon the voltage signal across it. The horizontal scale is the time scale and is selected at 25 micro-seconds per division. There is a 14ms delay between trigger and data acquisition. This allows power measurements to be made in steady state operating conditions. Open loop configuration of the control mode is also applied with a duty cycle of 0.45.

5.3 Application of K.V.L. to find the Voltage drops:

Based on all above measurements, the data was then shifted to matlab to do the data analysis and verify the repeatability and accuracy of the measurements. All of the voltage drops are being measured during different experiments. Thus it is necessary to examine

how repeatable is the process to determine if reasonable conclusions can be derived from this methodology. This was performed by comparing sums of voltages around loops to see if they do indeed sum to zero as required by Kirchoff's Voltage Law. Following figure shows the application of KVL across various components in the power supply.

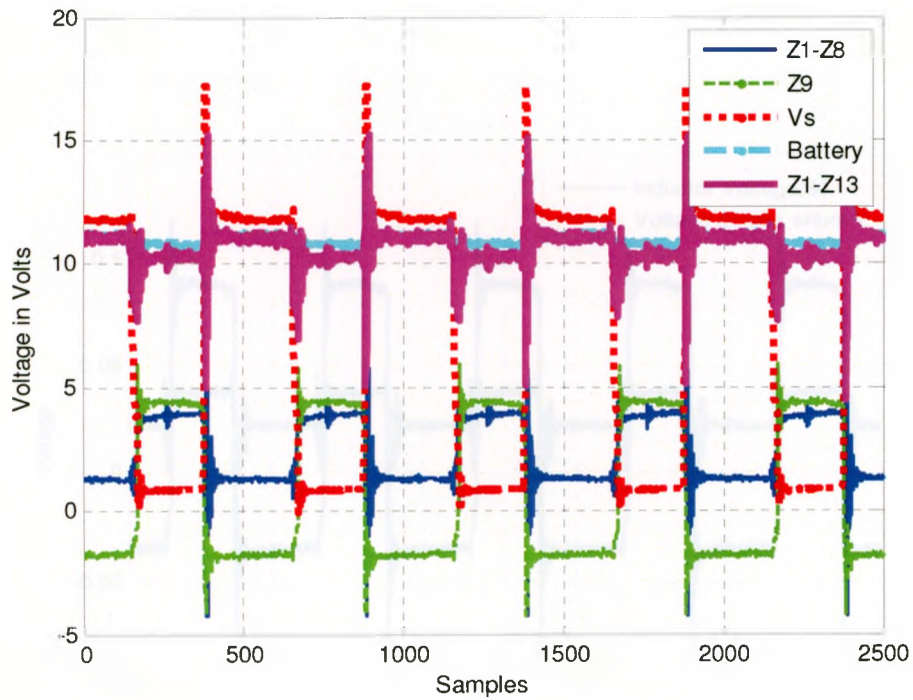


Figure 5.5 Voltage drops across various components of the power supply

Z9 is the voltage across the Inductor while V_s represents the voltage measured across the low-side MOSFET in the circuit. Battery represents the voltage measured across the battery terminals and Z1-Z13 is the addition of all voltages across all the components that come in direction of the flow of the current. The voltage measurement from Z4 to Z9 should equal those across Z_H . We see that when the low side transistor is off the measured voltage drops equal the voltage measured across the battery while there is a 0.5 volt discrepancy between battery voltage and sum of voltage drops when the high side

transistor is active. This discrepancy gives a bound on the accuracy of our measurement and is reasonable given the limitations of the 8 bit ADC in the oscilloscope.

5.4 Inductor current:

Figure 5.6 shows the plot of the inductor voltage and the voltage measured across shunt-2. The shunt resistance used in this measurement was $0.1\text{ m}\Omega$.

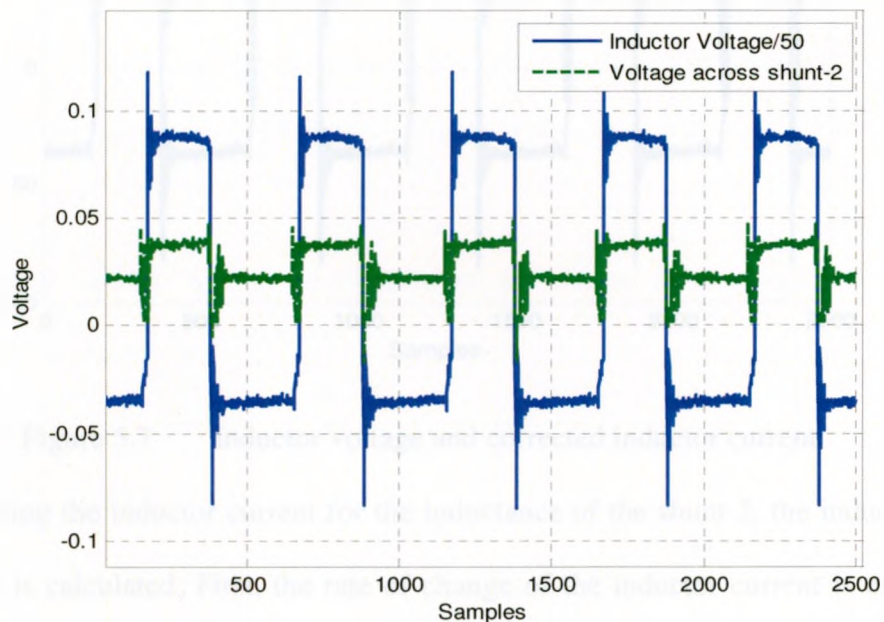


Figure 5.6 Inductor voltage and voltage across shunt-2

5.4.1 Correction of the inductor current:

In figure 5.6, it can be seen that the voltage across the shunt is discontinuous. If the shunt was purely resistive, this would imply a discontinuous current in the inductor which violates the laws governing inductors. It can thus be assumed that the shunt should be modeled as a resistor in series with an inductor. Thus the inductor current should be $I = 1/R (V - L di/dt)$. L can be found by finding the value of L ($1.53\text{ }\mu\text{H}$) such that the average of $L di/dt$ over a full period is zero. Figure 5.7 shows the signal of corrected

inductor current, which will then be used to measure the power losses across various components in the power supply.

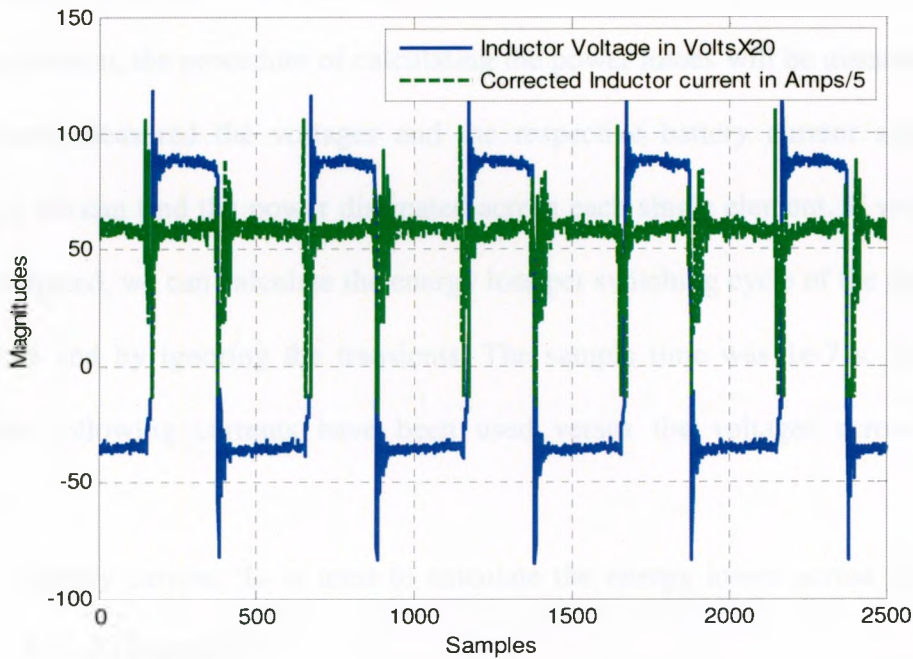


Figure 5.7 Inductor voltage and corrected inductor current

After correcting the inductor current for the inductance of the shunt-2, the inductance of the inductor is calculated. First, the rate of change of the inductor current is calculated during a switching cycle using above plot, which is 1.613×10^6 A/s and the voltage measured across the inductor as 6.1561 volts from figure to calculate inductance. We also know that $V = L \frac{di}{dt}$, so using this equation, the inductance value is calculated as 3.82 μ H.

The inductance of the inductor is also measured directly in the lab with the inductance meter LC-102 manufactured by SENCORE and which is 8 μ H. We can see the experimental inductance of the inductor is almost half than the inductance directly

measured with the meter. It can be assumed that inductance in practice will decrease for high currents as a result of decreasing permeability of the iron.

5.5 Calculation of Power Losses:

In this section, the procedure of calculating the power losses will be discussed. As we already have measured the voltages and the respective battery current and inductor current, so we can find the power dissipated across each single element. If we know the power dissipated, we can calculate the energy loss per switching cycle of the signal in the steady state and by ignoring the transients. The sample time was $1e-7$ s. To measure power, the following currents have been used versus the voltages across different junctions.

1. Battery current ' I_b ' is used to calculate the energy losses across Z1, Z2, Z3, Z11, Z12 and Z13.
2. Inductor current ' I_{ind} ' is used to calculate the energy losses across Z4, Z5, Z6, Z7, Z8, and Z9.
3. The method to measure Capacitor current ' I_c ' is described in the next section and is used to measure energy losses across the capacitor.
4. Current on high-side MOSFET ' I_{hs} ' is used to calculate the energy losses across it. The procedure of calculating the ' I_{hs} ' is discussed later in this chapter.
5. Current on low-side MOSFET ' I_{ls} ' is used to calculate the energy losses across it. The procedure of calculating the ' I_{ls} ' is also described later in this chapter.

5.5.1 Current through capacitor:

The capacitor in the circuit is connected to the power supply with the two copper strips. Therefore, the voltage drop across one of these strips can be used to measure the

capacitor current. Unfortunately the impedance of the metal strip has a reactive component that is comparable to its resistive component but is nevertheless too small to be measured by the inductance meter. To determine its precise value we identify a complete impedance model across the entire capacitor with its connectors using the voltages measured across the connector, V_1 , and across the connector and capacitor V_c and the resultant circuit schematic for these parameters has been shown in figure 5.8.

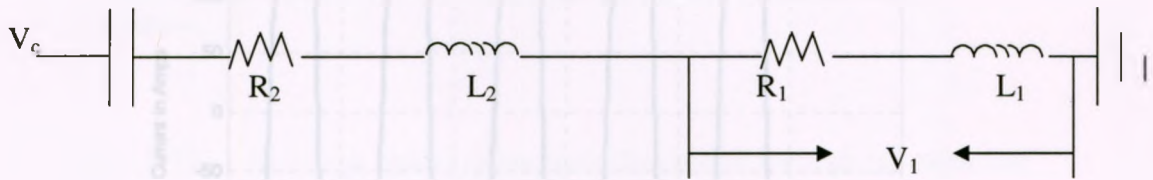


Figure 5.8 Block diagram to calculate current in the capacitor

The following state equations are applicable to the circuit of figure 5.8, when we realize it in the space state model.

$$\dot{X}_1 = \frac{V_1}{L_1} - \frac{R_1}{L_1} X_1 \quad (5.1)$$

$$\dot{X}_2 = \frac{1}{C} X_1 \quad (5.2)$$

where, X_1 represents the current into the capacitor and X_2 the voltage across capacitor respectively. R_1 represents the resistance of the copper strip and is measured as 0.24 m Ω in lab. R_2 and L_2 represents the effective series resistance and inductance of the capacitor while L_1 the inductance of the copper strip. The above state space equations were then implemented in simulink, see Figure 5.10, with

$$V_c = X_2 - L_2/L_1 * (V_1 - R_1 * X_1) - R_2 * X_1 \quad (5.3)$$

as the output. Educated guesses were then made for R_2 , L_2 and L_1 and these were then manual adjusted keeping in mind that we expected the capacitor current to be a square wave and to minimize the difference between the simulated and measured V_c . This gave $L_1 = 1.2\text{nH}$, $L_2 = 6\text{nH}$ and $R_2 = 8\text{ m}\Omega$. Figure 5.9 and 5.10 shows the plots of the capacitor current and measured and the simulated voltage V_c across the capacitor.

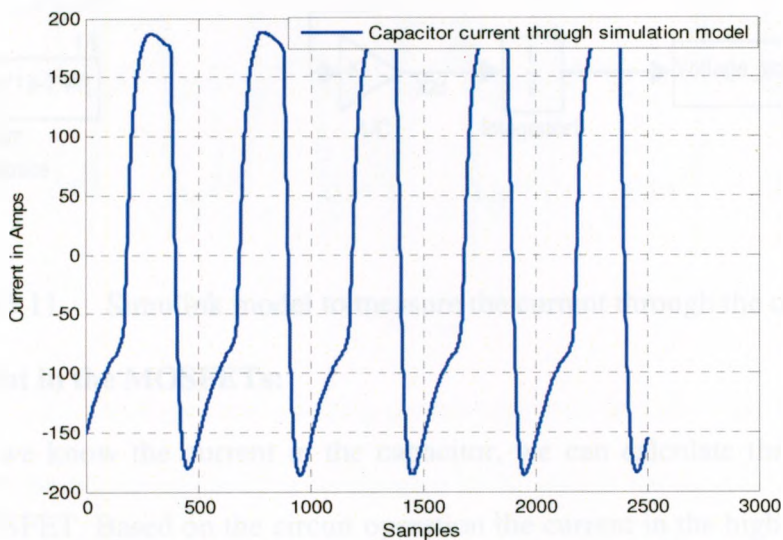


Figure 5.9 Capacitor current

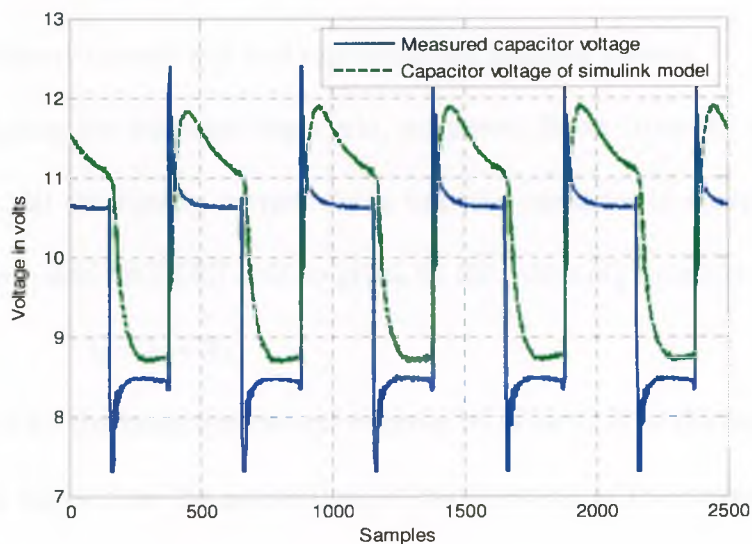


Figure 5.10 Measured and corrected capacitor voltage V_c

Figure 5.13 demonstrates voltages and current calculated across the high-side and low-side MOSFETs.

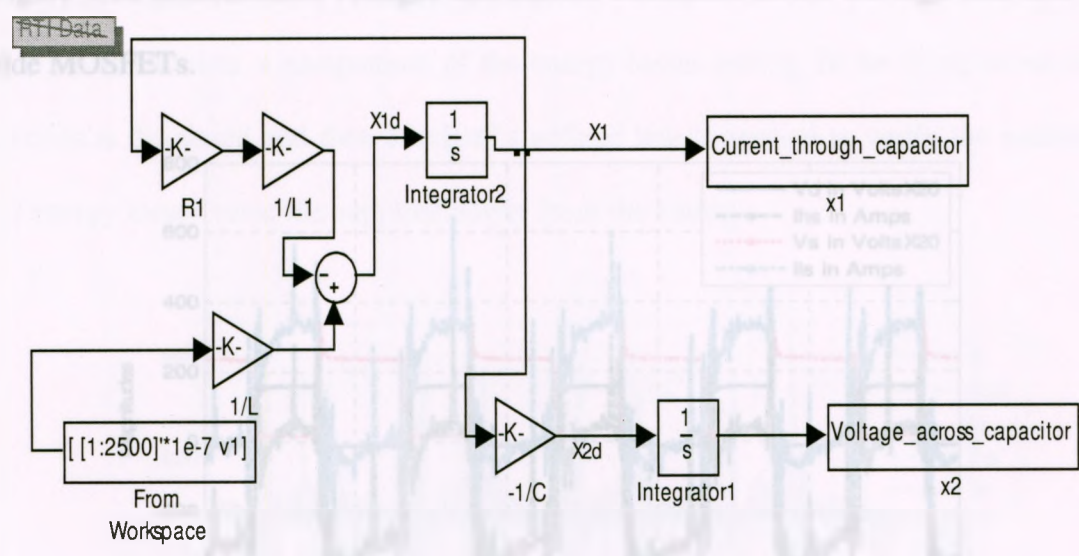


Figure 5.11 Simulink model to measure the current through the capacitor

5.5.2 Current in the MOSFETs:

Figure 5.12 Voltages and currents across high-side and low-side MOSFETs

Once we know the current in the capacitor, we can calculate the current in the high-side MOSFET. Based on the circuit operation the current in the high-side MOSFET

is given by the following equation which is represented in thesis by I_{hs} .

$$I_{hs} = I_b + X_1 - I_{ind} \tag{5.4}$$

where I_b is the battery current and I_{ind} represents the Inductor current.

As we know during the freewheeling cycle, no power flows from the battery into the load. Therefore, all the battery current flows into the capacitor to charge it. Hence the current on the low-side MOSFET will be given by the following equation:

$$I_{ls} = I_b + X_1 \tag{5.5}$$

Plus sign is used for the capacitor current because its polarity is in the opposite direction in the measured signal than the actual flow of the direction of the current in the circuit.

Figure 5.12 demonstrates voltages and current calculated across the high-side and low-side MOSFETs.

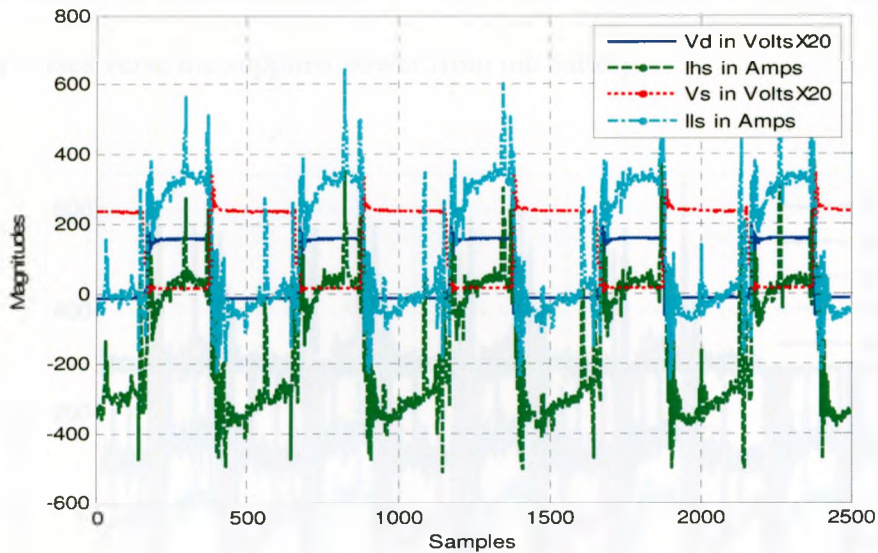


Figure 5.12 Voltages and currents across high-side and low-side MOSFETs

Following are the notations used for each signal in the plot of the figure.

- V_d = Voltage across the high-side MOSFET
- I_{hs} = Current across the high-side MOSFET
- V_s = Voltage across the low-side MOSFET
- I_{ls} = Current across the low-side MOSFET

Note that the currents found in both MOSFETs are only small when the MOSFETs are in off-state clearly indicating that our approach to finding the capacitor current needs to be improved. It is possible that neglecting the fact that, our capacitance is formed from a bank of capacitors with some impedance between the individual capacitors has introduced this error.

5.6 Comparison of the Energy Losses:

In this section, a comparison of the energy losses among all the components in the circuits is discussed and then Kirchoff's voltage law is applied to verify the addition of all energy losses verse the supplied power from the battery.

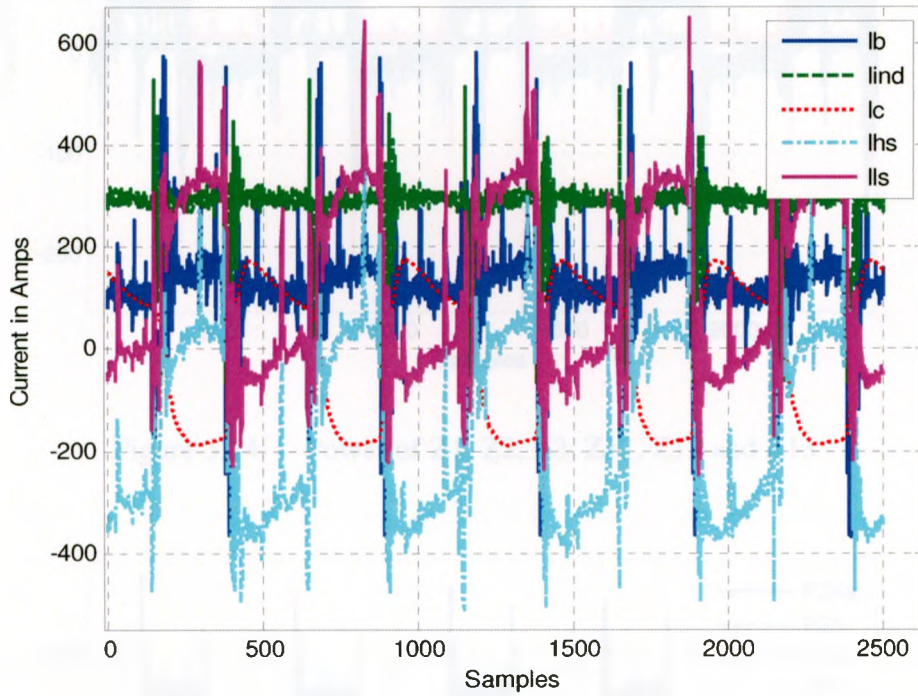


Figure 5.13 lb, lind, lc, lhs and lls

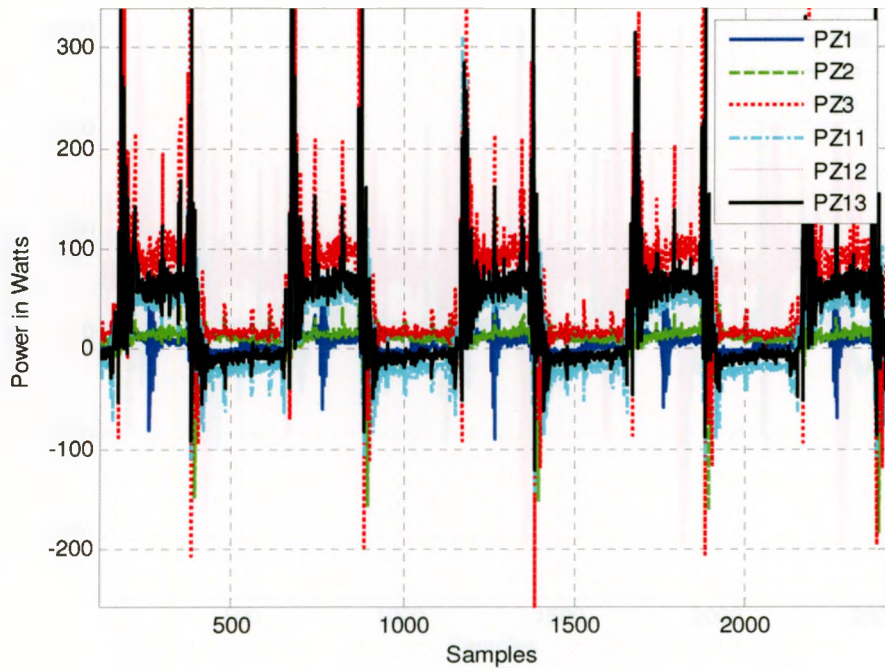


Figure 5.14 Power of Z1, Z2, Z3, Z11, Z12 and Z13

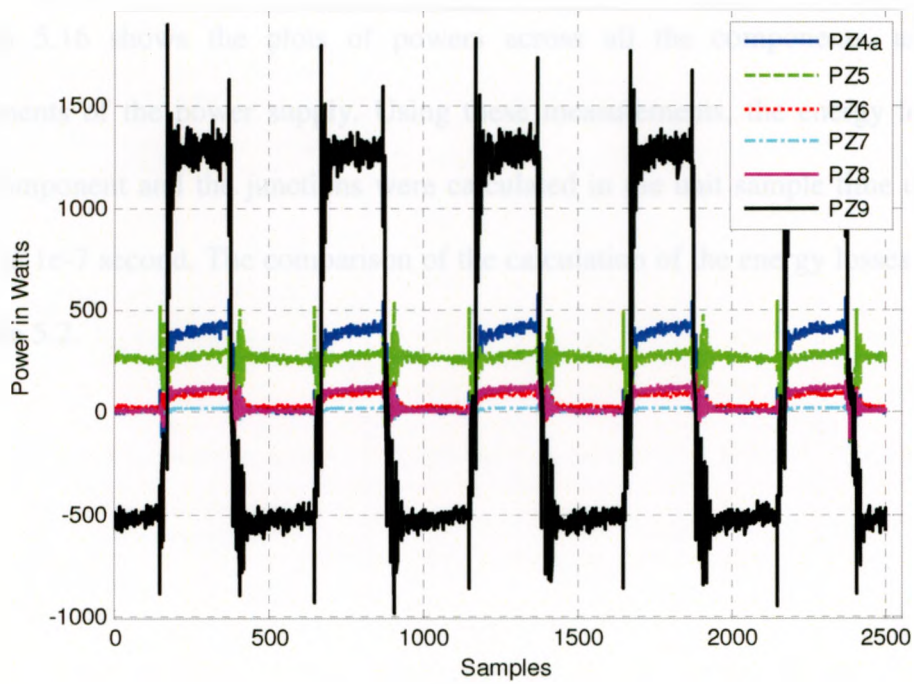


Figure 5.15 Power of Z4, Z5, Z6, Z7, Z8 and Z9

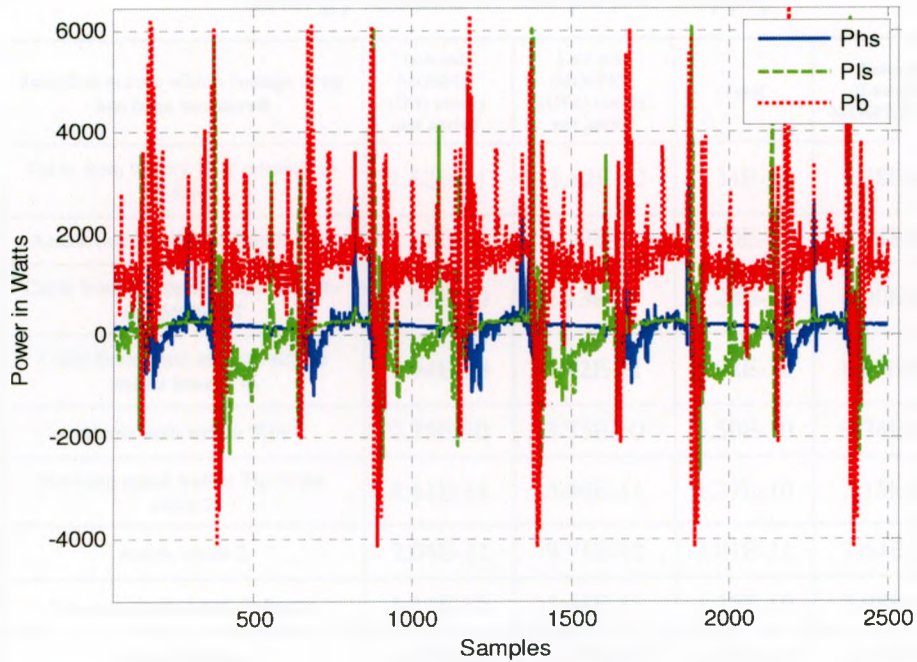


Figure 5.16 Pb, Pbs and Pls

Figure 5.5 shows the voltages, figure 5.13 shows the currents and figure 5.14 through 5.16 shows the plots of powers across all the components, and different components of the power supply. Using these measurements, the energy losses across each component and the junctions were calculated in the unit sample time of the signal which is $1e-7$ second. The comparison of the calculation of the energy losses is shown in the table 5.2.

Energy losses in the power supply						
	Junction across which voltage drop has been measured	Low-side MOSFET (ON) energy per period	Low-side MOSFET (OFF) energy per period	Total	Voltage (Lowside MOSFET ON)	Voltage (Lowside MOSFET OFF)
Z1	Cable from battery 12 V terminal to E-Stop	1.52E-11	-1.82E-12	1.34E-11	5.28E-02	1.32E-02
Z2	Across both sides of E-Stop Switch	1.51E-11	1.19E-11	2.70E-11	9.78E-02	8.41E-02
Z3	Cable from E-Stop to Drain of High-side MOSFET	1.07E-10	2.13E-11	1.28E-10	6.00E-01	1.40E-01
Z4	Cable from Drain of High-side to welder lower Tip	3.94E-10	1.42E-11	4.08E-10	1.40E+00	1.83E-02
Z5	Across both welder Tips	2.75E-10	3.75E-10	6.50E-10	9.74E-01	8.81E-01
Z6	Between upper welder Tip to the shunt-2	8.81E-11	3.90E-11	1.27E-10	3.15E-01	9.08E-02
Z7	Across shunt-2	2.04E-11	9.71E-12	3.01E-11	7.64E-02	1.68E-02
Z8	Between shunt-2 and Inductor	1.11E-10	1.44E-11	1.25E-10	3.98E-01	2.27E-02
Z9	Across Inductor	1.26E-09	-7.37E-10	5.23E-10	4.35E+00	-1.76E+00
Z10	Across the high-side MOSFET(without transition)	0.00E+00	2.56E-10	2.56E-10	7.90E+00	-5.50E-01
Z10	Across the high-side MOSFET(with transition)	0.00E+00	2.44E-10	2.44E-10		
Z10a	Across Low-side MOSFET(without transition)	3.49E-10	0.00E+00	3.49E-10	1.18E+01	8.70E-01
Z10a	Across Low-side MOSFET(with transition)	3.25E-10	0.00E+00	3.25E-10		
Z11	Cable between Source of Low-side MOSFET and shunt-1	6.13E-11	-2.21E-11	3.92E-11	3.27E-01	-1.61E-01
Z12	Across shunt-1	1.08E-11	-1.65E-12	9.15E-12	4.16E-01	-5.66E-02
Z13	Cable between shunt-1 and the negative terminal of the battery	7.59E-11	-5.41E-12	7.05E-11	4.09E-01	-5.66E-02
Pc	Energy loss across capacitor	-1.27E-09	1.80E-09	5.30E-10	8.46E+00	1.06E+01
	Total	1.51E-09	1.16E-09	3.86E-09	1.10E+01	1.03E+01
Vb	Across the battery terminal	2.83E-09	1.56E-09	4.39E-09	1.11E+01	1.08E+01
	Difference between Total losses and the battery terminal	1.32E-09	3.96E-10	5.35E-10	1.00E-01	5.00E-01
	Efficiency in Percentage	9.72%	24.04%	14.81%		

Table 5.2 Energy losses measured across the power supply

We can notice in the plots that the signals have two states in a period (a) low-side MOSFET-ON and (b) low-side MOSFET-OFF. In table 5.2, column-3 represents the

energy per period when the low-side diode is turned-on, while column-4 represents the energy per period when the low-side MOSFET is turned-off, which means both these two columns represents the energy per sample period. These calculations are also done after the switch current and voltages are in steady state thus excludes the transient energies. The total time of one period is 50-microseconds. Column-3 in the table is also multiplied by 22.5-microseconds and 0.45 because the low-side switch was on for this much duty cycle. Column-4 is multiplied by 27.5-microseconds and 0.55 because the low-side switch was off for this duration of the time. Then conservation of energy is applied to measure the total energy losses in whole power supply and added all losses. These losses were then compared with the energy of the battery to gauge whether variations in the experiments or measurement errors have made obvious discrepancies in our methodology. We can see that most of the energy losses are across the inductor and welder itself and the long wires in the power supply especially the wire of Z3 and Z4. These calculations only determine the steady state power losses. The switching losses have not been considered. However, because the power flow from the battery is smooth, the line P_b should include the switching losses. Thus the switching losses should be bounded by the difference between power supplied and measured power consumed plus the experimental uncertainty. The efficiency of the welding power supply is calculated using the output power across the welder and the input power supplied by the battery, which is also shown in the table. It can be seen in the table that the efficiency of the power supply is about 10 percent when the lowside MOSFET is ON. Similarly, the efficiency of the full period is almost 15 percent.

5.7 Conclusions:

Chapter 6

In this chapter, the voltage drops across each component of the power supply were being measured and these voltages around loops were added up to see if they sum to zero as required by Kirchoff's Voltage Law. We also noticed that when the low side transistor is off the measured voltage drops equal the voltage measured across the battery while there is a 0.5 volt discrepancy between battery voltage and sum of voltage drops when the high side transistor is active. There is another observation about the power supply that that most of the energy losses are across the wires and that since the steady state power consumed is not significantly less than the power supplied, switching losses are inconsequential for this circuit.

6.1.3 Output characteristics

The output characteristics for an n -channel power MOSFET with the drain current (I_D) as a function of drain-source voltage (V_{DS}) with gate-source voltage (V_{GS}) as a parameter are shown in Figure 6.1. It has three regions named as Linear, current-saturated and cut-off. In the cut-off region, the gate-source voltage is less than the gate-threshold voltage and the device is an open-circuit to V_{DS} . In the Linear region, the device acts as a resistor with almost a constant on-resistance ($R_{DS(on)}$) defined by V_{DS}/I_D . In the current-saturated region, the drain current is a function of the gate-source voltage and defined by:

$$I_D \approx K_n \times (V_{GS} - V_{GS(th)})^2 \approx g_m \times (V_{GS} - V_{GS(th)}) \quad (6.1)$$

Chapter 6

Simulations analysis of SSRSW

In this chapter, simulation results that have been done using Micro-cap software obtained from an SSRSW power supply are presented. This SSRSW power supply was implemented with Buck DC-DC converter as described in chapter 2. The efficiency of the welder power supply is shown, simulation waveforms obtained with this circuit are provided and conclusion about the performance of the circuits is made.

6.1 Power MOSFET Characteristics:

The static behaviour is defined by the output characteristics, on-resistance, and the transconductance of the device, while the dynamic behaviour is described by the switching characteristics that include the intrinsic capacitances, resistance, gate charge and the reverse recovery of the body diode.

6.1.1 Output characteristics:

The output characteristics for an N-channel power MOSFET with the drain current (I_{ds}) as a function of drain-source voltage (V_{ds}) with gate-source voltage (V_{gs}) as a parameter shown in figure 6.1. It has three regions named as Ohmic, current-saturated and cut-off. In the cut-off region, the gate-source voltage is less than the gate-threshold voltage and the device is an open-circuit or off. In the Ohmic region, the device acts as a resistor with almost a constant on-resistance, ($R_{DS(on)}$) defined by V_{ds}/I_{ds} . In the current-saturated region, the drain current is a function of the gate-source voltage and defined by,

$$I_{ds} = K \cdot (V_{gs} - V_{gs(th)})^2 = g_{fs} \cdot (V_{gs} - V_{gs(th)}) \quad (6.1)$$

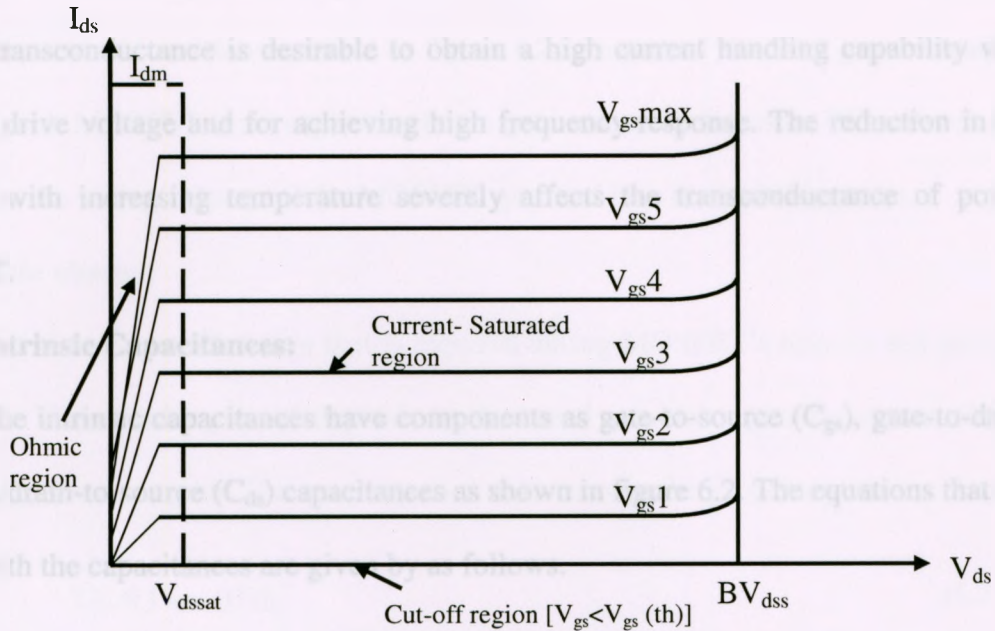


Figure 6.1 Characteristics of a N-channel Power MOSFET

6.1.2 On-Resistance $R_{DS(on)}$:

The on-resistance determines the conduction power dissipation and increases with increasing temperature and is defined by

$$R_{DS(on)} = R_{source} + R_{ch} + R_A + R_J + R_D + R_{sub} + R_{wcm1} \quad (6.2)$$

where, R_{source} = Source diffusion resistance, R_{ch} = Channel resistance, R_A = Accumulation resistance, R_J = "JFET" component-resistance of the region between the two-body regions, R_D = Drift region resistance, R_{sub} = Substrate resistance, R_{wcm1} = Sum of bond wire resistance, the contact resistance between the source and drain metallization and lead-frame contributions.

6.1.3 Transconductance g_{fs} :

The transconductance is defined as the change in drain current divided by the change in gate voltage for a constant drain voltage.

$$g_{fs} = dI_D / dV_{gs} \quad (6.3)$$

A large transconductance is desirable to obtain a high current handling capability with low gate drive voltage and for achieving high frequency response. The reduction in the mobility with increasing temperature severely affects the transconductance of power MOSFET.

6.1.4 Intrinsic Capacitances:

The intrinsic capacitances have components as gate-to-source (C_{gs}), gate-to-drain (C_{gd}) and drain-to-source (C_{ds}) capacitances as shown in figure 6.2. The equations that are related with the capacitances are given by as follows.

$$\text{Input capacitance,} \quad C_{iss} = C_{gs} + C_{gd} \quad (6.4)$$

$$\text{Output capacitance,} \quad C_{oss} = C_{ds} + C_{gd} \quad (6.5)$$

$$\text{Reverse transfer capacitance} \quad C_{rss} = C_{gd} \quad (6.6)$$

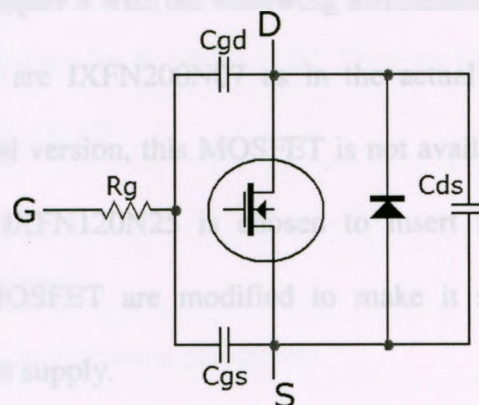


Figure 6.2 Power MOSFET parasitic components

6.1.5 Intrinsic resistance:

The intrinsic resistance shown in figure 6.2 is a part of the total gate resistance. Together with MOSFET input capacitance; the gate resistance forms an RC network that determines the voltage change at the MOSFET gate and thus the switching time.

6.1.6 Gate charge:

It is the amount of charge that is required during MOSFET's turn-on and turn-off transitions. The switching speed depends on the speed at which a gate driver can charge or discharge the input gate. The basic equation to determine the gate charge is

$$Q_G = \int i_{GG}(t) dt \quad (6.7)$$

The body diode exhibits very slow reverse recovery with large reverse recovery current. It is defined by $t_{rr} = t_r + t_f$. This time is also known as the storage time because it is the time that is taken to sweep out the excess charge, Q_{rr} .

6.2 Analysis with the small scale resistance spot welding:

Figure 6.3 shows the actual small scale resistance spot welding. The circuit is same as the model power supply of chapter 4 with the following differences.

- The MOSFETs used are IXFN200N07 as in the actual lab power supply. In Micro-cap professional version, this MOSFET is not available, so to do analysis, a similar MOSFET IXFN120N25 is chosen to insert in the circuit and the parameters of the MOSFET are modified to make it similar to actual used MOSFET in the power supply.

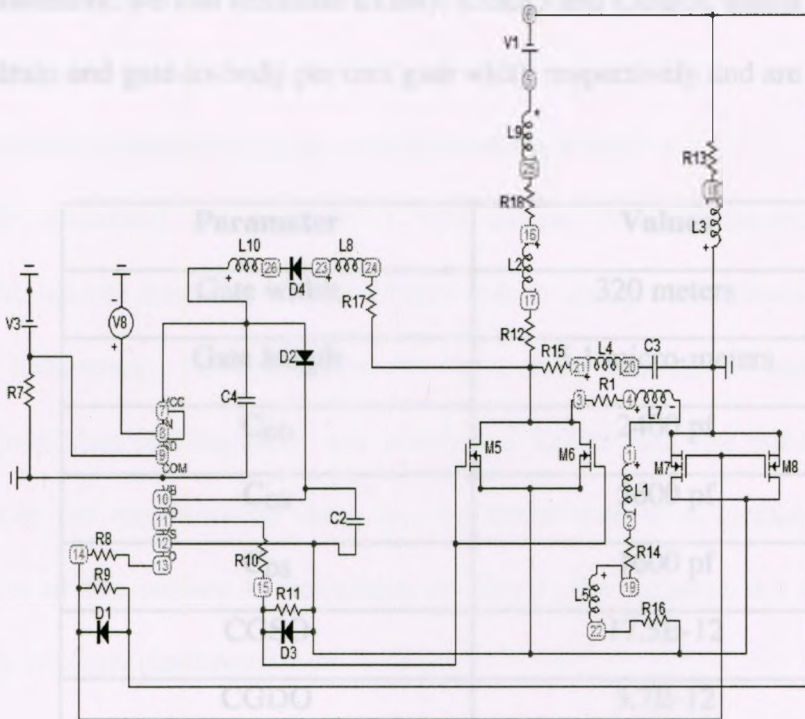


Figure 6.3 Small scale resistance spot welding used for simulation

As we have
$$I_D = K (V_d - V_{to})^2 \tag{6.8}$$

From the data sheet of IXFN200N07, we have the values of $I_d = 500$ A, $V_d = 10$ and $V_{to} = 5$. Therefore, we can calculate for K, which is 20. Then we have

$$K = W/L (K_p/2) \tag{6.9}$$

where

W = gate width, and L = gate length

$K_p = 1.0256E-6$ (Process transconductance parameter)

So the width and length of the gate can be calculated using equation 6.9. Also, in the data sheet, we are provided with the capacitances in the form of C_{iss} , C_{oss} , and C_{rss} . Using equation from 6.4 to 6.6, we can calculate C_{GD} , C_{GS} , and C_{DS} . Once we know the values of

these parameters, we can calculate CGSO, CGDO and CGBO, which are gate-to-source, gate-to-drain and gate-to-body per unit gate width respectively and are given in table 6.1.

Parameter	Values
Gate width	320 meters
Gate length	5.1 micro-meters
C_{GD}	2400 pf
C_{GS}	5600 pf
C_{DS}	1600 pf
CGSO	17.5E-12
CGDO	3.7E-12
CGBO	0
R_D	1.397525E-3
R_S	2.5E-3
R_G	5.1820
R_B	1.0000E-9

Table 6.1 Parameters values of the MOSFETs

- A capacitor is also added in parallel with the battery as in the actual power supply. This capacitor contributes during the power cycle. Because of the long wires from battery to the drain of the high-side MOSFET, battery can not provide the full power required during this cycle.
- Resistances and the inductances of the long wires have been added to figure 5.3, which accounts for the voltage drops in the power supply. These resistances and

inductances have been calculated using the experimental data, and figure 5.4 discussed in chapter 5.

6.2.1 Internal Inductance and resistance of the battery:

As described, the input is a 12V battery that has internal inductance and resistance, which needs to be considered while doing simulations. To calculate the internal inductance, the derivative of the battery current is calculated using the experimental data of Chapter 5, and which is 6.51×10^6 A/s. The voltage is 0.34 V, also taken from the experimental data. As we know that $V = L \frac{dI_b}{dt}$, so the internal inductance of the battery is calculated as 52-nH. To measure the internal resistance, following steps are performed.

- a) First, the open loop voltage of the battery terminals is measured using multi-meter in the lab and that is 12.66 volts.
- b) The average voltage of the experimental data is also calculated and which is 10.96 volts. The difference of both these voltages is noted and is 1.7 volts.
- c) Then used ohms law and divide this voltage by the battery current (150-Amp) to calculate the resistance of the battery which is 10.7 m Ω .

The manufacturer's nominal output resistance can be inferred based on cold cranking amps specified for the battery. The cold cranking amps are defined as the current output of the battery when its voltage has dropped to 7 V at 32 degrees F. $R_0 = 5.6/CCA = 5.6$ m Ω . There is discrepancy, if we compare this value with the experimental value. The possible reason can be that the battery used in these experiments is about 9-years old and from the comparison between the measured and cold cranking

amps effective series resistance of the battery, it can be concluded that, this is a time to replace the battery.

6.2.2 Calculation of Inductance and resistance of capacitor C3:

The capacitor in the SSRSW is connected with two copper strip and they are also accounted for the inductance and resistance of the capacitor in addition to its own effective series impedance. Here are the values of the inductance and resistance in the capacitor.

- a) R_1 represents the resistance of the copper strip and is measured as 0.24 m Ω and since it has two copper strips, this is multiplied by 2 to get R_1 's value. Therefore, $R_1 = 0.48$ m Ω . R_2 represents the effective series resistance of the capacitor and it was calculated as 3 m Ω . Hence the net series resistance is 3.48 m Ω .
- b) Similarly, the inductance of the copper strip is calculated as 1.2 nH and multiplied by 2, so the total of the two copper strips is 2.4 n-H. The series inductance of the capacitor is 6 nH. Therefore, the total inductance is 8.4 nH and these values are also given in table 6.2.

6.2.3 Calculation of inductance and resistance of long wires:

Table 6.2 shows the inductances and resistances of the long wires in the power supply. In the table L2 and R12 represents the combine inductance and resistance of Z1, Z2 and Z3, which has been calculated using the experimental data of the voltage across Z1, Z2 and Z3 and the battery current. L3 and R13 is the combine impedance of Z11, Z12, and Z13, and have been calculated using the experimental data of the voltage across Z11, Z12 and Z13 and the battery current. L5 and R16 show combine inductance and

resistance of Z4a, Z6, Z7, and Z8, and have been calculated using the experimental data of the voltage across Z4a, Z6, Z7 and Z8 and the inductor current. Z9 is the impedance of the inductor in the circuit. Z5 shows the impedance of the welder and also calculated by using the voltage across it and the inductor current. L4 and R15 is the impedance of the capacitor in the circuit. L9 and R18 is the impedance of the battery, while L8 and R17 shows the impedance of the wire from 12-V battery to the VCC pin of the driving chip. During the analysis, it was also noted that, the signals have too much noise, so to suppress this noise, inductor L10 (20 μ H) and diode D4 are used as a filter in the circuit as was already implemented on the actual welder.

Inductances and resistances of the wires in the power supply				
	Description	Inductance	Resistance	Length of wires
Z1	Cable from battery 12 V terminal to E-Stop	9.00E-09	3.90E-04	15"
Z2	Across both sides of E-Stop Switch	5.37E-10	2.33E-05	
Z3	Cable from E-Stop to Drain of High-side MOSFET	7.20E-08	3.10E-03	15"
Total		L2 = 8.15E-08	R12 = 3.85E-03	
Z4a	Cable from Drain of High-side to welder lower Tip	6.52E-07	4.50E-03	36"
Z6	Between upper welder Tip to shunt-2	1.10E-07	7.40E-04	9"
Z7	Across shunt-2	2.45E-08	1.70E-04	
Z8	Between shunt-2 and Inductor	1.75E-07	1.20E-03	15"
Total		L5 = 1.24E-06	R16 = 3.26E-03	
Z9	Across Inductor	L1 = 3.8E-06	R14 = 2E-03	
Z5	Across both welder Tips	L7 = 3.51E-08	R1 = 3.40E-03	
Z11	Cable between Source of Low-side MOSFET and shunt-1	7.82E-08	3.40E-03	15"
Z12	Across shunt-1	9.09E-11	1.20E-03	
Z13	Cable between shunt-1 and the negative terminal of the battery	7.34E-08	3.20E-03	15"
Total		L3 = 2.25E-07	R13 = 2.80E-03	
Cable between 12 V and VCC pin of IR-(2184) driving chip		L8 = 0.12E-07	R17 = 2.0E-02	
Capacitor (C₃)		L4 = 8.40E-09	R15 = 7.80E-03	
Internal Inductance and Resistance of Battery		L9 = 52.0E-09	R18 = 10.7E-03	

Table 6.2 Inductances and resistances of the long wires in the SSRSW power supply

6.3 Comparison of the Simulations with the Experiments:

The simulation results are compared with the experiments on equipment described in Chapter 5. Open loop voltage mode has been implemented. PWM signals with constant frequency (20 kHz) and constant duty ratio (45%) are applied to the high- and low-side MOSFETs. The simulation results are presented from figure 6.4 through figure 6.14. Measured data is collect 14ms from start of weld whereas simulation data is collected after 3ms at which it reached the steady state from start of weld.

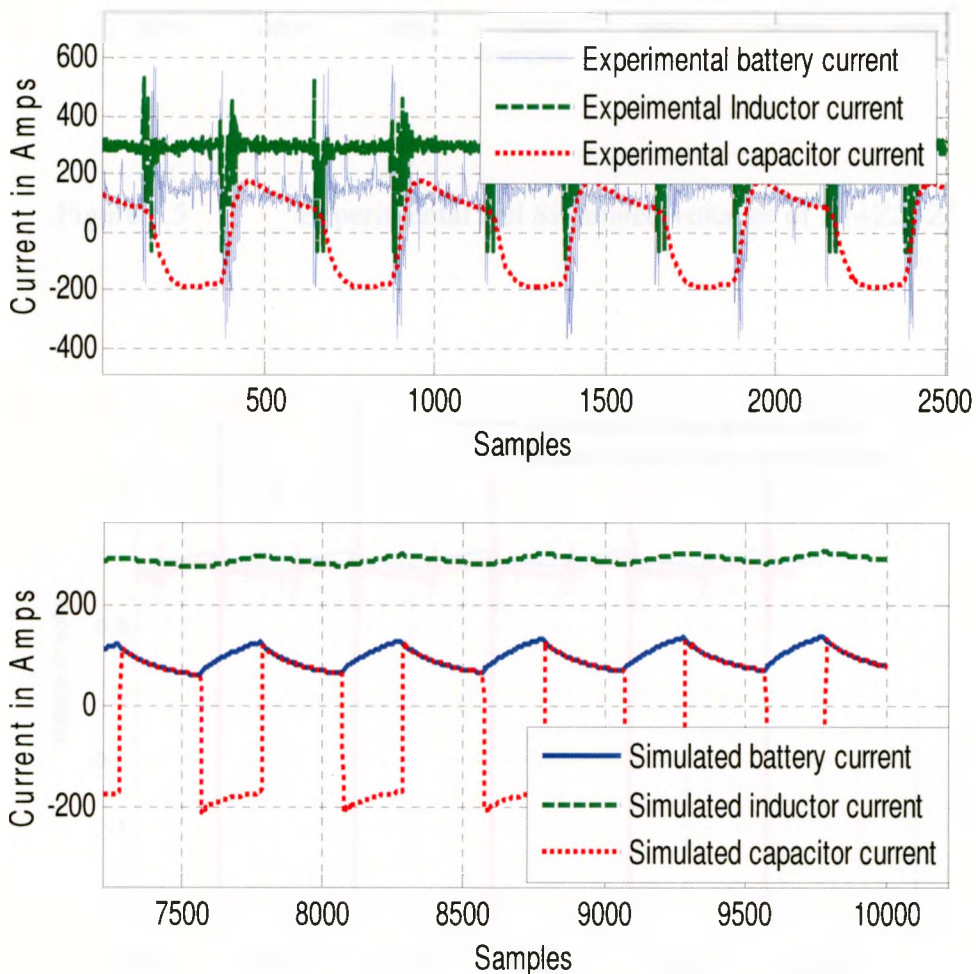


Figure 6.4 Experimental & Simulated current of Inductor, battery & capacitor

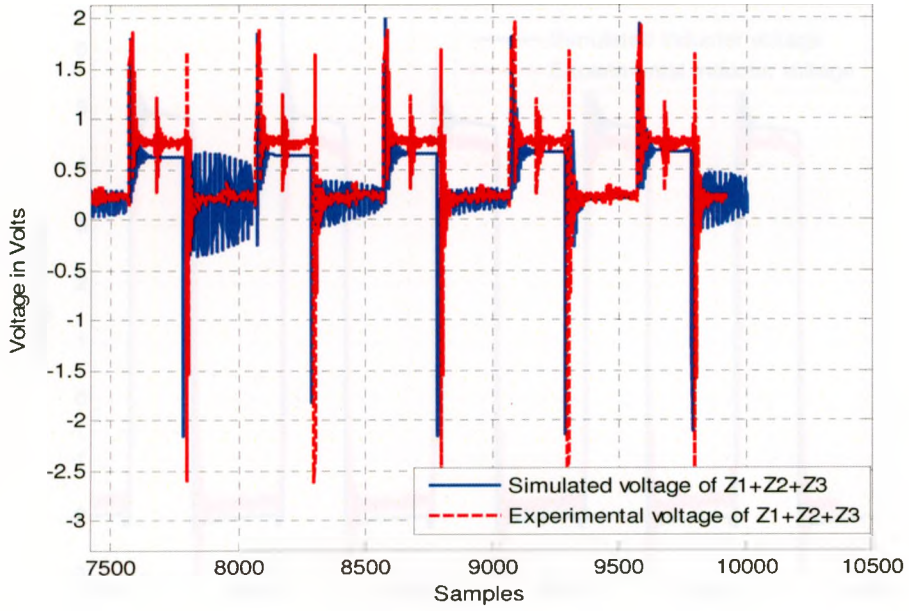


Figure 6.5 Experimental and Simulated voltages of $Z1+Z2+Z3$

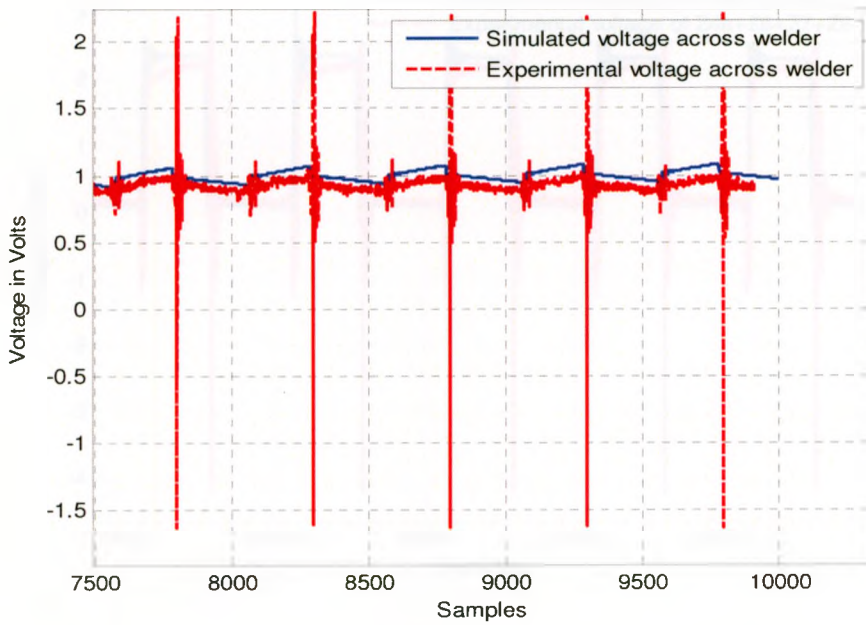


Figure 6.6 Experimental and Simulated voltages across the load resistor

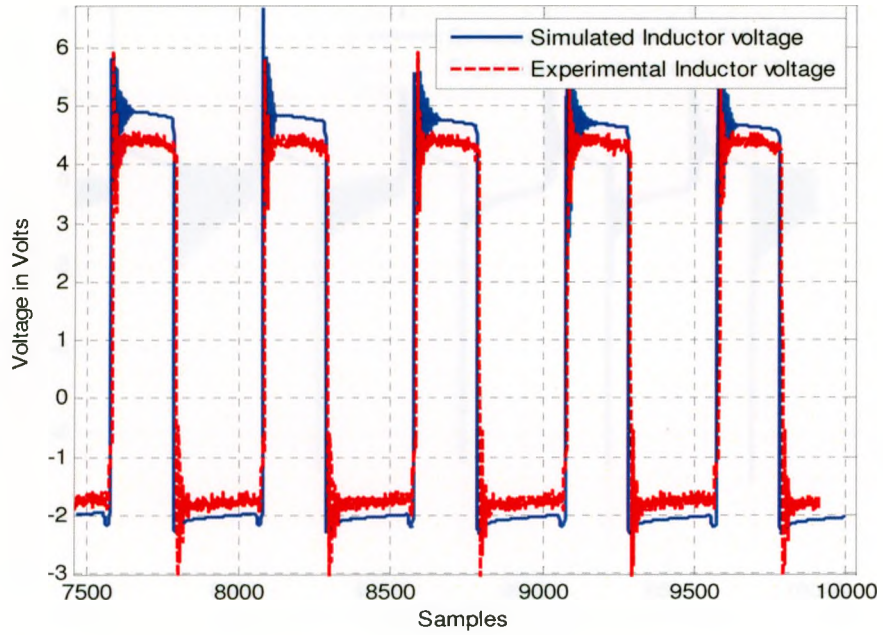


Figure 6.7 Experimental and Simulated Inductor voltage

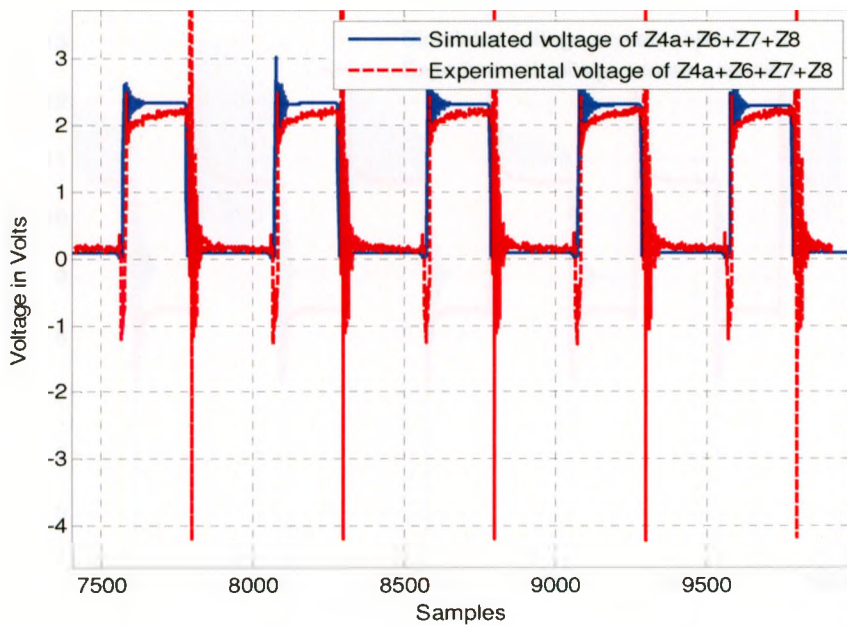


Figure 6.8 Experimental and Simulated voltages of $Z4+Z6+Z7+Z8$

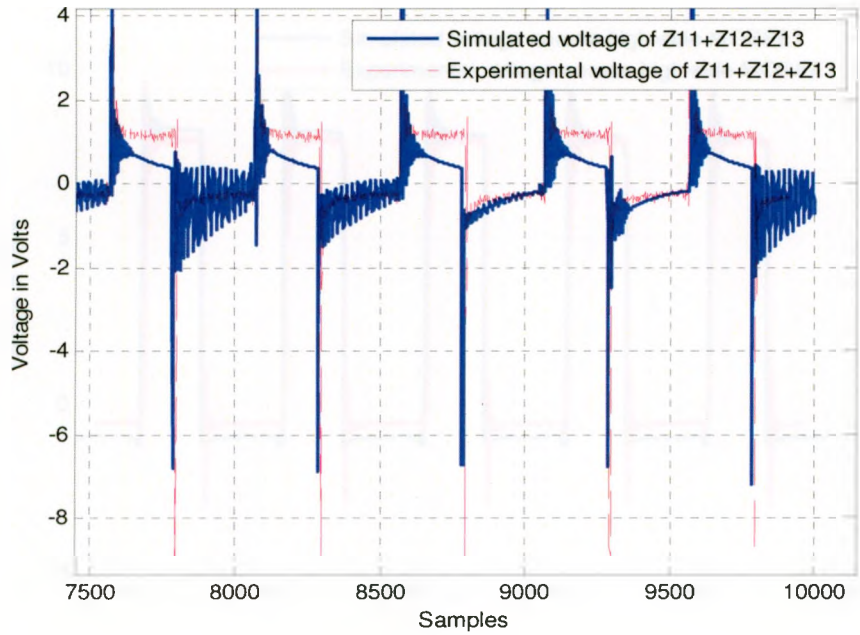


Figure 6.9 Experimental and Simulated voltages of Z11+Z12+Z13

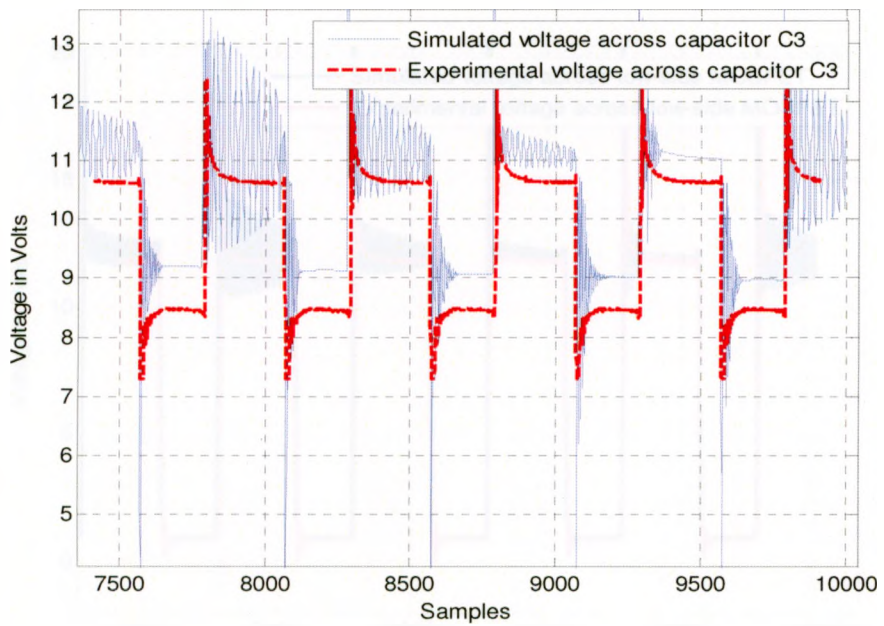


Figure 6.10 Experimental and Simulated capacitor (C3) voltage

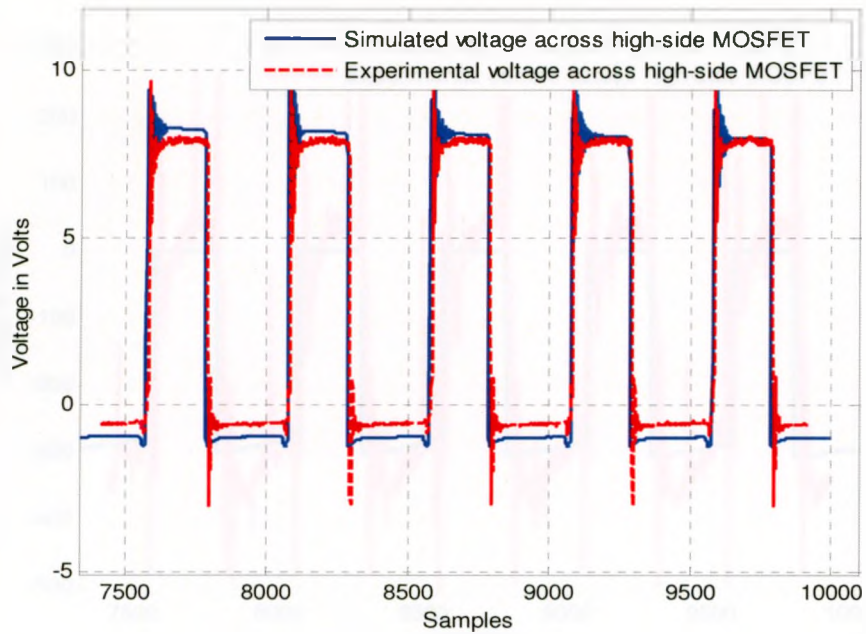


Figure 6.11 Experimental & Simulated voltage of high-side MOSFET

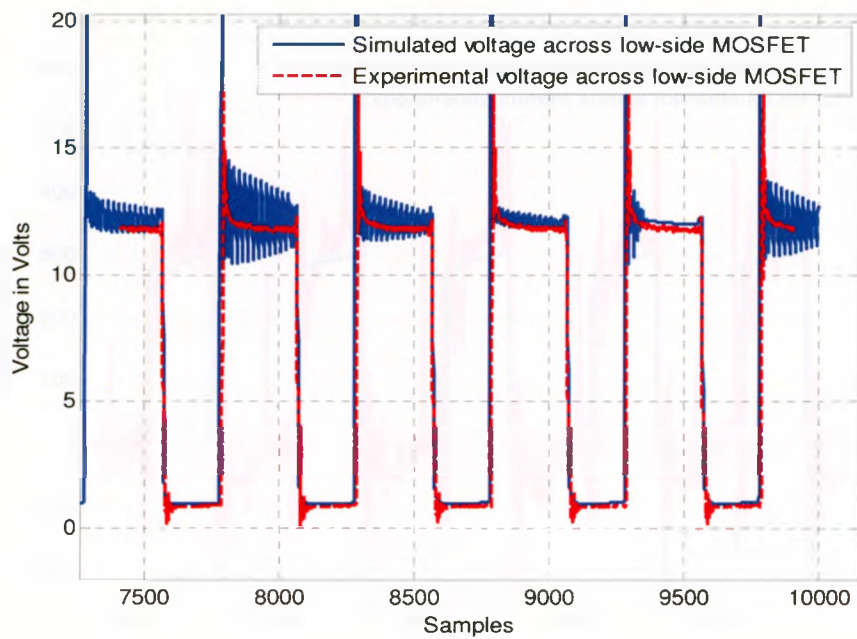


Figure 6.12 Experimental & Simulated voltage of low-side MOSFET

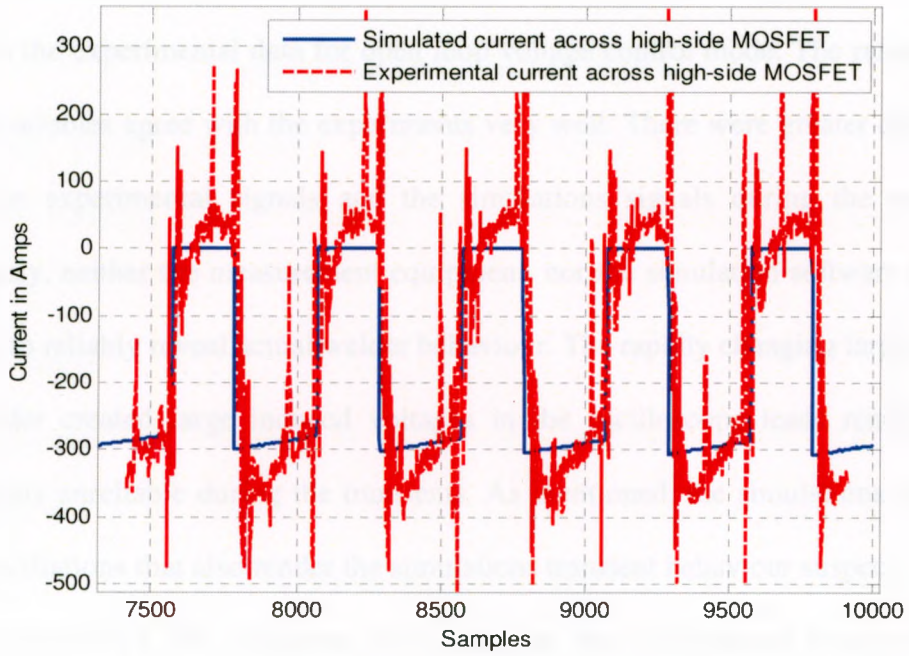


Figure 6.13 Experimental & Simulated current of high-side MOSFET

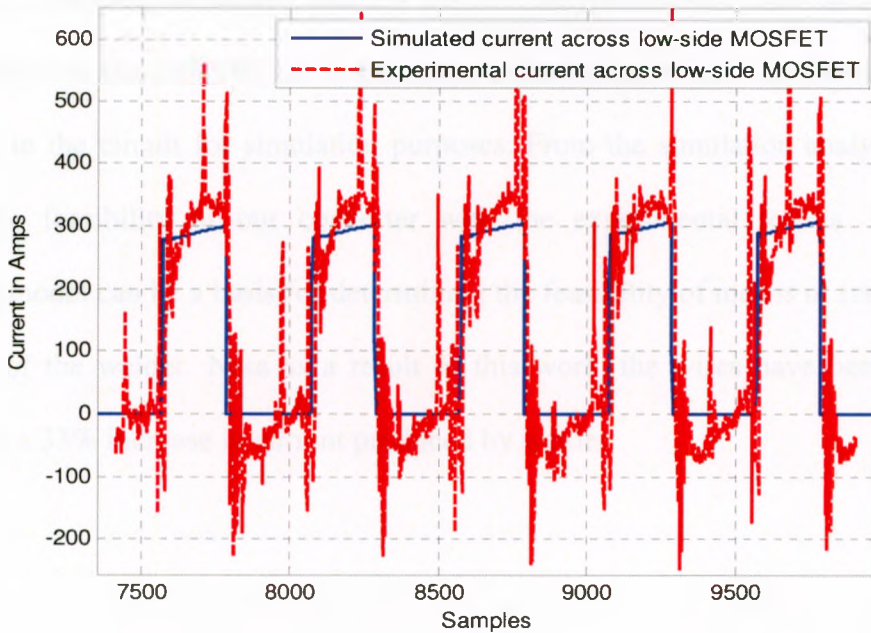


Figure 6.14 Experimental & Simulated current of low-side MOSFET

The figures indicate that the simulation waveforms can represent the real trends of the variables in the experimental data for open loop voltage control mode. The ranges of the simulated variables agree with the experiments very well. There were greater differences between the experimental signals and the simulations signals during the transients. Unfortunately, neither the measurement equipment, nor the simulation software could be considered to reliably reveal actual welder behaviour. The rapidly changing large currents in the welder created large induced voltages in the oscilloscope leads rendering the measurements unreliable during the transients. As mentioned, the simulations contained irregular oscillations that also render the simulations transient behaviour suspect.

The main purpose of the simulation is to compare the experimental results with the simulation results of the small scale resistance spot supply. In that sense the simulation has achieved quite satisfactory results.

6.4 Conclusion:

In this chapter, simulation analysis has been performed with small scale resistance spot welding. For the SSRSW, the inductances and resistances have also been calculated and added in the circuit for simulation purposes. From the simulation analysis, we can confirm the feasibility of our converter with the experimental results. Further the simulation model can be a basis for determining the feasibility of means of improving the efficiency of the welder. Note as a result of this work, the wires have been upgraded resulting in a 33% increase in current produced by welder.

Chapter 7

Conclusion and Future Work

In this chapter, the major works of the thesis are summarized, the main contributions resulting from the thesis are stated, and suggestions for future work are given.

7.1 Summary:

High frequency operation of pulse width modulated (PWM) DC-DC buck converters allows for the reduction of the size and weight of their magnetic and filtering components; however, at high switching frequency, switching losses become significant and must be minimized. It has been accepted by power electronics researchers that the most efficient switching PWM converters with high frequency are zero-voltage transition (ZVT) PWM converters. These DC-DC buck converters contain MOSFETs as an active switch and passive LC elements. The purpose of main power switch, typically a MOSFET is to turn-on with zero-voltage switching (ZVS).

There have been many circuits for ZVS-PWM converters that have been previously proposed by power electronics researchers. Most, if not all, of these circuits are either one of two general types; an auxiliary circuit can be a non-resonant circuit or a resonant circuit. The auxiliary switch in a non-resonant circuit has considerable loss at turn-off as the flow of a significant amount of current through the switch is interrupted when the switch is turned off. The auxiliary switch in a resonant circuit has much lower turn-off loss, but the resonant circuit itself creates additional circulating current that increases conduction losses and the peak current stress of the main power switch.

The main objective of this thesis was to propose a passive technique by using capacitors between drain and source of the high-side and low-side MOSFETs used in the buck DC-DC converter of the small scale resistance spot welding to reduce the energy losses and to study, characterize and examine the properties and characteristics of this new type of circuit through mathematical analysis and experimental work. Experimental results obtained from a model circuit DC-DC PWM buck converter were presented.

7.2 Conclusions:

The following conclusions can be made based on the work done in this thesis:

- Primary losses are resistive losses in the cables and inductor.
- Switching losses are not significant as compared to losses in cables.
- The passive technique of having capacitors between drain and source of the MOSFET was also implemented on model of the small scale resistance spot welding. Gains were insufficient to consider applying this technique to the actual welding power supply.
- It was also observed that the capacitor current is not correct during the comparison between experimental and simulated signals. A more sophisticated and accurate model of the capacitor bank is required for calculating the capacitor current.
- Thus it does not make sense to expend resources reducing the switching losses until cable losses are addressed.

7.3 Contributions:

The principal contributions of this thesis are as follows:

- Analysis on a circuit was performed so that the properties and the steady-state characteristics of the circuit were determined and an understanding of the circuit was developed. Main limitations and their primary sources have been identified.
- The operation of the circuit was experimentally confirmed with results obtained from a model and the existing small scale resistance spot welding. It was determined that the simplest modification to reduce switching losses was not a viable strategy for improving the welder.
- The voltage drops across each component of the SSRSW power supply were being measured and analyzed. These voltages around loops were then added up to see if they sum to zero as required by Kirchoff's Voltage Law.

7.4 Future Work:

Based on the achievements of this thesis, the following tasks are recommended for the future research and study:

- First and foremost, upgrade and shorten the cables used in welder. The existing cables were long (1-foot & 2-feet) and of the higher guage (0.6 AWG) that means its per unit length resistance and inductance is high, which adds to the losses of the circuit. Therefore, shortening the wires and by using 0.2 AWG wires, these losses can be reduced in future.
- Upgrade the inductor. Parameters like coil material, tolerance, device dimensions, shielding are very important. The reduction of coupling allows shielded inductors to be placed closer together without having an adverse effect on the performance of the circuit. This can be exploited to reduce overall size. Additionally, the use of shielded parts reduces the circuit's electromagnetic interference.

- Use the micro-cap model with improved inductor and short wires of 0.2 AWG (with less resistance and inductance per unit length) to optimize welder performance.

[1] Angela Brannon and Ernest Delgado, "Analysis and design of magnetic circuits for high power GTO DC-DC converters", © IEEE Transactions on Power Electronics, Vol. 9, No. 1, January 1994.

[2] Hong-Mau Jaber, A. Abu-Ordah, Shihong Qiu, Jueqiang Wu, and Ibrah Bateman, "Transfer function model for current double rectifier in voltage source inverter system", School of Electrical Engineering & Computer Science, University of Central Florida, Orlando, Florida, USA. © 2005.

[3] Yuhui L. Kazianka, "Improved Buck and Boost converters for Alpha Power applications", Institute of Semiconductor Physics, Novosibirsk, Russian Federation. © 2007 IEEE.

[4] Dong-hui Kwak, Seung-Ho Lee and He-Young Jung, "A new Buck-Boost DC-DC converters of high efficiency by self-switching inductor", Professional Doctoral School of Dynamic Precision, Kangwon National University, Korea.

[5] Chang-hong Yang and Chen-Lan Chen, "A passive inductor smoother cell for non-reduced PWM DC/DC Converter", 1998.

[6] Yoshitaka Kimachi, Yung-Pi Huang, "Self-switching Buck Boost converter using passive inductor composed of pulsed current superconducting resonant circuit", Power Conversion Laboratory, Industrial Technology Research Institute Hsinchu, Taiwan © 2007 (IEEE).

References

- [1] Angelo Brambilla and Enrico Dallago, “*Analysis and design of snubber circuits for high power GTO DC-DC converters*”, © IEEE Transactions on Power Electronics, Vol. 9, No. 1, January 1994.
- [2] Hong Mao, Jaber A., Abu-Qahouq, Weihong Qiu, Yangyang Wen, and Issa Batarseh, “*Lossless snubber circuit for current double rectifier to reduce reverse recovery losses*”, School of Electrical Engineering & Computer Sciences, University of Central Florida, Orlando, Florida, USA. © 2003.
- [3] Yuriy I. Kransnikov, “*Improved Buck and Boost converters for high Power applications*”, Institute of Semiconductor Physics, Novosibirsk, Russian Federation © 2007 IEEE.
- [4] Dong-kurl Kwak, Seung-Ho Lee and Do-Young Jung, “*A new Buck-Boost DC-DC converter of high efficiency by soft switching techniques*”, Professional Graduate School of Disaster Prevention, Kangwon National University, Korea.
- [5] Ching-Jung Tseng and Chern-Len Chen, “*A passive lossless snubber cell for non-isolated PWM DC/DC Converters*”, 1998.
- [6] Yoshihiro Konishi, Yung-Fu Huang, “*Soft switching Buck Boost converter using passive snubber composed of pulse current regenerative resonant circuit*”, Power Conversion Laboratory, Industrial Technology Research Institute Hsinchu, Taiwan © 2007 IEEE.

- [7] Rui Liu, “*Comparative study of snubber circuits for DC-DC converters utilized in high power off-line power supply applications*”, Bell Labs, Lucent Technologies, Mesquite, Texas © 1999 IEEE.
- [8] Xiaodong Sun, Xuanson Cai, “*A novel soft switching PWM converter with active energy recovery snubber*”, Institute of Beijing Bilin Power Electronics, Beijing, China.
- [9] Luiz Carlos de Freitas, Paulo Roberto Coelho Gomes, “*A high power high frequency ZCS-ZVS PWM Buck converter using a feedback resonant circuit*”, Universidade Federal de Uberlandia Av. Universitaria, Uberlandia, Brazil © 1993 IEEE.
- [10] River T.H. Li, Henry S.H. Chung, “*A passive lossless snubber cell with minimum stress and wide soft-switching range*”, City University of Hong Kong, Honk Kong © 2009.
- [11] A. K. Panda and Aroul K., “*A novel technique to reduce switching losses in a synchronous buck converter*”, International Conference for Power Electronics, Drives and Energy Systems, PEDES, © 2006.
- [12] Gert Fregien and Jacobus D. Van Wyk, “*Non-linear capacitors in snubber circuits for GTO-Thyristors*”, ABB, Mannheim, Germany, © 1989.
- [13] Philip C. Todd, “*Snubber circuits, theory, design and application*”, © 1993.
- [14] Yu-Kransikov, “*New solution to the old problems of buck and boost Converters*”, Power Electronics Co., Ltd, Novosibirsk, Russian Federation © 2005.
- [15] C. U-Yaisom, W. Khamgern and S. Nitta, “*The study and analysis of the conducted EMI suppression on power MOSFETs using passive snubber circuits*”, Faculty of

Engineering and Research Center for Communication & Information Technology,
King Mongkut Institute of Technology, Ladkrabang, Bangkok, Thailand, © 2002.

[16] Francisco K.A. Lima, Cicero M.T. Cruz and Fernando L.M. Antunes, “*A family of turn-on and turn-off non-dissipated passive snubbers for soft-switching single-phase rectifier with conduction losses*”, Federal University of Ceara, Fortaleza-CE, Brazil, © 2004.

[17] Alexander Isurin and Alexander Cook, “*Passive soft-switching snubber circuit with energy recovery*”, Vanner Inc., Hilliard, Ohio, © 2008.

[18] Bill Andreycak, “*Active clamp and reset technique, achieve zero voltage transition (ZVT), higher efficiency, higher frequency switching and reduced EMI/RFI*”, October-1994.

[19] Vlad Grigore and Jorma Kyyra, “*A new Zero-Voltage –Transition PWM Buck Converter*”, Electronics and Telecommunication Faculty, Politehnica University, Bucharest, Romania, © 1998.

[20] LJ. DJ. Varga and N.A. Losic, “*A novel lossless snubber*”, Institute Mihajlo Pupin, Beograd, Yugoslavia, © 1989.

[21] Jian Sun, Kenneth F. Webb and Vivek Malhotra, “*Integrated Magnetics for Current-Doubler Rectifiers*”, © 2001.

[22] Ionel Dan Jitaru and Alexandru Ivascu, “*Quasi-Integrated Magnetic an avenue for higher power density and efficiency in power converters*”, Rom-power Inc., Tucson, Arizona © 1997 IEEE.

- [23] R.C. Fuentes and H.L. Hey, "*A comparative analysis of the behavior and of the switching losses for a group of ZCS-PWM converters using IGBT's*", Federal University of Santa Maria, Santa Maria, Brazil © 1997 IEEE.
- [24] Alexander Isurin and Alexander Cook, "*Passive Soft-Switching Snubber Circuit with energy recovery*", Hilliard, Ohio © 2008.
- [25] C. U-Yaisom, W. Khamgern, S. Nitta, "*The study and the analysis of the conducted EMI suppression on power MOSFET using passive snubber circuits*", Bangkok, Thailand © 2002.
- [26] Tingting Song, Niachi Huang, "*A zero voltage and zero current switching three level DC-DC converter with secondary assisted regenerative passive snubber*", Sichuan University, China © 2004.
- [27] J. Lin, "*power supply designed for small-scale resistance spot welding*", "Master's thesis. The University of Western Ontario, London, ON, Canada 2005." Jin He, An improved energy recovery soft-switching Turn-ON/Turn-OFF passive boost snubber with peak voltage clamp, Mesquite, TX © 2000.
- [28] Pritam Das and Gerry Moschopoulos, "*A comparative study of Zero-Current-Transition PWM Converters*", © IEEE Transactions on Industrial Electronics, Vol., 54, No. 3, June 2007.
- [29] Jian Sun, Kenneth F. Webb and Vivek Mehrotra, "*Integrated magnetics for current-doubler rectifiers*", © 2004.

- [30] Praveen Jain, Harry Soin and Martin Cardella, “*Constant frequency resonant DC-DC converters with zero switching losses*”, Bell Northern Research, Ottawa, Ontario © 1994.
- [31] Andre St-Martin, Praveen K. Jain and Gray Edwards, “*Asymmetrical Pulse-Width – Modulated resonant DC-DC converter topologies*”, Bell Northern Research, Ottawa, Ontario, © IEEE Transactions on Aerospace and Electronics Systems, Vol., 30, No. 2, April 1995.
- [32] Robert Streit and Daniel Tollik, “*High efficiency telecom rectifier using a novel soft-switched Boost-based input current shaper*”, Ascom Energy Systems, Berne, Switzerland © CH 2970-2/91/0000-0720, November 1991.
- [33] J. W. Baek, C.Y. Jung, J.G. Cho, and G.H. Rim, “*Novel zero-voltage and zero-current switching (ZVZCS) full bridge PWM converter with low output current ripple*”, Power Electronics Research Division, Korea Electro-Technology Research Institute, Korea © 1997 IEEE.
- [34] Dhaval B. Dalal, “*A 500 KHz Multi-Output Converter with zero voltages switching*”, Digital Equipment Corporation, Maynard, MA, USA © IEEE, CH 2853-0/90/0000-0265, 1990.
- [35] K. Mark Smith and Keyue M. Smedley, “*A comparison of voltage soft switching methods for PWM Converters*”, Dept. of Electrical & Computer Engineering, University of California, Irvine, California © 1996 IEEE.

- [36] Praveen K. Jain, Andre St. Martin and Gary Edwards, "Asymmetrical pulse-modulated resonant DC/DC converter topologies", © IEEE Transactions on Power Electronics, Vol., 11, No. 3, May 1996.
- [37] Guichao Hua, Ching-Shan Leu, Yimin Jiang and Fred C. Y. Lee, "Novel Zero-voltage transition PWM converters", © IEEE Transactions on Power Electronics, Vol., 9, No. 2, March 1994.
- [38] Byeong-Ho Choo, Byoung-Kuk Lee, Sang-Bong Yoo, Dong-Seok Hyun, "A novel secondary clamping circuit topology for soft switching Full-Bridge PWM DC/DC converters", Dept. of Electrical Engineering, Hanyang University, Seongdong-Ku, Seoul, Korea, © 1998 IEEE.
- [39] Yingqi Zhang, P.C. Sen, "A new soft switching technique for Buck, boost and Buck-Boost Converters", Department of Electrical & Computer Engineering, Queen's University, Kingston, Ontario, © 2002.
- [40] "Digital Integrated Circuits Analysis and Design", by John E. Ayers by CRC press 2004.
- [41] Miniature type Aluminum Electrolytic Capacitors "HN type" www.nichicon.co.jp
- [42] D. Steinmeier. *Downsizing in the world of resistance welding*. Welding Journal, Vol. 77, PP39-47, July 1998.
- [43] K.J. Ely and Y. Zhou. *Microresistance spot welding of Kovar, steel, and nickel*. Science and Technology of Welding and Joining, Vol.6, No.2, PP 63-72, 2001.
- [44] Wen Tan, *Small-Scale Resistance Spot Welding of Thin Nickel Sheets*, Ph.D. Thesis, Doctor of Philosophy in Mechanical Engineering Waterloo, Ontario, Canada, 2004.

[45] "*Electrical Engineering Principles and Applications*", (Fourth Edition) by Allan R. Hambley, Pearson Prentice Hall, New Jersey, 2008.

[46] "*Introduction to Modern Power Electronics*", by Andrzej M. Trzynadlowski, John Wiley & Sons, Inc., 1998.